Feasibility study of oil immersed power electronic based high voltage test source for onsite testing purpose

By

Getssy Prathiba Lourduraj

in partial fulfilment of the requirements for the degree of

Master of Science in Electrical Engineering

Department of Electrical Sustainable Energy

at the Delft University of Technology,

to be defended publicly on Wednesday August 21, 2019 at 9:00.

Student number:	*4716175*	
Responsible Supervisor:	*Prof. Ir. Peter Vaessen*	*TU Delft*
Daily Supervisor:	*Dr.Ir. Mohamad Ghaffarian Niasar*	*TU Delft*
Thesis committee:	*Prof. Ir. Peter Vaessen*	*TU Delft*
	Dr.Ir. Mohamad Ghaffarian Niasar	*TU Delft*
	Dr.Ir.Alex Stefanov	*TU Delft*
Company supervisor:	*Dr.Ir.Benjamin Baum*	*DNV GL*

If the only prayer you ever say in your entire life is thank you, it will be enough.

Meister Eckhart

Acknowledgement

"Alone we can do so little; together we can do so much."
Helen Keller

I take this opportunity to thank everyone who had been a great support during my thesis work. I would like to express my sincere gratitude to the chairperson, *Prof. Ir. Peter Vaessen*, for giving me the opportunity and supporting me to do my master thesis in collaboration with DNVGL - KEMA Laboratories. His remarkable guidance coupled with eye for detail on my work were very helpful to improve the quality of thesis report. I thank my daily supervisor *Dr. Mohamad Ghaffarian Niasar* who was always very patient with me. His constant encouragement and valuable comments were extremely useful to refine my thesis work. I would like to thank *Dr. Alex Stefanov* for accepting my request for being a part of my thesis committee. As a part of this thesis was based on experimental analysis, I extend my sincere thanks to my lab supervisor *Ing. Remko Koornneef*. The experimental work wouldn't have been possible without his support. His immense experience, along with witty humor, made the assembly of test setups a delightful experience. In a short period of time, two functional test setups were built in the laboratory. I am also thankful to *Ir. Radek Heller, Mr. Wim Termorshuizen* and *Ing. Paul Van Nes* from the High Voltage Laboratory. Despite practical difficulties, these people had constantly supported me throughout my thesis.

I thank my company supervisor *Dr. Benjamin Baum* from DNVGL – KEMA Laboratories for his continuous support. His technical expertise helped me to work on developing a practical solution for the problem definition. I would also like to thank *Dr. Cornelis Plet, Ir. Edwin Pultrum* and *Mr. Sjoerd Smeenk* from DNVGL for their valuable technical guidance. I would like to convey my heartfelt thanks to *Dr. Ir. Thiago Batista Soeiro* for his constant technical support and expert advice on regular basis in the field of power electronics. My sincere thanks to *Stefaan Heirman* from PVMD group and *Dr. Ing. Bart Roodenburg* from DCES group for their timely support by providing equipment for building the test setups. I extend my gratitude to 'Eurofins', material science laboratory in the Netherlands and *Carry Hermans* from Eurofins who helped me with the internal analysis of test samples.

I have to express my unfeigned gratitude to *Ing. Hari Nagarathinam* for vigilantly proofreading my report work and providing valuable feedback. I thank *Ir. Dhanashree Ganeshpure* for providing technical and moral support throughout my thesis work. I also want to thank a very special team of friends: *Rahul (Possum), Ragav, Padmapriya, Naveen, Balaji, Arun, Nivee and Samyuktha* without whom my student life at TU Delft wouldn't have been lively. Finally, I would like to thank my parents for their constant moral and spiritual support during my entire thesis.

Getssy Prathiba Lourduraj
Delft, August 2019

Summary

There is an increasing demand for compact onsite dielectric test systems of medium and high voltage equipment. Though there are commercially available mobile high voltage (HV) test sources, they have some important drawbacks such as limitation in voltage capability, complexity in building up the test setup and lack of versatility to test different equipment. Alternatively, the present challenges in these conventional test sources could be resolved by constructing a power electronics based test source. Amongst various converter topologies, Modular Multilevel Converter (MMC) is considered as a suitable topology for this application because of its high efficiency, modular structure, and reduced filter requirement. In order to achieve a compact solution, an oil immersed design of MMC, instead of the typical air insulated converter design is proposed in this master thesis. Oil can act both as a coolant and an effective insulating medium, thereby reducing the dimensions of the test system.

This master thesis demonstrates the feasibility of oil immersed MMC based HV test source, covering both system level and component level aspects. The extent of compactness of the test source in oil was estimated at a system level. It was found that for the given trailer dimensions, the voltage capability of test source is around 4 times higher in oil when compared to air, This shows the effectiveness of oil as an insulating medium. The feasibility of oil immersed converter design depends on the degree of compatibility of its components under oil. Hence, experimental investigation was conducted on Insulated Gate Bipolar Transistor modules (IGBT) under oil as they are considered to be a pivotal component in MMC. Preliminary results show the penetration of oil into the IGBT chip surface. Despite oil migration, the operation of IGBT was not hindered during the test. Based on the results obtained from experimental work, a road map of future tests is suggested that need to be performed to realize an oil immersed HV mobile test source.

Keywords – submodule, MMC, converter layout, IGBT, insulation, oil, silicone gel, thermal cycling.

Contents

1

Introduction

"Testing, we will never do enough of it."
Greg LeMond

1.1 General Background and Motivation

Numerous high-voltage (HV) and medium voltage (MV) equipment such as switchgear, transformers, power cables, insulators, and generators play an important role in the successful operation of the electric power system. An ever-increasing demand for electrical energy by various consumers has resulted in an increased number of installations with this equipment in the power system infrastructure. The reliable and safe operation of these installations is paramount to ensure grid reliability. According to the Eaton Blackout tracker, faulty equipment is one of the common cause of power outages [1]. This calls for the need of rigorous testing procedures and monitoring techniques of all power equipment installed in the grid. The whole life cycle of any power equipment is accompanied by a variety of tests. In particular, insulation failure in equipment results in unexpected breakdowns and creates a huge impact on grid operation. Therefore, various high voltage tests are conducted to ensure the healthiness of insulation.

As per IEC 60071-1, HV tests are based on the principle that the applied test voltage shall simulate stresses which can occur during the service condition of equipment [2]. HV testing can be conducted in different locations such as laboratory, manufacturing facility (factory) and on site. This thesis focusses on the feasibility study of an on-site test source which will be used for high voltage testing purposes.

According to IEC 60060-3, *"an on-site test is defined as a test executed at the place of use of the equipment or installation that is to be tested, and with the test object as far as possible in its service condition"* [3]. The onsite HV testing is typically conducted on equipment such as power transformers, rotating HV machines, cable systems, and complete substations. At present, HV tests are applied on site for the following purposes:

(1) *Tests after installation* - as a part of the commissioning of new equipment on site to demonstrate that transportation from the manufacturer and erection have not caused any new dangerous defect in insulations.
(2) *Tests after field repair* - to verify and validate the reliable operation of the equipment after an onsite repair/service.
(3) *Technical due diligence* - to demonstrate that the service-aged equipment is still free of defects and for the assessment of residual lifetime.

Besides the above-mentioned reasons, there is a growing demand for onsite HV testing with new applications. For instance, **planned outage** (PO) of electrical installations in a substation is rapidly becoming one of the biggest challenges for grid operators. Increasing grid size and complexity, combined with the required high degree of grid reliability develop as major challenges to have a planned outage. The duration of the PO is very critical and needs to be accomplished without any delay, which if not achieved, would result in significant negative consequences. There are upcoming possibilities of bypassing a complete substation with the help of a mobile HV substation thereby aiding in implementing planned outage effectively [4]. In this case, testing of mobile HV substation is inevitable on-site before bypassing the main substation. In addition, the time taken for HV testing should also be as short as possible. The proposed HV on-site test source could be used for such application requirements as well.

There are various commercially available conventional mobile test systems used for on-site testing purpose based on the test requirement. Typical mobile test systems of Power Diagnostix Instruments GmbH (PDIX) and KEMA Laboratories are shown in figure 1.1 and 1.2 respectively [5, 6].

Figure 1.1: Mobile test system of PDIX [5]

Figure 1.2: Mobile test system of KEMA Laboratories [6]

As per IEC 60060-3, several voltages have been defined for onsite testing. Based on field experience, many test voltages are in use for testing and diagnosis based on the equipment type [7]. For example, withstand voltage tests on extruded cables can be performed using the high voltage AC resonant test system after cable installation. An internal view of such a test system manufactured by HIGHVOLT is shown in figure 1.3 [8]. It mainly consists of a high voltage reactor which forms a resonance circuit with the cable to be tested. A detailed schematic of this test system is given in appendix A.1.

Figure 1.3: Internal view of the mobile test system manufactured by HIGHVOLT [8]

Though there are mobile test systems available, they have the following drawbacks,

(1) **Limited voltage capabilities -** The maximum voltage capability of an individual test system that could fit in a trailer is limited. For example, the mobile test system shown in figure 1.3 in a trailer is designed for tests of up to 260 kV [8]. Several such test systems should be connected in cascade configuration for higher voltages.
(2) **Complexity in building up the test setup -** The effort and time taken for the erection of the HV test system on-site should be as short as possible. If the voltage or power requirement exceeds the capability of the individual test system, then multiple trailers should be transported onsite to make a parallel or cascaded connection. This increases transportation cost. In addition, time taken to configure this type of connection of test system is very long (typically a day) when compared to the average duration of the test (≈ 1 hour).
(3) **Lack of versatility –** There are dedicated mobile test systems used for different equipment. For example, there are two different mobile test systems available for cables and power transformers. Therefore, the conventional test sources lack the versatility to test multiple equipment.

These constraints create a need to have a one-stop solution of a versatile high voltage test source with higher voltage and power capability to effectively test the equipment. Hence, this project opens a new platform to extend the capabilities of the testing facilities of KEMA Laboratories to meet the upcoming demands for onsite testing.

1.2 Problem definition

As a viable alternative, the above-mentioned challenges in the conventional test systems could be resolved by constructing a power electronic based test source [9-11]. However, a compact solution for a high voltage test source that fits in a standard trailer is difficult to build with traditional air insulated power converters since air insulation calls for large dimensions.

For example, in an HVDC converter station, the converter is usually installed in a building called the valve hall. Typically, more than 60% of the total volume of valve hall is occupied by air for insulation. The remaining volume is occupied by the converter. Alternatively, if oil is used as an insulating medium, the volume required for insulation could be significantly reduced, because the dielectric strength of oil is higher than that of air. Oil is used as an insulating medium in many types of electrical equipment - transformers, bushings, cables, and capacitors. Hence, an oil immersed design of the test source is proposed in this thesis. This can be a promising solution because oil can act both as a coolant and as an effective insulating medium, thereby helping to reduce the size of test system. The problem definition boils down to:

"Is it feasible to have an oil immersed power electronic based test source for onsite testing?"

1.3 Research scope

This thesis is a first step towards the ultimate goal of building a compact mobile test system. According to the results obtained in [9], Modular Multilevel Converter (MMC) topology has been proven to be a promising solution for this high voltage test source. Hence, in this thesis, all analysis and experiments were conducted considering the MMC topology. The two preliminary aspects mentioned below are examined in this thesis to demonstrate the feasibility of the oil immersed test source.

Primarily, the extent of compactness that can be achieved by using oil as an insulating medium in the test source has to be estimated in order to validate the proposed solution.

Secondarily, if the test source is immersed in oil, then the long-term viability of the test source can be guaranteed if its components are compatible in oil. As the proposed test source is MMC based, its reliability is critically limited by the lifetime of power semiconductor devices, which in this case is Insulated Gate Bipolar Transistor (IGBT). Hence, the operation of IGBTs when immersed in oil will be investigated.

1.4 Research objectives

The research objectives grouped in section 1.4.1 and section 1.4.2 are based on the two aspects mentioned in section 1.3.

1.4.1 First design and dimensioning of the test source

(1) To create a first **conceptual design** for the stacked modular architecture of the test source for onsite testing
(2) To estimate and compare the **achievable percentage of size reduction** of the test source under oil in comparison with air as the insulating medium
(3) To estimate and compare the **maximum voltage capability of the test source** that can be fitted into a (standard) trailer with oil and air as the insulating medium

1.4.2 Experimental investigation on the electrical performance of IGBT immersed in oil

(4) To conduct a preliminary test to understand the **influence of external electric field** on the behaviour of the IGBTs when immersed in oil
(5) To design the test setup, test procedure and perform tests to investigate the **long term stable operation** of IGBTs when immersed in oil
(6) To propose a plan regarding the remaining **test procedures and validation methodologies** that need to be performed for realizing an oil immersed mobile test source.

2

First design and dimensioning of the test source

"Design is the intermediary between information and understanding."
Hans Hoffman, artist and teacher

The aim of this chapter is to elucidate the methodology followed to design the converter layout of test source. Based on the proposed design, the voltage capability of the test source is estimated when air or oil is used as an insulating medium. With these inputs, the extent of compactness that could be achieved using oil is evaluated.

2.1 Need for the design of the test source

The primary aim of immersing components in oil is to reduce the external clearance requirements, thereby building a compact test source. Clearance is understood as the shortest distance in the insulating medium (e.g., air, oil, epoxy, etc.) between two conductive parts [12]. It is often misunderstood with another term 'creepage', which in turn is the shortest distance along the surface of a solid insulator between two conductive parts [12]. Hence, the concept of clearance and creepage between two conductors is illustrated with the help of figure 2.1.

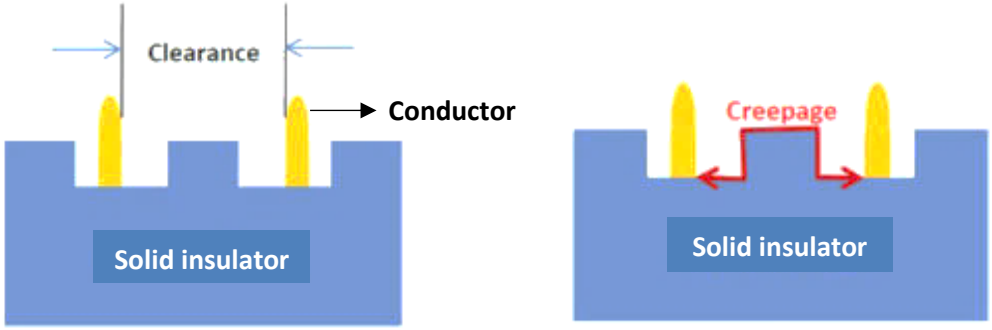

Figure 2.1: Clearance vs. Creepage [13]

The determining factors for clearance are the highest peak voltage present and the dielectric strength of the insulating medium. The clearance distance is inversely proportional to the dielectric strength of the insulating medium. The dielectric strength of oil is higher than the dielectric strength of air. Thus, clearance requirements in oil are lower than that of air for the same given voltage. The physical size of components will remain the same despite the insulating medium. Hence, the primary reduction in size is due to the reduction in clearance requirements in oil. Therefore, it is important to evaluate the extent of size reduction of the test source in oil when compared to air as an insulating medium. This requires a primary design which is to be used as a basis for this comparison. From the design, the voltage capability of the test source can be compared when air or oil is used as an insulating medium.

2.2 Steps involved in the design and dimensioning of the test source

As mentioned in section 1.3, Modular Multilevel Converter (MMC) is considered as the most suitable topology for this test application [9]. Hence, a conceptual design of MMC for the test source was created by following the steps as indicated in figure 2.2. Firstly, a detailed literature study was carried out to review the existing converter layouts of MMC topology. As a next step, the main design specifications and constraints for the test source were gathered and listed. Based on the inputs, a primary design of the MMC was created in accordance with the given specifications. Each step is explained in detail in sections 2.3, 2.4 and 2.5

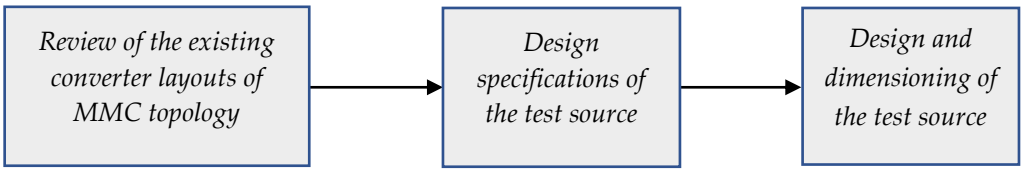

Figure 2.2: Steps involved in the design and dimensioning of MMC based test source

2.3 Review of the existing MMC converter layouts

The MMC has become the most promising multi-level voltage source converter (VSC) topology for high-power applications because of its high efficiency, modular structure, and reduced filter requirement. MMCs are built up of several series-connected submodules (SMs) mainly containing power semiconductor devices and a DC storage capacitor. Each submodule contains two or four IGBTs as switching elements, depending on the design (half bridge or full bridge). Figure 2.3 shows the basic schematic of a single-phase MMC with half-bridge submodule, proposed for the test source. A detailed description of the submodule design is given in section 2.3.1. MMC consists of two arms per phase leg where each arm comprises of N series-connected SMs, a series inductor L_a and a resistor R_a. The test object (TO) is modelled as a capacitor indicated as C_{load}.

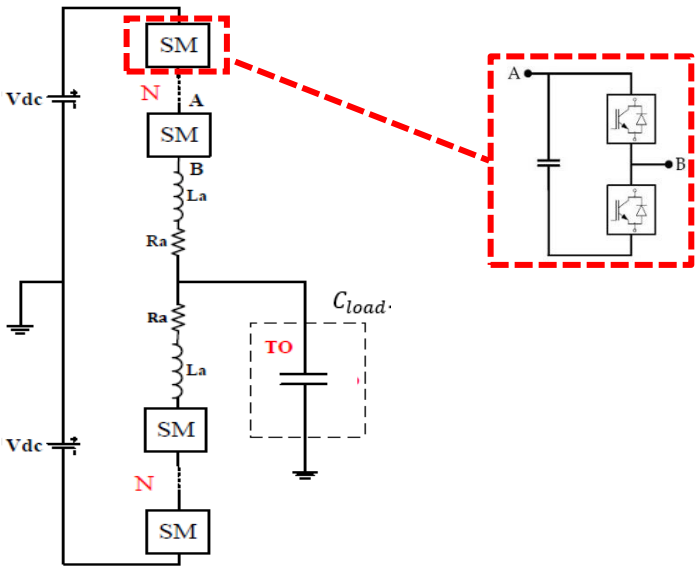

Figure 2.3: Schematic of a single phase MMC topology and a half bridge submodule [9]

The mechanical arrangement of MMC is a modular architecture in order to facilitate ease of manufacturing, testing, transportation, installation, and maintenance. The subsystems which constitute to the converter design is shown in figure 2.4 and each block is described in detail in the following subsections.

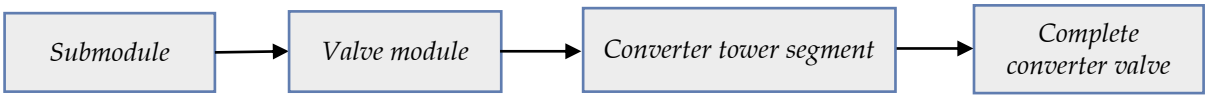

Figure 2.4: Hierarchy of the converter arrangement

2.3.1 Submodule

One major feature of the MMC is that it is a scalable technology. The voltage level of the converter can be increased by connecting more submodules in series. Hence, **the submodules are the elementary building blocks of MMC system**.

Several converter manufacturers such as Siemens, Alstom Grid, Toshiba and Hyosung have constructed their own designs of MMC for applications like HVDC transmission and STATCOM. The MMC submodules are designed differently in detail, but with a very similar appearance [14] as shown in figure 2.5.

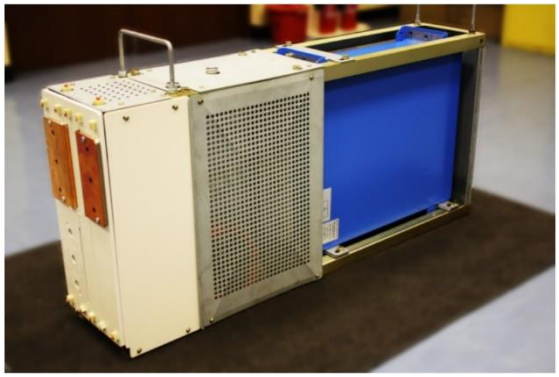

(a) Alstom Grid/GE

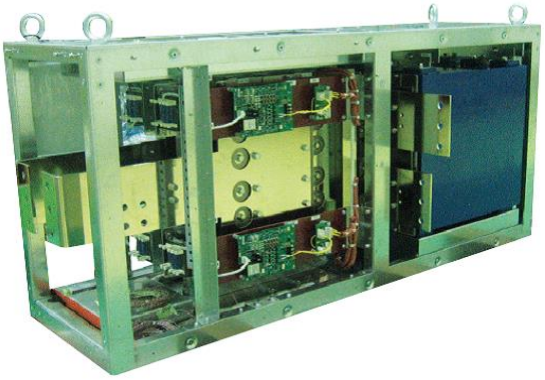

(b) Mitsubishi

(c) Hyosung

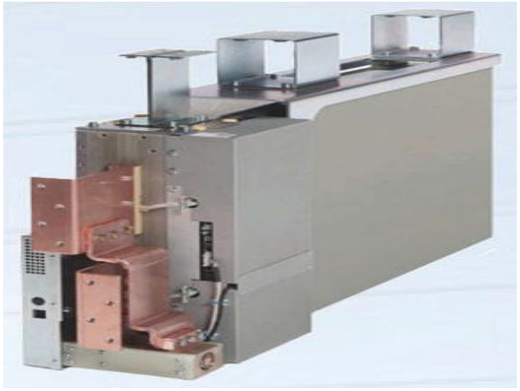

(d) Siemens

Figure 2.5: Images of MMC submodule from different manufacturers (the images are not to scale) [14]

Figure 2.6 shows the components in an Alstom Maxsine half-bridge submodule [15]. Amongst the different packages of IGBTs available, Alstom employs standard off-the-shelf wire-bonded IGBT modules with plastic cases which are rated for 1.5 kA and 3.3 kV [16]. These IGBT modules are mounted on water-cooled heat sinks. A detailed explanation regarding these wire-bonded IGBT modules is given later in section 3.2. Metallized polypropylene film capacitor is mostly used as a DC capacitor which acts as a voltage source for the submodule [17]. The submodule consists of a thyristor which will be triggered to protect anti-parallel diodes in case of a dc-side short-circuit. If the wire-bonded IGBT fails in an open circuit, the submodule is equipped with a mechanical bypass switch to short circuit the submodule. A laminated bus bar is used to connect IGBT power modules together with a capacitor bank. Bleed (discharge) resistors are used for safe handling of the DC capacitor. In addition to these components, the gate drives for IGBTs are also present in the submodule. The top view of a typical submodule is shown in figure 2.7. As observed in figure 2.7, half **the volume of the submodule is occupied by the DC capacitor** [18].

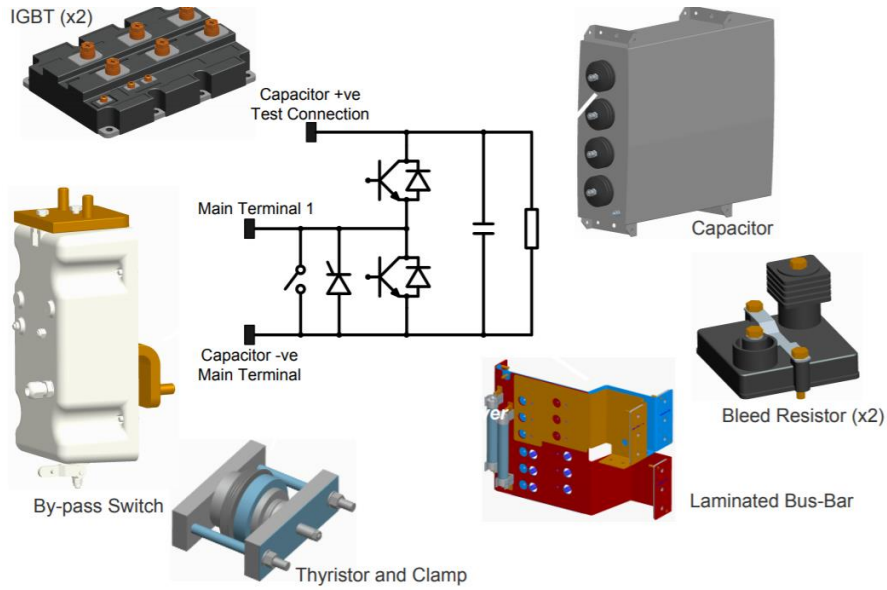

Figure 2.6: The main components of Alstom Maxsine half bridge submodule (the images are not to scale) [15]

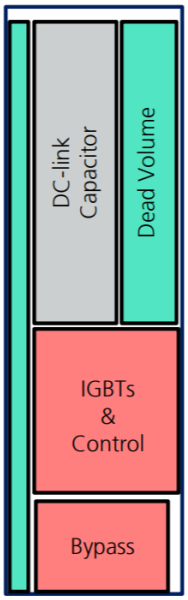

Figure 2.7: typical submodule design - top view [14]

2.3.2 *Valve module*

As a next stage, the submodules are mounted in a rack to form a valve module or power module (the terminology could vary between manufacturers). For example, in an HVDC converter configuration, six to eight submodules are physically grouped together with shared mechanical supports and coolant pipes. A valve module is the next higher level basic unit over submodule in an MMC converter. Figure 2.8 shows the valve module design of two manufacturers, Hyosung and Alstom Grid/GE respectively [19, 20]. The former design has six submodules and the latter has eight submodules as indicated in the image.

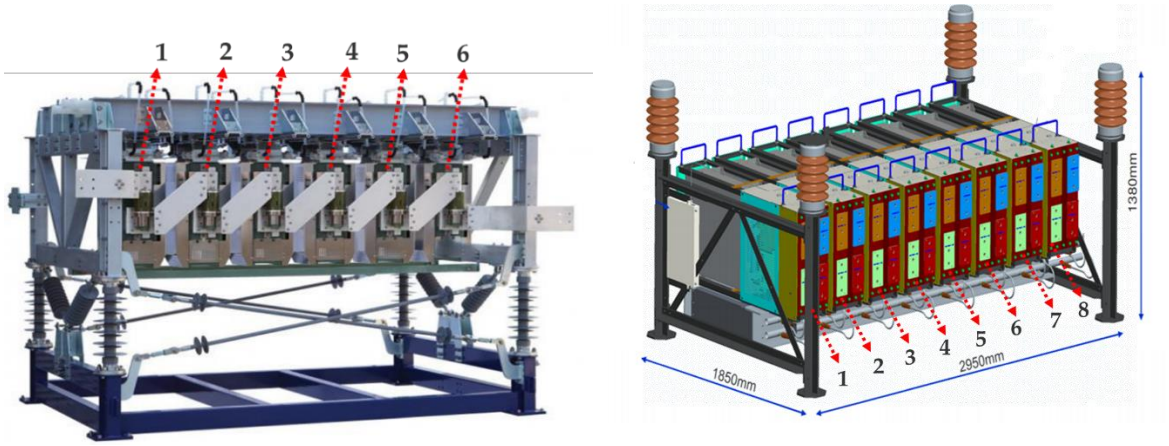

(a) Hyosung – 6 submodules [19] (b) Alstom Grid – 8 submodules [20]

Figure 2.8: Valve module design (the images are not to scale)

2.3.3 *Converter tower segment*

The next higher level modular unit of MMC is a converter tower. It usually comprises of three to four layers of valve modules which are separated by composite post insulators [21]. The main functions of a converter tower are to provide mechanical support and electrical connection. Figures 2.9 (a) and (b) show converter tower structures of Alstom Grid and C-EPRI respectively [22,23]. The converter tower design by Alstom Grid has 4 layers of valve modules. The converter tower of C-EPRI has 3 layers of valve modules, but the difference is that there are two rows of valve modules in each layer of the tower. Hence, they are sometimes called 'double tower'. The height of the insulators in the tower will depend on the voltage level of the converter. The metal structures at the top, bottom, and sides of the tower in figure 2.9 (b) are added to shape the electric field around the converter tower.

(a) Alstom Grid – 4 levels [22] (b) C-EPRI– 3 levels [23]

Figure 2.9: Converter tower design

2.3.4 Converter valve

A converter valve is formed by the interconnection of the converter towers together. These converter valves are housed in a valve hall at the converter station. A study on three different ways of connecting converter tower segments is explained as follows.

Type I – Figure 2.10 shows the type I connection of a converter valve representing a converter arm [21]. The layers are numbered from bottom to top. In this configuration, the AC line is connected to the left-most submodule of the first layer. All the submodules are connected in series in this layer. Then the rightmost submodule in the first layer is connected to the left-most submodule in the second layer, and so on. Finally, the right-most submodule in the top layer is connected to the DC bus.

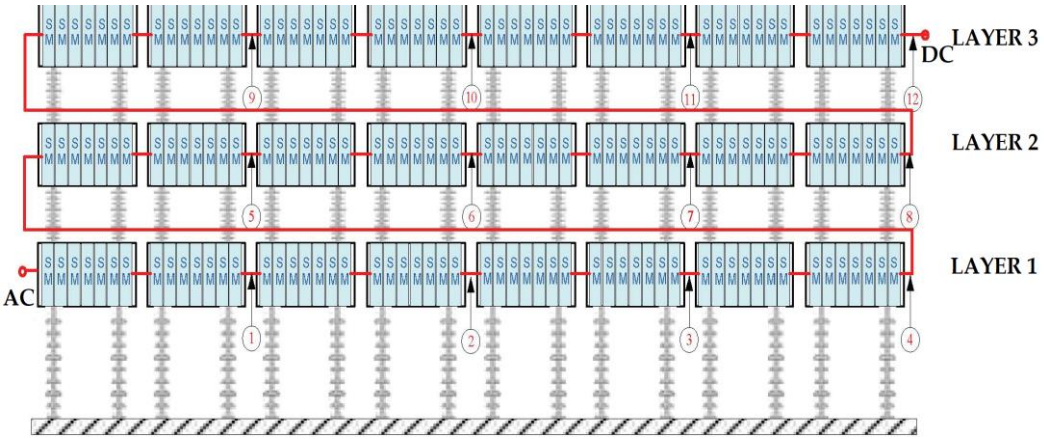

Figure 2.10: Type I connection of a converter arm [21]

Figures 2.11 and 2.12 shows the front and rear view of type I connection of converter valve of Trans Bay cable project [24,25], the first HVDC system to incorporate MMC. The MMC converter was delivered by Siemens. The DC voltage level of the converter is ±200 kV. The total number of submodules in one converter arm is 216 (spares 16). The front view shows the series connection of submodules and rear view shows the long connection from one layer to other of the converter tower (as indicated in figure 2.10).

Figure 2.11: Front view of the converter valve – Trans Bay cable project (Siemens) [24]

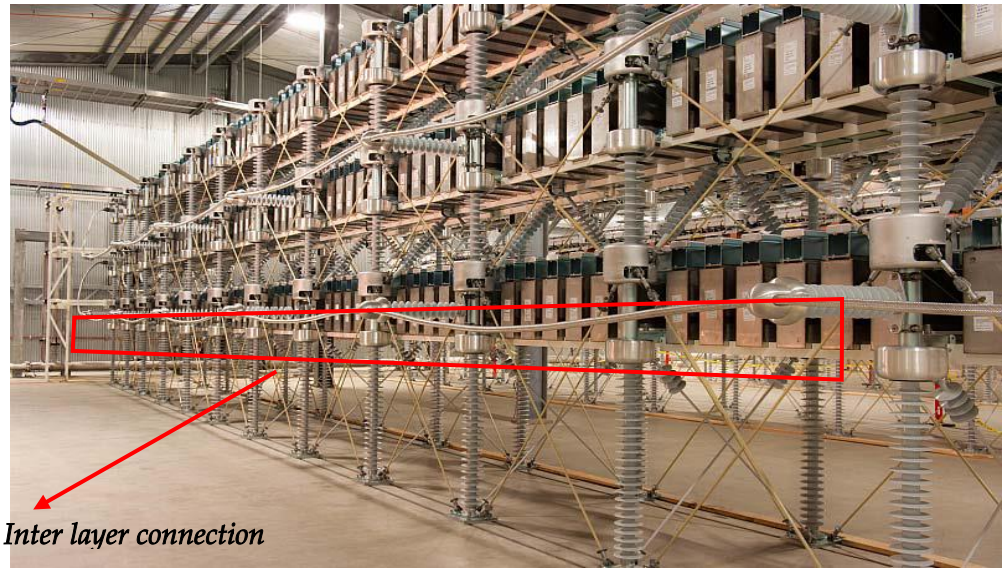

Figure 2.12: Rear view of the converter valve – Trans Bay cable project (Siemens) [25]

Type II – For higher voltages, two valve structures of type I are connected in a spiral connection to form a converter arm as shown in figure 2.14 [26]. There are 4 layers in the converter valve where the input and output connections are also indicated. Therefore, in every layer, there are two rows of valve modules connected in series. Figure 2.13 indicates the terminologies of layer and row for clear understanding.

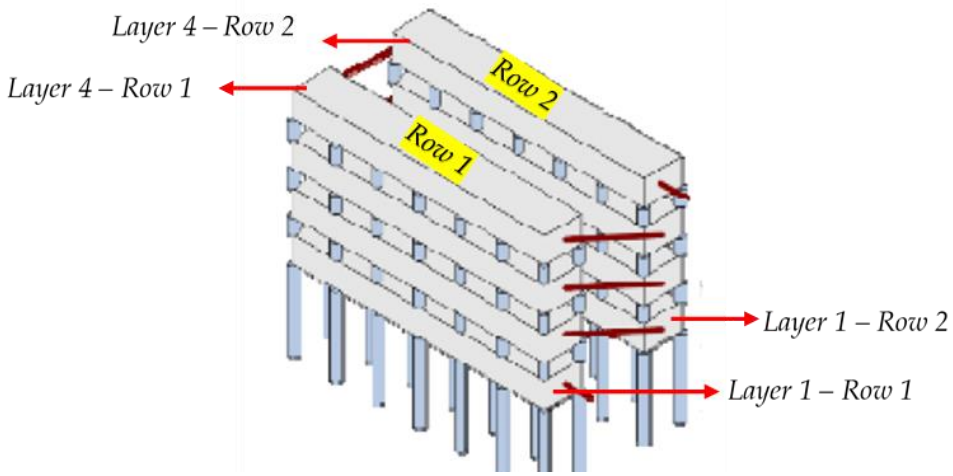

Figure 2.13: Terminologies used in type II connection of a converter arm [26]

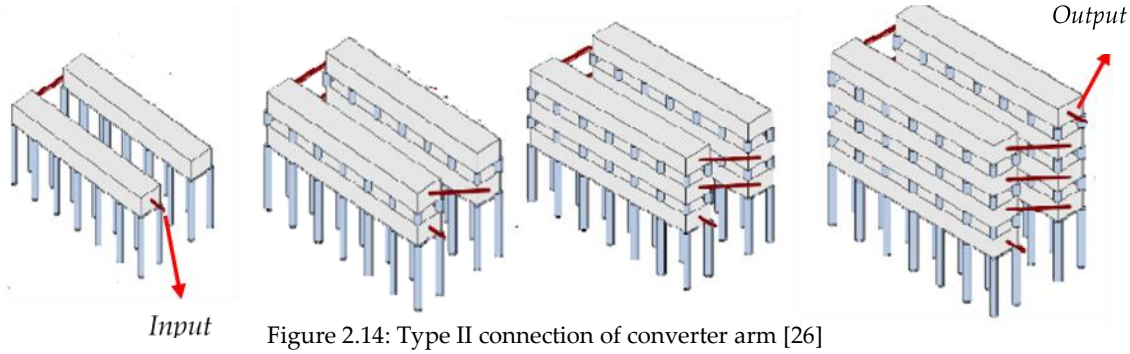

Figure 2.14: Type II connection of converter arm [26]

Figure 2.15 shows the image of type II connection of converter valve delivered by Alstom Grid [27]. There are three converter valves, each corresponding to a converter arm. Each converter valve has 4 layers of valve modules and each layer, in turn, has two rows of valve modules in series. The row and layer terminologies in the valve are highlighted in figure 2.16 (a) and (b) respectively.

Figure 2.15: Internal view of the converter valve hall (Alstom Grid) with type II connection [27]

(a) Row 1 in a layer 1 (b) Layer 1 in the valve

Figure 2.16: Terminologies used in type II converter valve [27]

Type III – As observed in figure 2.15, type II connection demands more floor area (lengthwise). For applications with higher voltage requirement, but with the limited floor area, type III connection can be a promising solution. This connection is made up of interconnecting the converter tower segments as shown in figure 2.9. In this type, valve modules inside one single tower are connected in series first, and then converter towers are connected in series to form a converter valve as shown in figure 2.17 [21]. A disadvantage of type III connection is that converter towers will need higher air clearance between its first layer and the ground. Thus the composite post insulator to the ground is longer.

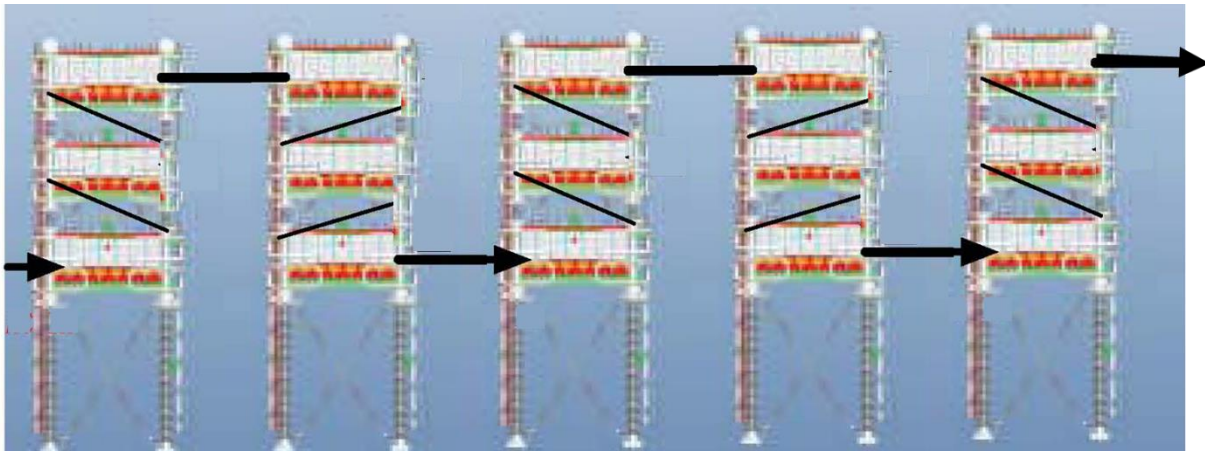

Figure 2.17: Type III connection of a converter valve [21]

Figure 2.18 shows the image of type III connection of converter valve delivered by Siemens in Büttel, Germany, built with 'double tower' as shown in figure 2.9 (b) [28]. One converter tower is highlighted in the image.

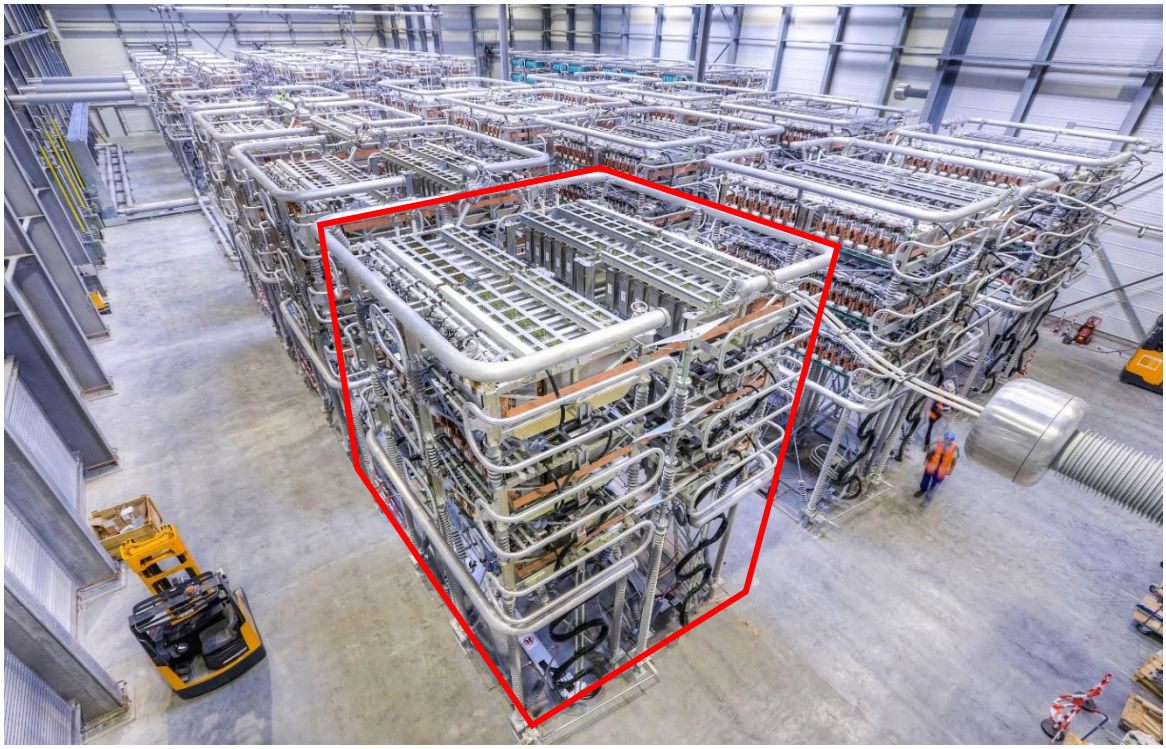

Figure 2.18: Internal view of Type III connection converter valve (Siemens) [28]

An advantage of this type of connection is that the design can be very flexible where the converter towers can be arranged based on available space as shown in figure 2.19 [29]. It can be observed that one tower could also be placed on top of another. This design is especially useful for offshore converter station where there is limited floor area and fewer restrictions on the height of the valve hall.

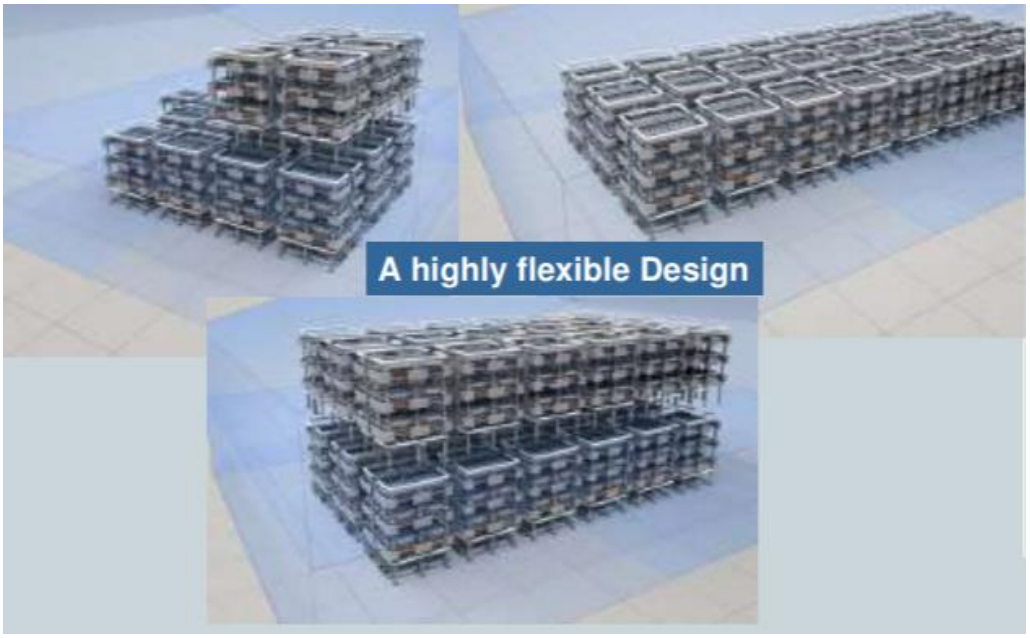

Figure 2.19: Flexible design of Type III connection (Siemens) [29]

2.3.5 *Clearances required in the converter design*

With air as an insulating medium, careful considerations are required regarding the clearance distances in the converter design. Each submodule is enclosed in a metallic box to provide shielding of the submodule from the surrounding electric field. The potential of the metallic enclosure of every submodule is referenced to its corresponding negative capacitor bank terminal [30]. The arrangement is in such a way that voltage increases linearly across each subsequent submodule in the string when all the submodules are inserted. This means that there should be sufficient clearance distance between each subsequent submodule. Apart from that, clearances are also required on a system level. Henceforth, all clearance distances required for converter arrangement are classified into the following zones.

1) Zone 1 - between the submodules
2) Zone 2 - between the rows of the converter tower
3) Zone 3 - between the layers of the converter tower
4) Zone 4 - between the converter towers
5) Zone 5 – between the converter arm
6) Zone 6 - from all the sides of the converter hall enclosure (including the ground)

2.4 Design specifications of the test source

2.4.1 Inputs from a previous master thesis

Some of the functional requirements of test source were obtained from the results of a previous master thesis which proved the feasibility of an MMC-based high voltage test source through mathematical modelling. The following design specifications were taken from [9].

1) Most HV equipment behaves as a capacitor when their insulation is tested with HV voltage. Hence, the test object is modelled as a **capacitance** (C_{load}).
2) Unlike the traditional three-phase MMC, a **single-phase leg of the MMC** will be sufficient to generate single-phase wave shapes across the test object as shown in figure 2.3. Hence the MMC based test source will have only **two converter arms** (upper and lower).
3) The chosen submodule topology is a **half bridge topology** as shown in figure 2.6 with IGBTS as power semiconductor devices.

2.4.2 Choice of the main-circuit parameters

It is important to note that the design and dimensioning of the converter valve of the test source is only created in this thesis. Dimensioning of the DC source required for MMC is not included in this thesis. In addition, size estimation of other components like the arm resistance and inductance of the test source need more detailed inputs regarding the test source requirements. Hence, based on primary inputs obtained as given in section 2.4.1, the choice of main parameters required for a first design of the converter valve were made and are explained hereafter.

Rating of the IGBT module – There are two different packages of IGBT modules which are currently available for high voltage applications. The most common type is industrial power module with an isolated base plate and a non-hermetic plastic cover. The second type is hermetically sealed press-pack modules. A detailed overview of these packages is given in section 3.2. The industrial power modules are commonly used in MMC for HVDC applications [17]. The industrial IGBT power modules used for high voltage applications are usually rated for 3.3 kV, 4.5 kV, and 6.5 kV. The 6.5 kV IGBT is chosen for this application where the devices are typically operated at 4 kV to allow for safety margins.

Choice of the number of submodules per arm – A good estimate of the number of submodules per arm (N) is found from equation (2.1) [17]:

$$N = \frac{2\,V_{dc}}{V_{avg}} \tag{2.1}$$

where $2\,V_{dc}$ is the total DC pole to pole voltage and V_{avg} is the average submodule capacitor voltage. The choice of V_{avg} depends on several factors as mentioned in [17]. As a first approximation, a suitable choice of $\boldsymbol{V_{avg}}$ for a 6.5 kV IGBT can be **4 kV**.

For a 200 kV test source, V_{dc} will be 200 kV and the number of submodules per arm is 100 as per equation (2.1). It is very important to note that N represents the number of submodules per arm. As mentioned earlier, the test source has two converter arms. So, the total number of modules in the test source will be twice that of N, which is 200 submodules for a 200 kV test source. This is also a reason for not choosing lower-rated IGBTs which in turn would increase the number of submodules in the converter.

Choice of submodule capacitance - The design criterion for submodule capacitance is different for test source when compared to traditional power application. According to [9], the submodule capacitance C_s for test source is calculated as follows.

$$C_s = \left[2.round\left(\frac{N+1}{2}\right) + \frac{N+2}{2}\right].\frac{V_{dc}}{N\Delta v_{uT}}\ C_{load} \tag{2.2}$$

where Δv_{uT} is the total submodule capacitor voltage ripple. The submodule capacitance primarily depends on the capacitance of the test object C_{load} and voltage rating (V_{dc}) of the test source. The number of submodules per arm (N) is related to (V_{dc}) by equation 2.1. A load capacitance (C_{load}) of 0.6 µF was considered in this thesis. For example, in case of power cable testing, this load corresponds to a 200 kV rated cable with an approximate length of 3 km (with a typical consideration of capacitance per unit length to be 0.2 $\frac{\mu F}{km}$ [31]). A choice of 10% of ripple in the submodule capacitor voltage (V_{avg}) was considered from [9]. Hence, for a 200 kV test source and with C_{load} of 0.6 µF the submodule capacitance is estimated as 100 μF.

2.4.3 Constraints on the dimensions of test system

Since the mobile test source is mounted on a standard trailer, it must fit into the dimensions of trailer. Hence the typical dimensions of the existing mobile test system of KEMA Laboratories are given below and indicated in figure 2.20.

- The length of entire test system is 14.5 m (including the truck)
- The height of trailer is 4 m from the ground level
- The width of trailer is 2.5 m

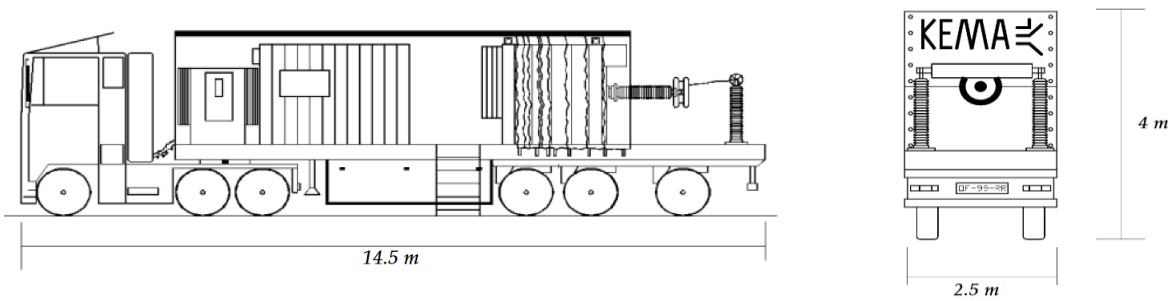

(a) Side view (b) Rear view

Figure 2.20: Dimensions of the mobile test system [32]

Hence the effective dimensions ($L_{trailer} \times W_{trailer} \times H_{trailer}$) of converter valve arrangement inside the trailer is initially chosen to be 9 m x 2 m x 2.5 m taking into consideration about the space required for other components of the test source.

2.5 Design and dimensioning of the test source

As mentioned in section 2.4.3, converter valve arrangement needs to fit into the specified dimensions of trailer (9 m x 2 m x 2.5 m). Inputs from section 2.3.4 on existing three types of MMC layouts were taken as a reference while designing the converter layout. Amongst the three types, the most suitable type of design is the one which can accommodate the maximum number of submodules in available space which in turn primarily depends on the dimensions of submodule. A similar procedure is followed with oil as an insulating medium and the voltage capability of the test source is compared with that of air. Hence, the first step of design is to estimate the dimensions of submodule based on the available inputs from section 2.4.2.

2.5.1 Size estimation of the MMC submodule

Though submodule consists of many components, half of its volume is occupied by DC capacitor as already pointed out in section 2.3.1. In traditional power application, submodule capacitance is in the mF range. However, for the test application, the value of the capacitance was calculated to be 100 μF from section 2.4.2. The size of the DC capacitor depends mainly on the application and on several other design parameters which are currently unknown. Henceforth, it is very difficult to predict the exact dimensions of capacitor. Therefore, based on the available data from manufacturers, the volume of a 100 μF capacitor rated for 4 kV is estimated to be 0.005 m^3. As mentioned in 2.3.1, DC capacitors are usually metallized polypropylene film capacitors, typically available in cuboid-shaped housings and the terminals have voltage-adapted bushings. The capacitor is chosen to be 0.2 m long, 0.18 m high, and 0.15 m thick from a manufacturer's datasheet [33]. The weight of the chosen capacitor is 10 kg.

The first part of submodule consists of semiconductor devices along with auxiliary components as shown in figure 2.21 [17].

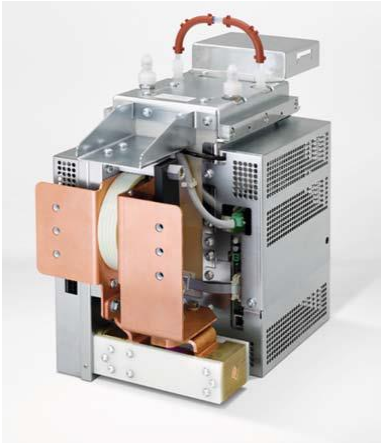

Figure 2.21: Photograph of a Siemens half-bridge submodule excluding the submodule capacitor [17]

The size of this part of submodule mainly depends on the size of IGBT modules and its cooling arrangement. Since the test source is meant for high voltage testing, the output current is in the form of pulses which are required only for charging and discharging of the load capacitance (test object). Hence the current rating of IGBT modules used in the test source is relatively low. This facilitates the usage of IGBT modules rated for 6.5 kV with a lower current rating, unlike the traditional modules. Currently, the IGBT modules used for power application are typically 190 mm long and 140 mm wide. Figure 2.22 shows an IGBT module of Infineon whose voltage and current ratings are 6.5 kV and 750 A respectively [34]. Figure 2.23 shows a 6.5 kV rated IGBT module but with a lower current rating of 250 A [35]. This module is only 73 mm long and 140 mm wide. Both modules have an integrated antiparallel diode.

Figure 2.22: IGBT module - 6.5 kV and 0.75 kA [34] (the image is not to scale)

Figure 2.23: IGBT module - 6.5 kV and 250 A [35] (the image is not to scale)

Hence, based on the above-mentioned arguments, there is certainly a room for size reduction of the submodule which will be used in the test source. The traditional submodule manufactured by Alstom Grid is 1.5 m long, 0.65 m high, and 0.3 m thick [16]. These modules are operated between 1.8 - 2.0 kV and 1000 – 1200 A. Considering these dimensions as a reference along with the above-mentioned DC capacitor size, **the dimensions of the submodule for a 200 kV test source was estimated to be 0.6 m long, 0.3 m high and 0.25 m thick. The weight of the complete submodule is estimated to be 20 kg.** The corresponding volume of the submodule was 0.045 m^3. This volume is taken as a reference. For example, if the maximum voltage capability of the test source in air is found to be 100 kV, then the submodule capacitance (C_s) will be 50 µF according to the equation (2.2) for the same C_{load} of 0.6 µF. The corresponding volume of the submodule was reduced by half, considering the reduction in the size of the submodule capacitor. This assumption was found to be reasonable for the first design. It is inappropriate to use fixed module dimensions for all the voltage rating of the test source, which will lead to severe under estimation. Henceforth, this relation was incorporated during the dimensioning of the test source, having the dimensions of the submodule for 200 kV as a reference.

2.5.2 Choice of the design layout

A logical approach - Two different types of orientation of converter tower are possible in the trailer. Orientation I have submodules stacked along the length of the trailer whereas orientation II have submodules stacked along the width of the trailer. Hence, type I design is only applicable to the first orientation. The classification of converter layout types possible under these orientations is shown in figure 2.24.

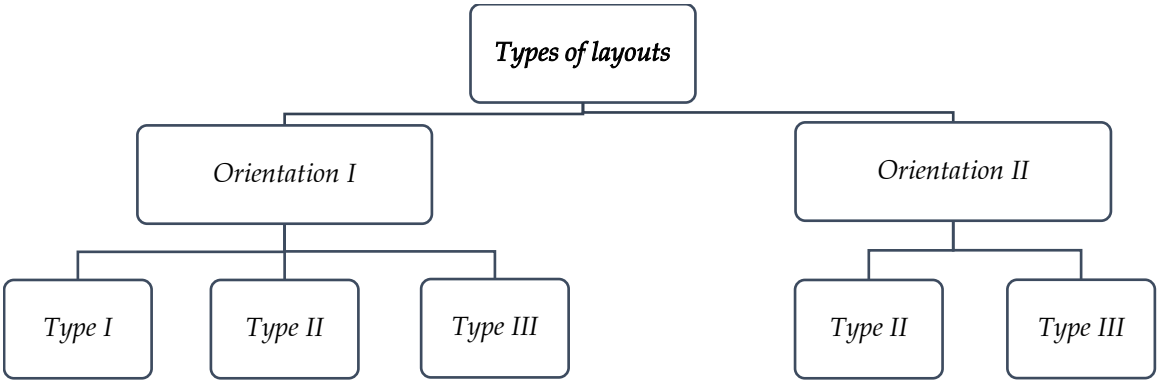

Figure 2.24: Classification of the converter layouts

Figure 2.25 and 2.26 show 3D views of type II design inside the trailer in two orientations for illustrative purpose. As indicated in figure 2.25, the x, y and z-axis correspond to the length, height and width of the trailer respectively. However, in first orientation, width of the trailer poses a constraint to the layout. For the given dimensions of trailer, the number of submodules that could be fitted in all possible types are calculated for both orientations. Amongst all types, the converter layout that accommodates the largest number of modules per arm (N) is chosen to be the final choice.

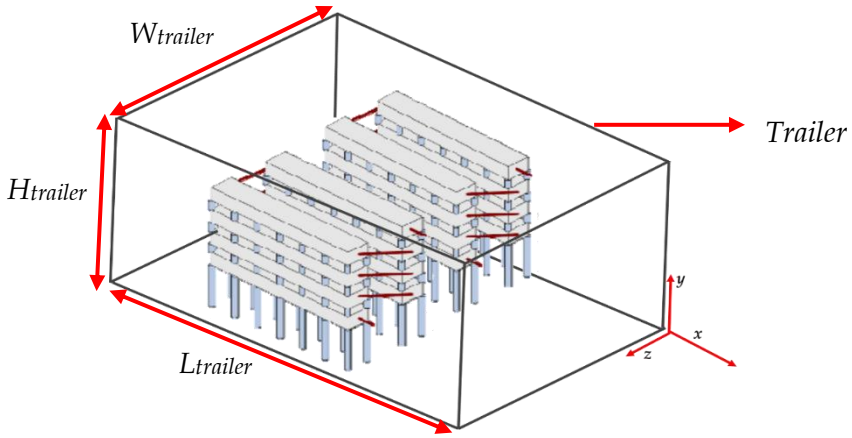

Figure 2.25: Representation of type II – orientation I connection inside the trailer

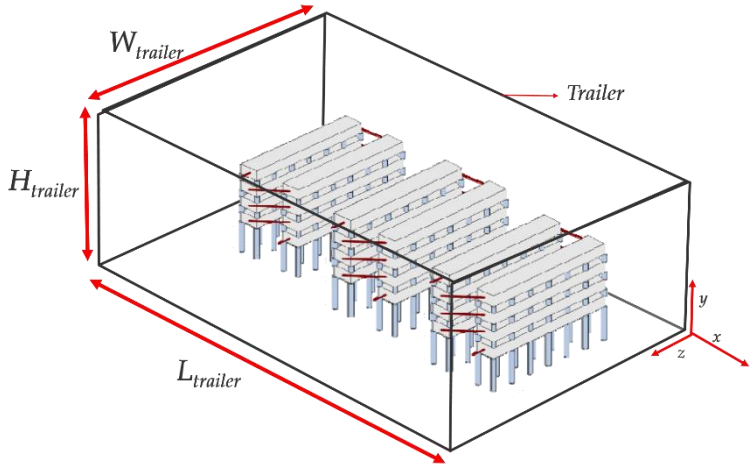

Figure 2.26: Representation of type II – orientation II connection inside the trailer

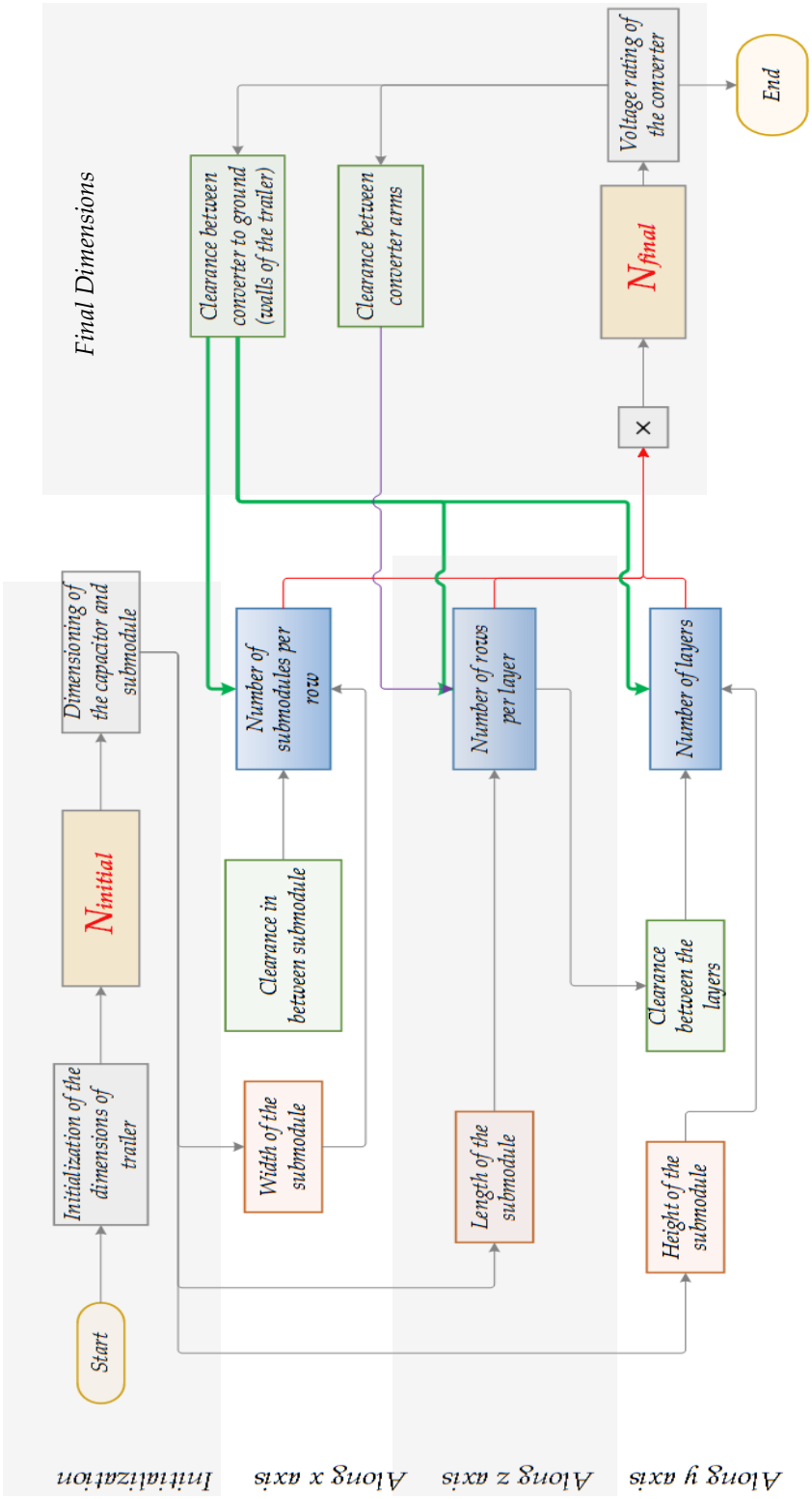

Figure 2.27: Flowchart for dimensioning type II connection of the converter valve

Non-sequential procedure - The flowchart in figure 2.27 shows the dimensioning procedure followed for the type II connection with first orientation. A similar procedure is followed for other converter designs, with variation according to the type of layout. It can be clearly seen from flowchart that the dimensioning procedure is not sequential. The clearances required for zones 5 and 6 (as mentioned in section 2.3.5), depend on the voltage rating of the test source. Hence an optimisation algorithm was used in MATLAB to calculate the number of modules. In addition, an initial value of the number of submodules per arm ($N_{initial}$) is assigned based on which the size of the submodule is estimated as explained in section 2.5.1. After completing the dimensioning procedure, ($N_{initial}$) is compared with the final estimate (N_{final}). This procedure is iterated for many several values of $N_{initial}$ until the minimal difference between the initial value and the final estimate (N_{final}) was obtained.

The number of submodules that could fit it all the types of layouts in air is discussed below. It is to be noted that the design methodology of type I is similar to that of type II, but only with one row in each layer. Hence, this type can be considered as a special case of type II connection. So, feasibility of type II connection is explained first followed by type I connection.

Number of submodules in type II connection - Figure 2.28 shows a 3D view of two converter arms of type II connection in first orientation. This figure is similar to figure 2.25, but with detailed construction of submodules. The modules in type II connection (first orientation) are arranged in such a way that width of submodule (w_{module}) is along x axis, height of submodule (h_{module}) along y axis and submodule length (l_{module}) along z axis as represented in figure 2.28. The clearance required between each module d_{module} is also shown in the image.

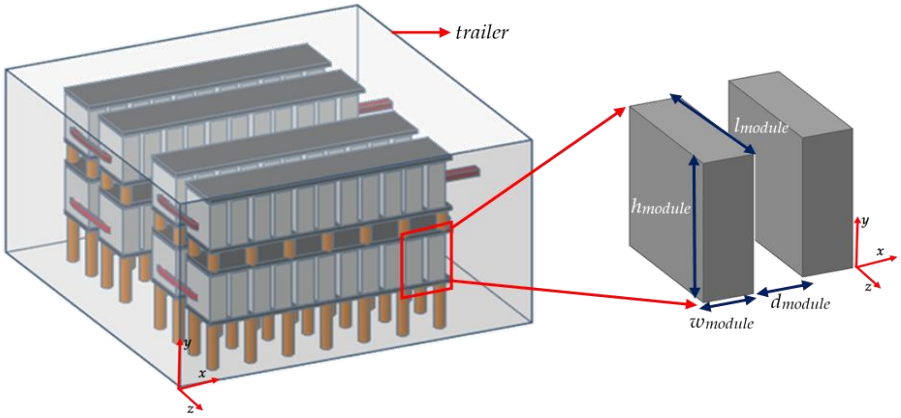

Figure 2.28: Submodule arrangement of type II connection in orientation I

For the chosen trailer dimensions ($L_{trailer}$×$W_{trailer}$×$H_{trailer}$) of 9 m x 2 m x 2.5 m, it was found that only 4 modules can fit along the trailer in orientation I with type II. To accommodate more modules, the effective width of more than 2 m was needed. Hence, type II connection is not suitable with the specified dimensions of submodules. However, in second orientation, multiple rows could be accommodated as observed in figure 2.29. In this orientation, length of the module is along the length for the trailer unlike the first orientation. A maximum of 36 modules can be accommodated in converter arm using this type of connection in air.

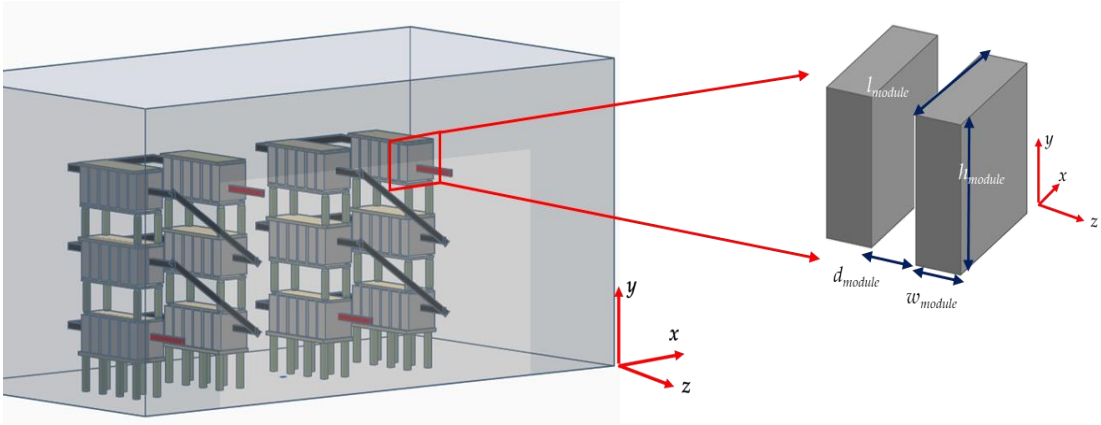

Figure 2.29: Submodule arrangement of type II connection in orientation II

Number of submodules in type I connection – The next step is to calculate the number of submodules that could fit into the trailer using type I connection. A 3D representation of the type I connection with the submodule arrangement of two converter arms is shown in figure 2.30. It can be seen that there is only one row per arm. Hence, this design is only applicable to the first orientation.

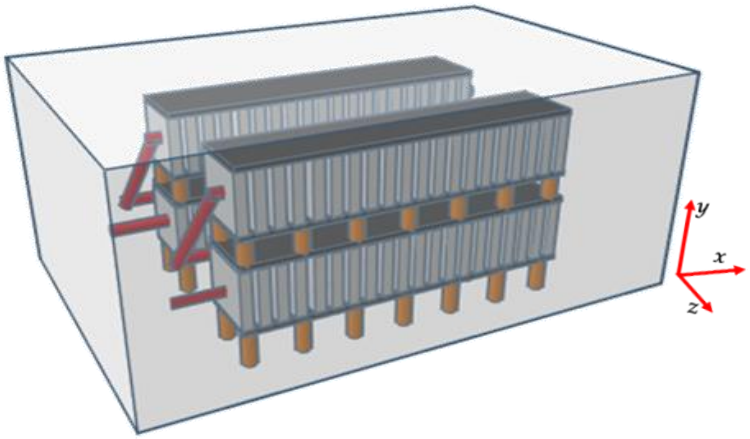

Figure 2.30: Submodule arrangement of type I connection inside the trailer (the image is not to scale)

It was found that only 18 modules can be accommodated per converter arm with air as the insulating medium with this type.

Number of submodules in type III connection – The next step is to calculate the number of submodules that could fit into the trailer using type III connection. A 3D representation of the type III connection with first and second orientation is shown in figure 2.31 and figure 2.32 respectively. In this type, the submodules in one converter tower segment are connected in series before moving to the next tower as shown in figure 2.17. It was found that 24 modules can be accommodated per converter arm using type III with air in orientation I and 36 modules could be fitted in orientation II.

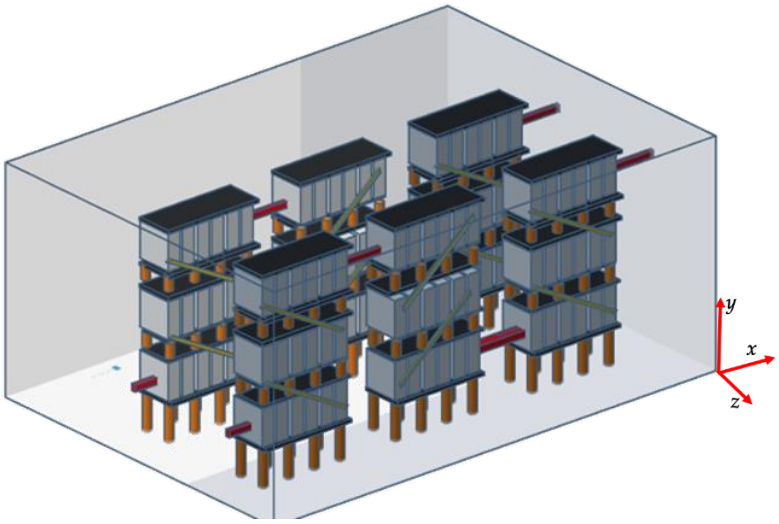

Figure 2.31: Submodule arrangement of type III connection (orientation I) (the images not to scale)

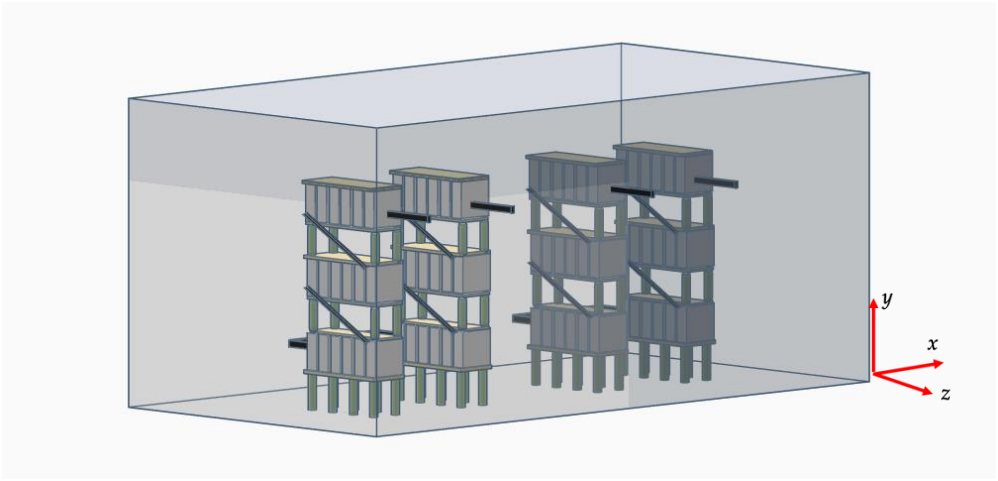

Figure 2.32: Submodule arrangement of type III connection (orientation II) (the image is not to scale)

2.5.3 *Dimensioning tool for the MMC*

It is very important to note from the above-mentioned design considerations that the size and shape of the module highly influence the design criteria and choice of converter layout. For example, currently estimated module dimensions resemble a brick similar to traditional modules. But, it is expected that after the actual design of submodule for the test source, its dimensions will vary in future. Hence, a MATLAB based dimensioning tool was developed wherein trailer dimensions can be entered by the user. The tool can perform the following tasks:

1) Choose the converter layout based on specified trailer dimensions. It can also provide a converter layout for a stationary test source by providing the details of the available space since the design procedure remains the same.
2) Calculate the number of submodules that could fit into trailer and thereby calculate the voltage rating of test source with air as an insulating medium.

3) Estimate the number of submodules if oil is used as an external insulating medium for the converter instead of air. Subsequently, the voltage rating of test source when immersed in oil could also be calculated and compared with that of air.

2.6 Comparison of the converter in air and oil

As mentioned in section 2.1, the primary idea of creating a first design of the mobile test source was to create a reference for comparing the converter with air and oil as an insulating medium. Hence, the same design procedure as mentioned in section 2.5.2 is applicable when oil is used as an insulating medium. However, the clearances in the test system will reduce in oil. Six insulation zones were identified, characterized by different working voltages, and requirements for insulation coordination in section 2.3.5. The clearances in air for the zones 1,2,4,5 and 6were calculated according to the IEC standard 60071-1. In between the levels of the converter tower, insulators are present. Hence, the clearance between the levels of the converter tower was calculated according to a typical height of the insulators for the corresponding voltage level from a reference guide of a manufacturer [36]. The clearance distances in oil were calculated considering the breakdown strength of 2.5 $\frac{kV}{mm}$. This typical permissible field strength for oil was chosen based on the values provided in [37] for AC voltage. It is to be noted that these values were used since this is the first step in the procedure of designing the test source.

2.6.1 Voltage capability in air vs oil

With the chosen dimensions of trailer, the number of modules in the converter of the test source was estimated in air and oil. The voltage capability of the test source can then be calculated using equation 2.1. These values are tabulated for air and oil in table 2.1.

	Connection type		Air	Oil
Orientation - I	Type I	Number of modules per arm	18	144
		Voltage capability	36 kV	288 kV
	Type II	Number of modules per arm	4	16
		Voltage capability	8 kV	32 kV
	Type III	Number of modules per arm	24	162
		Voltage capability	48 kV	324 kV
Orientation - II	Type II	Number of modules per arm	36	125
		Voltage capability	72 kV	250 kV
	Type III	Number of modules per arm	36	150
		Voltage capability	72 kV	300 kV

Table 2.1: Comparison of voltage capability in air and oil

From table 2.1, it is clearly visible that oil immersed design can accommodate a large number of modules with respect to air. In air, amongst all possible design layouts, 36 submodules could be fitted per arm, hence a maximum voltage capability of 72 kV. However,

in oil, amongst all the types, a maximum of 162 submodules could be fitted in, which results in a maximal voltage capability of 324 kV. Hence with respect to air, the voltage rating of the converter in oil is around 4 times higher.

2.6.2 Utilisation of volume in air and oil

The available volume inside the trailer to accommodate is 45 m^3 with the available dimensions of 9 m x 2 m x2.5 m. But, the actual volume occupied by the converter in air and oil is tabulated in table 2.2 to have the maximum voltage capability of 72 kV and 324 kV respectively.

	Air	Oil
Volume of the converter	34 m^3	42 m^3

Table 2.2: Comparison of volume occupied by the converter in air and oil

As observed in table 2.2, for a test source of 72 kV in air, 34 m^3 is required. This is due to the fact that, with an increase in the number of submodules, the clearance in the converter system also increases. This limits the expansion of the converter. The maximum utilisation of the available volume is obtained with oil wherein the converter volume is 42 m^3 for a test source rated for 324 kV.

2.6.3 Weight of the trailer

An important consideration of oil immersed design is the weight of the trailer. For a converter volume of 42 m^3, the weight of mineral oil (Shell Diala S4 ZX-I) is calculated to be 37590 m^3 (considering the density of oil to be 895 $\frac{kg}{m^3}$ [57]). As mentioned in section 2.5.1, the weight of submodule was estimated to be 20 kg. Considering a total of 324 submodules (number of submodules in both the converter arms), the total weight of the submodules is 6480 kg. Hence a total weight of nearly 44070 kg is constituted by oil and submodules. However, the weight of other components of the converter tower (insulators, corona rings, and busbars) was not included in this calculation. The weight of the existing mobile test system is 43000 kg [32]. Hence, the weight of the trailer is a crucial factor during the design of the converter.

2.7 Electric field simulation of the converter layout in air

While dimensioning the converter in air, clearances in different zones were considered as per the criteria mentioned in section 2.6. To observe whether the electric field distribution of the proposed converter design meets the basic insulation requirement, a FEM based simulation study was conducted.

The electrostatic field simulation was conducted in COMSOL Multiphysics software. A parameterized 3D model of the converter tower was built in COMSOL. The basic building block, submodule was built in Solid works and imported in COMSOL. Care was taken to avoid sharp edges on the submodule enclosure and avoid high electric field. This was done by adding fillet to the vertices of the submodule. Each submodule is enclosed in a metallic box, to provide shielding, protection and shaping of the surrounding electric field. The submodules

are mounted on a rack to form a valve module. The valve section support structure has metallic frames at each end held together by insulating material to which the submodules are fixed as shown in figure 2.33. The metal frames are connected to the enclosure of its closest submodule. Each submodule defines the enclosure potential, which is referenced to its negative submodule capacitor terminal.

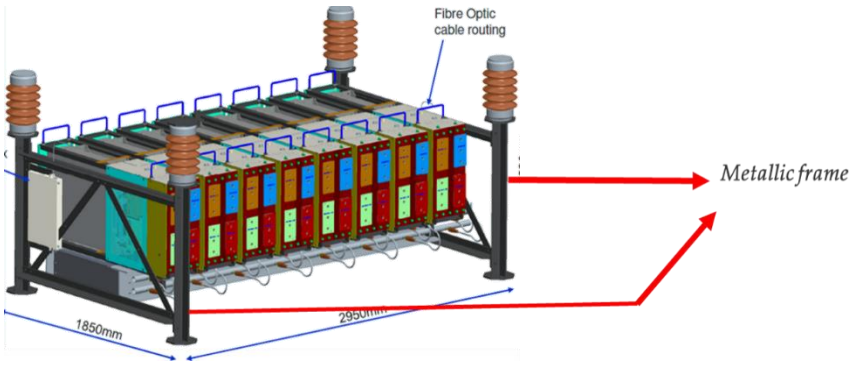

Figure 2.33: Valve section support structure [20]

Amongst the design layout, type II design in orientation II was found to fit in a maximum of 36 submodules. Hence, the electric field analysis is conducted for this design. A 3D representation of this converter design is shown in figure 2.29. In figure 2.29, there are two rows with 3 layers of submodules per converter arm. In each row, 6 submodules are arranged. Similarly, the design to fit it 36 submodules included 6 rows with 2 layers of submodules in each row. There are 3 submodules in each row. A 3D representation of the actual layout (type II – orientation II) proposed by the dimensioning tool is shown in figure 2.34. All the submodules in the first layer are connected in series followed by the submodules in the second layer. As indicated in figure 2.34, the location of rows 1 and 6 in the converter arm is given.

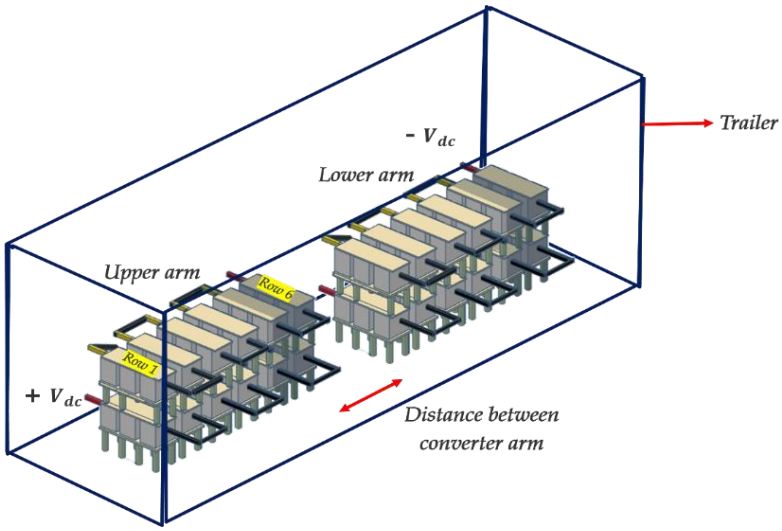

Figure 2.34: Type II (orientation II) – proposed layout

Since the voltage increases linearly across each subsequent submodule in the string, the field distribution will be similar between every row. Hence, a subsection of the converter arm as indicated in figure 2.35 is chosen to show the electric field distribution A simplified 3D model of the submodule arrangement of this section in COMSOL is shown in figure 2.36. The supporting insulators, in between the layers and from the ground were not included in the model.

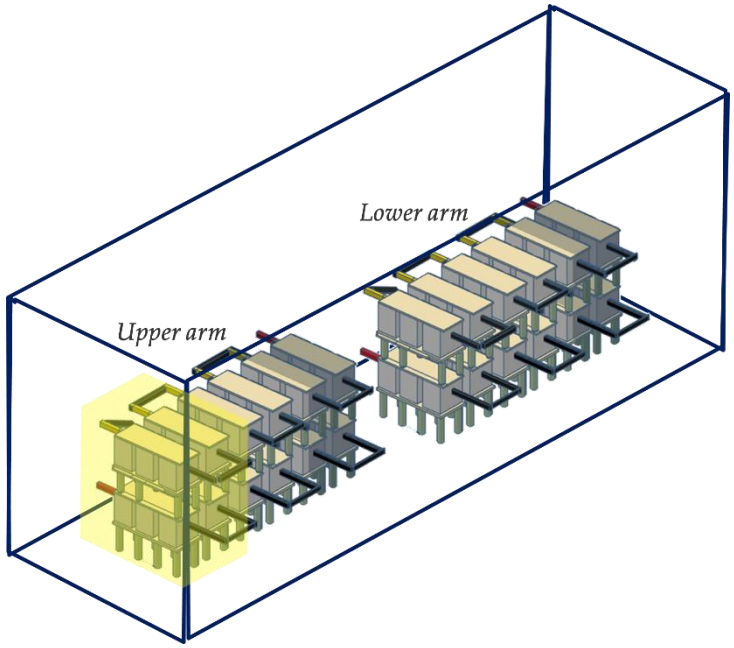

Figure 2.35: Subsection of the converter arm under analysis

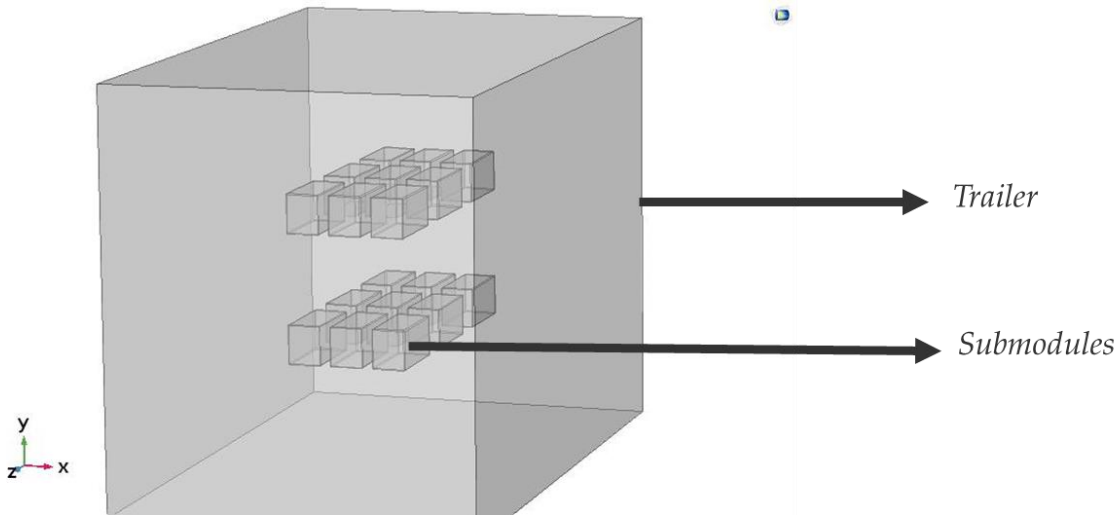

Figure 2.36: Simplified 3D model of the subsection of converter tower in COMSOL

Figure 2.37 shows the potential distribution of the subsection shown in figure 2.36, when all the modules in the upper arm are inserted ($N_u = 36$) and all the modules in lower arm are bypassed ($N_l = 0$).

The output voltage for this state of the converter is -V_{dc} which is -72 kV in this case. A detailed explanation regarding the switching states and the corresponding output voltage levels is given in [9]. The potential of submodules decreases along the row of the arm in the first layer and then reaches the second layer. The ground reference is chosen to be the walls of the trailer.

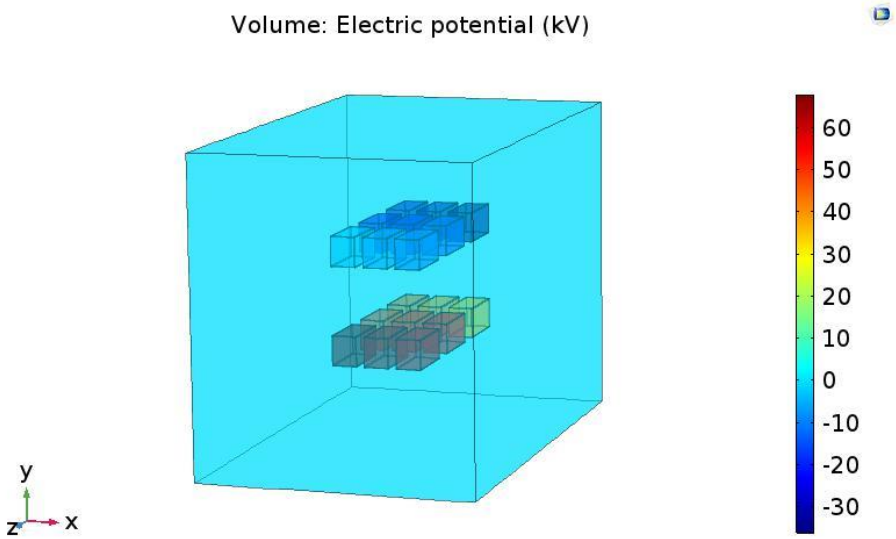

Figure 2.37: Potential distribution of submodules in the subsection of converter arm

The field distribution on the surfaces of the submodule is shown in figure 2.38. It can be seen that there is a relatively higher electric field on the edges and corners of the submodule. A maximum electric field of nearly 3 kV/mm was observed.

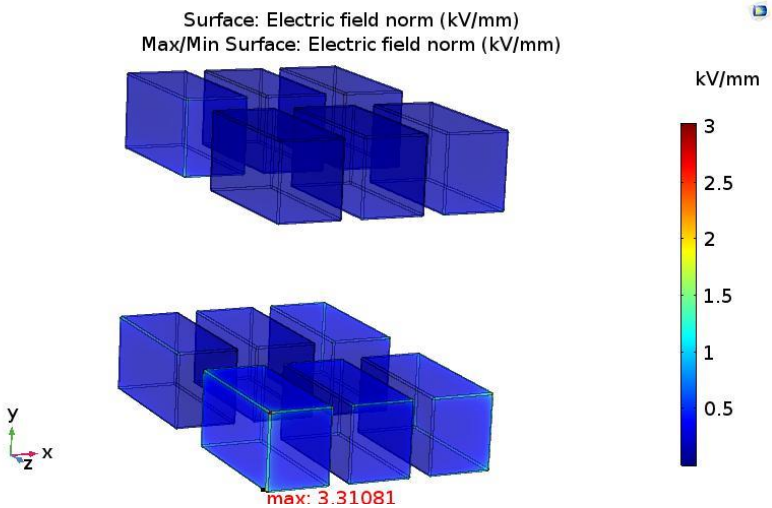

Figure 2.38: Electric field distribution of submodules in the chosen section

At the most serious condition, if the electric-field distribution of metal fittings of valve tower is 2-3kV/mm, this will suggest that the metal fittings of valve tower cannot have the corona discharge dangerous as per [38]. However, in order to improve the electric field distribution, it is a common practice to add shield and corona rings in a converter tower design. The design of these rings differs based on the manufacturer as shown in figure 2.39.

(a) RXHK

(a) Siemens

(c) Alstom/GE

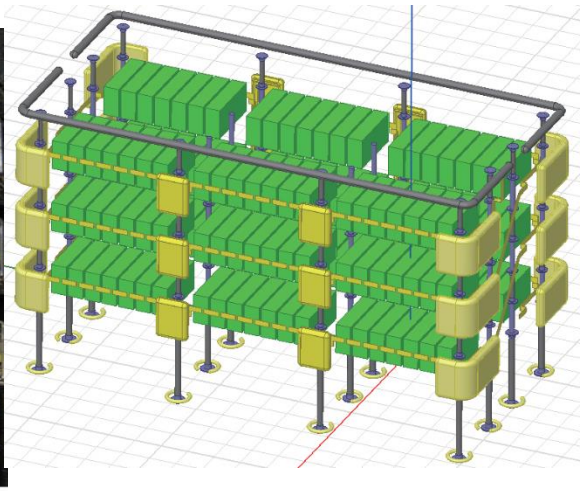

(d) Model of Sunan converter valve

Figure 2.39: Types of shields and corona rings (by different manufacturers)

The influence of the corona ring on the electric field distribution is illustrated below. The corona ring is connected to metallic frames at the ends of the converter tower. Hence, the corona ring is electrically connected to the negative potential of the closest submodule capacitor. Upon addition of a corona ring structure to one side of the frame, the electric field enhancement has reduced at the corners of the adjacent submodule whereas on the other end, the vertex of the submodule without the corona ring indicates a higher electric field of nearly 2.7 $\frac{kV}{mm}$. This can be observed in figure 2.40.

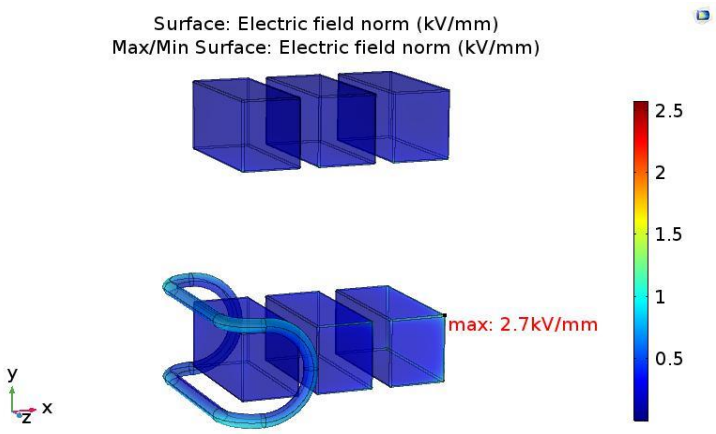

Figure 2.40: Electric field distribution after addition of a corona ring at one end of the tower

Upon addition of corona ring on both the ends, the electric field has reduced to nearly 1.17 $\frac{kV}{mm}$. This is shown in figure 2.41. A similar analysis was conducted for another type of converter layout (type I – orientation I) which is included in appendix A.4.

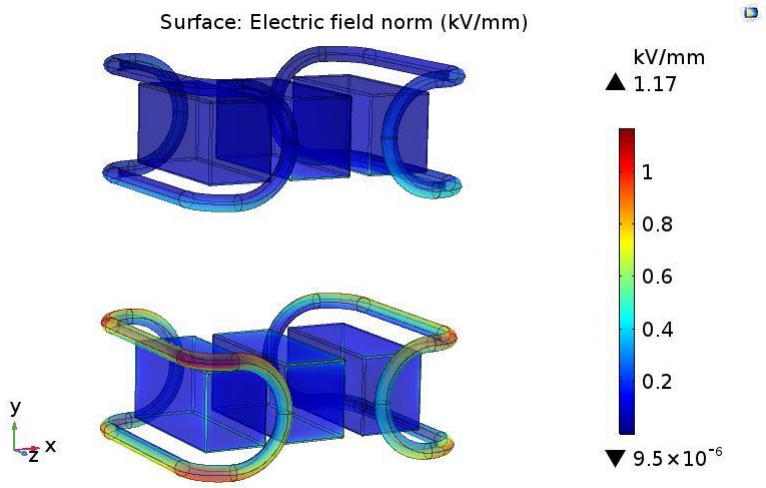

Figure 2.41: After addition of corona ring at both the ends of the tower

This design for corona ring was only for illustrative purpose to validate the clearance distances in air, as calculated by the tool. Upon optimisation of the radius of curvature of the fillet and proper design of the corona ring or shields for the converter tower, electric field values below 1 $\frac{kV}{mm}$ can be achieved with the proposed dimensions of the converter layout.

Meshing strategy - Since the converter structure involved sharp regions, meshing them required careful considerations. The meshing strategy followed to build the entire model is elucidated. The fillets present at the vertices of the submodule and the edges of the submodule were meshed using edge nodes. Triangular meshes were used to mesh the surfaces of the submodule. Tetrahedral mesh elements were used to mesh the external trailer.

2.8 Customisation of the submodule capacitor

The first design proposed for the test source is based on the existing MMC designs by different manufacturers. From the dimensions of the submodule, half the volume of the submodule is occupied by the DC capacitor. In order to effectively optimise the size of the capacitor, a novel idea for the capacitor design could be thought of. One such proposal of a capacitor design is as follows:

The submodule is a primary building block in a traditional MMC. The modular design of MMC is mainly to ensure reliable operation since these converters are used in applications where they are under continuous operation like HVDC applications. On the contrary, the test source will be utilised only for testing purpose which lasts for a (relative) short duration. Hence, the modularity of the converter design could be reduced by combining a group of submodules with a single capacitor housing with multi terminals, consisting of several capacitors intrinsic to the package. In this way, the capacitor could be smaller in size instead of connecting individual capacitors in series. A diagrammatic representation of this idea is

shown in figure 2.42. However, the feasibility of this design and the achievable percent of size reduction by this design should be investigated.

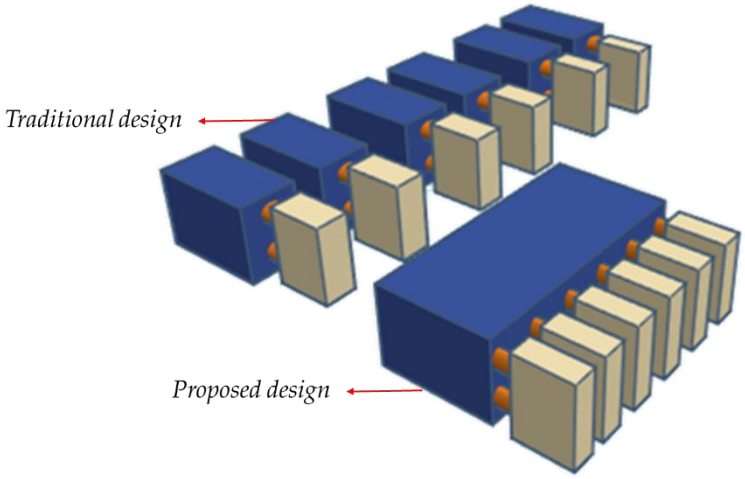

Figure 2.42. Traditional vs. proposed design of submodule capacitor

2.9 Summary

In this chapter, the methodology followed to design the test source was elucidated. Existing physical layouts of converter were reviewed from the literature. With the available dimensions of trailer, an optimisation script was developed in MATLAB to find a suitable design. The script also acts as a tool to provide the maximum voltage capability of test source based on the design layout in both insulating medium (air and oil). It is found that the voltage capability of test source is around 4 times higher in oil when compared to air. A preliminary electric field study was conducted to illustrate that the clearances considered during the dimensioning of test source in air are closer to realistic design.

3

Experimental investigation on the performance of IGBTs immersed in oil

[...] everything we know is only some kind of approximation, because we know that we do not know all the laws as yet. Therefore, things must be learned only to be unlearned again or, more likely, to be corrected. The test of all knowledge is experiment. Experiment is the sole judge of scientific "truth".

Richard Feynman - Lectures on Physics Volume I, Introduction

This chapter explains the experimental investigation conducted on IGBTs when immersed in mineral oil. Based on the results obtained from experimental work, future test procedures and validation methodologies are proposed that need to be performed to realize an oil immersed mobile test source.

3.1 Need for the experimental investigation

As discussed in chapter 1, the MMC based test source is to be used for on-site testing purposes. Failure of such a test system on site will incur a large financial loss. Hence, the availability of the test source is very crucial and must be given utmost importance.

Currently, most of the traditional power electronic converters employed in different industrial applications are built by considering air as the external insulating medium. Hence, every component constituting the converter is tested for its reliability with air as the external environment. The idea of 'oil immersed test source' calls for the need to immerse the components of MMC in oil, similar to the concept of 'oil immersed transformers'.

There is no scientific literature available regarding any application where MMCs are immersed in oil and operated at a high voltage[1]. There are few publications available which discuss the usage of oil immersed thyristor valves for HVDC application. One example was the ± 533 kV Cahora Bassa - Apollo HVDC station, first commissioned in 1975, wherein oil insulated outdoor thyristor valves were used. Figure 3.1 shows an image of oil-filled thyristor valve enclosures [40]. But, this oil-based design is not in operation anymore as the converter station was later upgraded with water-cooled, thyristor valves [39].

[1] The voltage classes used in this report is in accordance with the EN 50160 standard.

Figure. 3.1 Outdoor thyristor valves immersed in oil at Apollo HVDC station [40]

Currently, there is another stream of research, ongoing in the field of pressure tolerant power electronic converters for subsea applications. This concept considers the power electronic converters placed in vessels completely filled with dielectric liquid and able to operate at pressures from 1 bar up to several hundred bars. These converters are operated at medium voltage range. Detailed information regarding this application is provided in [41,42]. However, there is no commercial product available for this liquid-immersed converter as this project is still in the testing phase.

Therefore, from the literature study, it is found that there are no existing power converters available with the oil immersed design in other high voltage applications such as HVDC and FACTS. Hence, experimental investigation on the reliability of components when immersed in oil needs to be conducted. Though off-the-shelf components are tested for reliable operation with air as the external environment, it is extremely important to assess the performance of the devices under oil to ensure long term stable operation.

3.2 *The choice of component for the experimental investigation*

Since the proposed test source is power electronic based, its reliability is critically limited by the power semiconductor devices and their lifetime. Figure 3.2 shows the failure distribution of components in power electronic systems based on a survey [43]. It can be seen from the pie chart that the power semiconductor devices and capacitors are the most fragile components in power electronic systems. There are existing oil-filled high voltage capacitors available in the market which already showcases the feasibility of this design [44].

However, it is not common practice to have power semiconductors immersed in oil. Hence, the primary focus is required on investigating the behaviour of power semiconductor devices in oil.

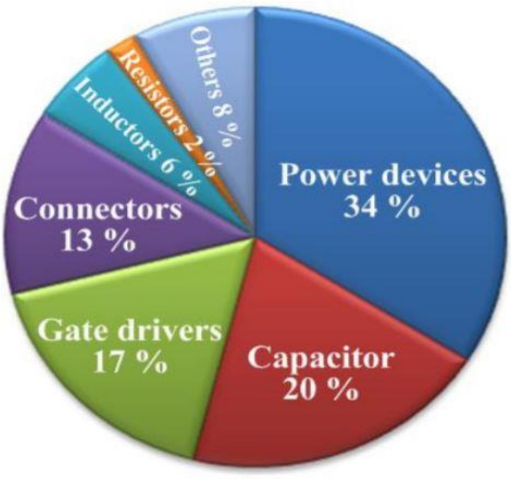

Figure 3.2: Failure distribution of components in power electronic systems [43]

As already mentioned in the previous chapter, amongst various power semiconductors, IGBTs are the most suitable choice for the MMC due to a multitude of reasons [17]. Hence, in this thesis, a compatibility study of IGBTs when immersed in oil is carried out. An IGBT is a switching device which combines the advantages of Metal Oxide Semiconductor Field Effect Transistor (MOSFET) and Bipolar Junction Transistor (BJT) and is represented by the circuit symbol as shown in figure 3.3. The IGBT has three terminals, Collector (C), Gate (G) and Emitter (E).

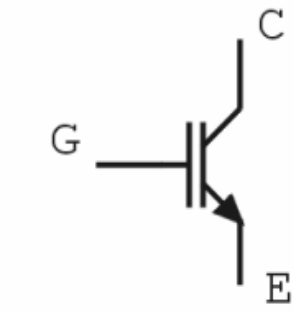

Figure 3.3: Circuit symbol of IGBT [45]

There are different types of packaging technologies for IGBTs based on the power range as shown in figure 3.4. The three main packages are discrete, wire-bonded isolated power modules and press-pack power devices.

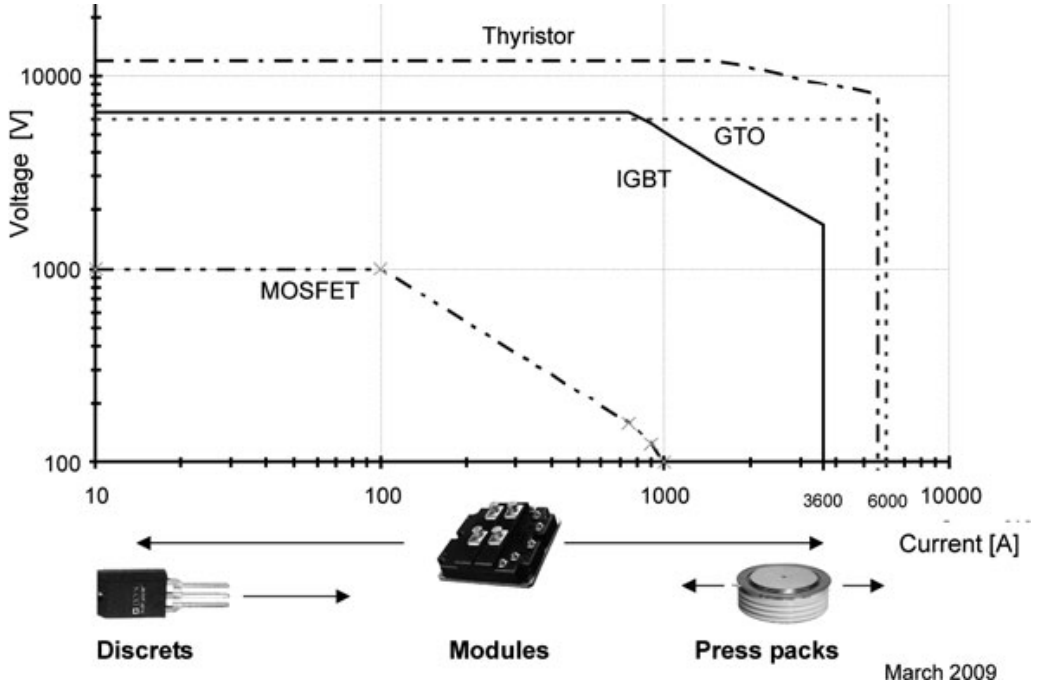

Figure 3.4: Power range of semiconductor devices along with the predominant package type [46]

An overview of these packages is presented as follows.

Discrete IGBTs – These packages are predominantly used for low power applications. Amongst various types of discrete packages, "transistor outline" (TO) package is the most common type. Popular representatives of the TO package family are the TO-220 and the TO-247 package. In these packages, the IGBT chip is soldered directly to a solid copper base, which acts as a mounting surface. Therefore, the package does not have inherent electrical insulation. The contact leads of the IGBT are fixed by a "transfer mould" housing. These leads are connected to the chip by bond wires. IGBTs in TO-247 package are typically available up to 1200 V [47]. The internal design of the IGBT along with an external appearance of the TO-247 package is shown in Figure 3.5.

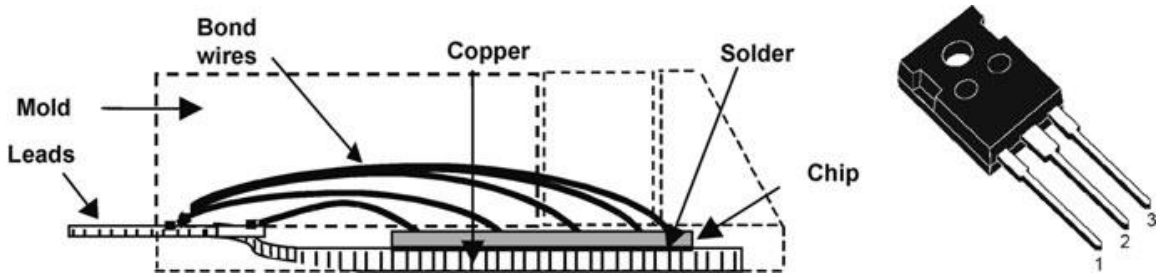

Figure 3.5: Internal design and typical external appearance of TO - 247 IGBT [46]

Press pack IGBTs – Figure 3.6 shows the internal construction of a press pack IGBT [49]. The IGBT chip is mounted between two metal discs in order to homogenize the pressure and to avoid pressure peaks. The connections to the chips are made by physical contact pressure via external clamping between electrodes and strain buffers, as indicated in figure 3.6.

The package is hermetically sealed. Hence, these packages are suitable for oil immersion [48] and there will not be any penetration of oil into the IGBT. However, a complete electrical and the thermal contact will only be established by the application of a defined pressure to the package, which typically ranges from 10–20 N/mm^2. Amongst press pack IGBTs, there are other construction methodologies too, which are discussed in detail in [49]. Press pack IGBTs are available up to a blocking voltage of 6.5 kV.

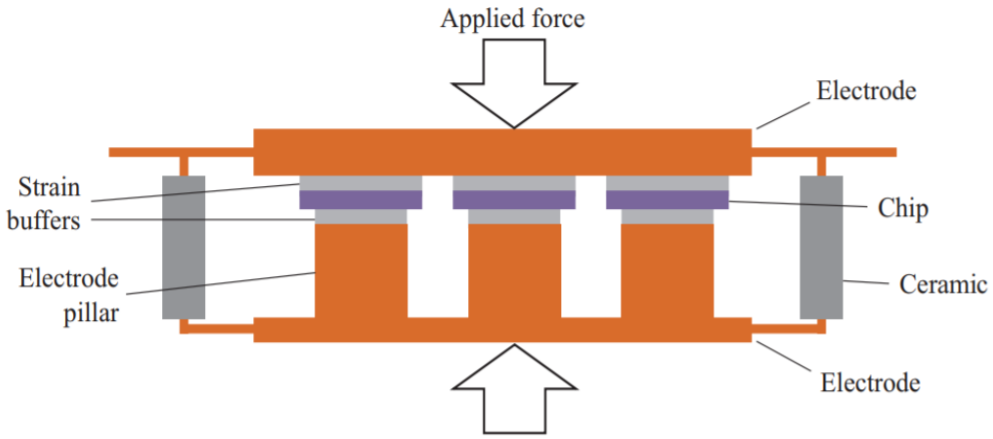

Figure 3.6: Internal construction of a typical press-pack IGBT [49]

Figure 3.7 shows a press-pack IGBT where the upper lid is removed [50]. All the connections to the chip are established through pressure contact alone.

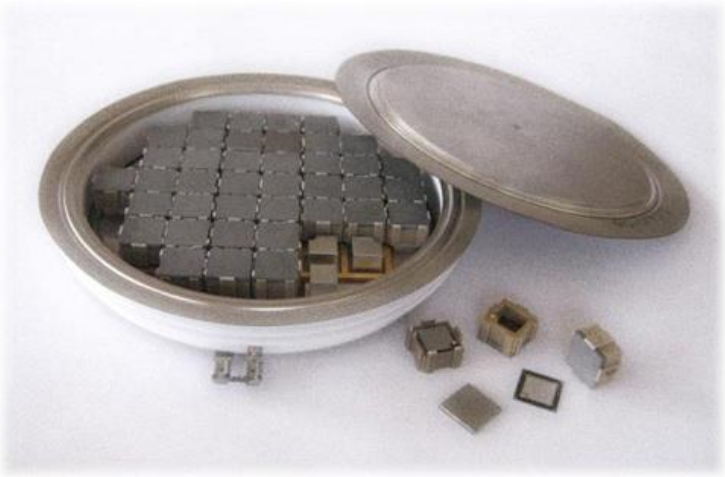

Figure 3.7: 1.6 kA, 4.5 kV conventional press-pack IGBT (the upper lid is opened) [50]

Standard power modules - Power modules are dominating in the current range of more than 10 A, for blocking voltages of 1200 V and above [47]. These modules are wire-bonded and are the most popular choice of package construction for IGBTs used in many high power industrial applications. Figure 3.8 shows the internal layout of a typical IGBT module. Six identical sections are placed in parallel on a baseplate. One section is highlighted in the image. The number of sections in the module depend on the rating of the power module. Each section comprises of two IGBT chips and corresponding antiparallel diodes. The layout displayed in

figure 3.8 is obtained after removing the plastic housing, silicone gel covering all active elements[51]. Unlike the press packs, these modules are not hermetically sealed and the oil can penetrate into the module. The chemical compatibility of the silicone gel with the oil is explained in section 3.6.1. Photographs of IGBT power modules are shown in figure 2.22 and 2.23.

Figure 3.8: Internal view of an IGBT power module without housing, silicone gel, and terminals [51]

Choice of the IGBT package - As shown in figure 3.4, wire-bonded power modules and press-packs are available for higher power ranges, thereby suitable for MMC based HVDC application. Commercially available MMCs by different manufacturers like Siemens, Alstom Grid and Mitsubishi use the wire-bonded power modules [52]. However, the hardware design of press pack IGBT based MMC, implemented in the Nan'ao multi-terminal HVDC project is explained in [21]. This project is the world's first MMC HVDC that is based on press pack devices for submodules. A detailed comparison between press packs and modules is given in [21].

The main drawback of press packs is the complexity in their mechanical assembly. Moreover, the usage of press pack IGBTs is preferable in applications demanding higher current carrying capability. But, as mentioned in section 2.5.1, the current rating of IGBTs used in the test source will be lower when compared to the HVDC application. Hence, the usage of press pack IGBTs is not necessary for this application. In addition, the cost of the press pack devices is higher than the wire-bond modules[49]. Due to the large quantities of IGBTs involved in building the MMC, price is a key consideration. Due to the above considerations, the most suitable package for the test system is chosen to be wire-bonded IGBT modules. Henceforth, the primary focus in this thesis was to analyse and investigate the extent of compatibility of the wire-bonded IGBT power modules when immersed in oil.

Before starting the experimental work, several manufacturers of the wire-bonded IGBT modules were contacted to inquire regarding the availability of any IGBT power modules which are compatible with oil. It was found that there are no such commercial IGBT modules which can be immersed in oil. The reliable operation of off-the-shelf wire-bonded IGBT modules under oil could not be guaranteed by the manufacturers.

A detailed overview of the existing construction procedure of these type of IGBT modules is presented in the following section.

3.3 Typical construction of the IGBT power modules

Figure 3.9 (a) shows a cross-sectional image of an IGBT module which is composed of two sections. It can be seen that the IGBT module consists of two IGBT chips each having an external antiparallel diode chip. A traditional IGBT in principle is not reverse conductive. However, it is mostly used in applications involving inductive load which requires a freewheeling branch to conduct current in reverse direction. Henceforth, IGBTs are always equipped with an antiparallel diode and integrated into a power module always as a separate chip type. A region of the IGBT module in figure 3.9 (a) is zoomed in figure 3.9 (b) to show the internal layer sequence which is required to mount the IGBT chip in the module.

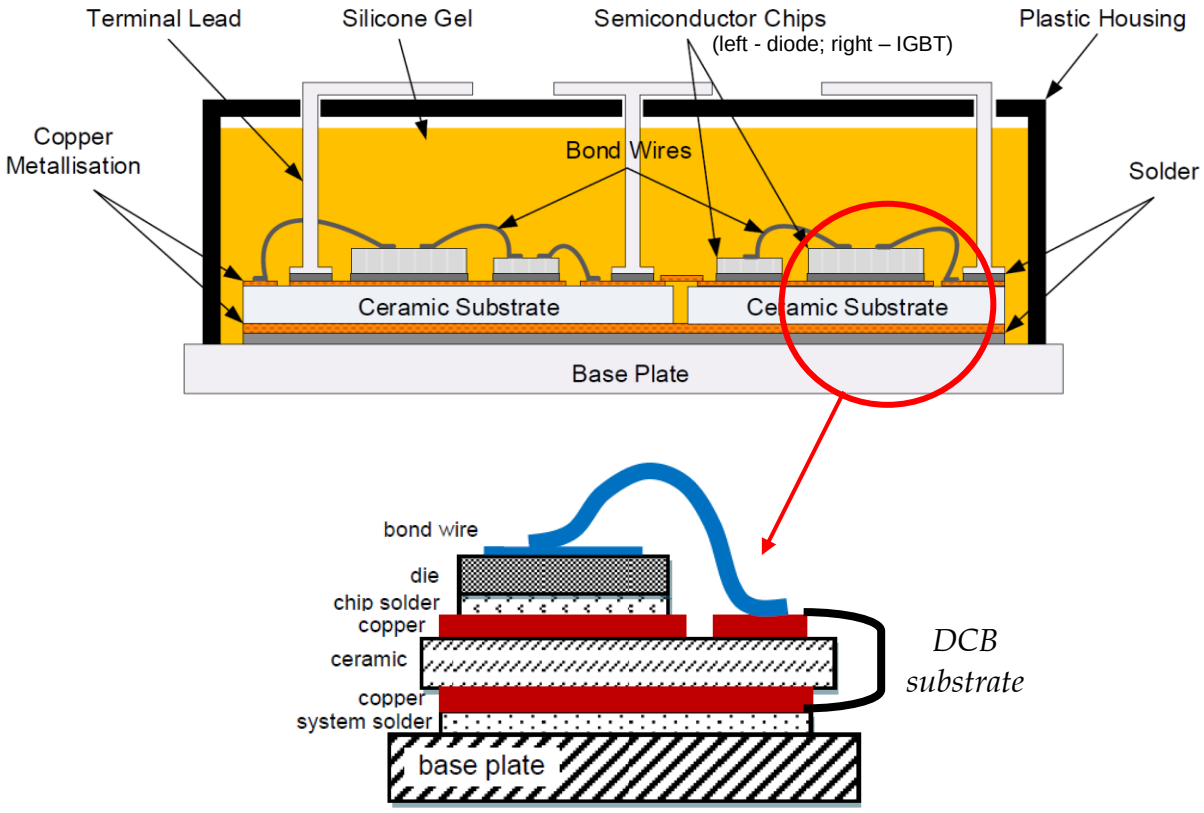

Figure 3.9 (a) Cross sectional image of IGBT power module including the external housing [53]
(b) Layer sequence of IGBT module [54]

The different layers of the internal structure of an IGBT are explained from bottom to up starting from the base plate.

Base plate – The base plate is mostly made of copper and is 3mm to 8mm thick, with a nickel coating [47]. The primary reason for this choice of material is its high thermal conductivity and the mechanical compliance with the bottom copper layer of the DCB substrate [51]. Certain applications like high-power traction systems sometimes use Aluminium Silicone Carbide (AlSiC) baseplates instead of copper. For the experimental investigation, IGBT modules with copper base plates were used in this thesis.

System solder – System solder layer is present to join the substrate to the baseplate. The soldering process should be carefully executed in order to avoid air-pockets or cavities in the solder layer. Presence of cavities increases the thermal resistance, which eventually leads to premature ageing of the IGBT module.

Substrate - Direct Copper Bonded (DCB) substrates, are the most widely used substrate materials in power electronics. DCB substrate comprises a ceramic tile bonded to the copper layers on the top and bottom by means of a high-temperature melting and diffusion process. Figure 3.10 shows the construction of the DCB substrate. The main ceramics used in DCB substrates are aluminium oxide (Al_2O_3) or aluminium nitride (AlN) [47]. Al_2O_3 is commonly used in most of the IGBT modules. AlN substrates are especially used in IGBT modules to achieve higher power density because of its higher thermal conductivity[2] than that of Al_2O_3, The purpose of ceramic layer is to electrically isolate the chips from the base plate. In addition, DCB substrate has to conduct the current via the copper tracks and must also provide a path for the heat from the chip to the base plate. The IGBT modules with a ceramic layer of Al_2O_3 is used in this thesis.

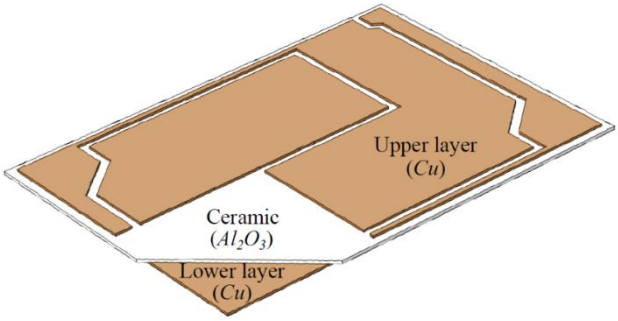

Figure 3.10 Construction of DCB substrate [51]

Chip solder - The metallic backside of the semiconductor chip is connected electrically and thermally to the DCB substrate in a vacuum soldering process [47]. As with system soldering, air pockets should be avoided during chip soldering process too.

[2] The capability of a medium (solid object, liquid or gas) to transport thermal energy in the form of heat is described as thermal conductivity [47].

Die - This is the region where the silicon-based main IGBT chip is present.

Bond wire - Bond wires are used to make interconnections from the chip to the external contact area and the diode chip. The most commonly used assembling technology is ultrasonically wedge (US) bonding. Al-based bond wires are used in most of the IGBT modules [51]. In some cases, small amounts of other elements are added to the wire for corrosion control and to increase wire hardness.

Silicone gel – After the construction of the layers, the entire structure is covered with silicone gel as shown in figure 3.9 (b). Silicone gel acts as a protection layer against environmental effects and as a secondary cooling path. As observed from 3.9 (a), the silicone gel does not completely 'fill' the housing and there is a general empty space at the top.

Hard encapsulation/ Plastic housing - Finally, the entire module is encapsulated in a hard plastic cover which made of one of five different materials. These are polyphenylene sulfide (PPS), polybutylene terephthalate (PBT), polyphthalamide (PPA), polyamide (PA) and polyethylene terephthalate (PET). The latter three are often used for high-voltage modules. The materials are chosen based on specific application requirements. PBT was used as encapsulation material in the IGBT modules used in this thesis.

The material content datasheet of the IGBT module used for the experimentation purpose is given in [55]. Before conducting the main experimental work, a preliminary study was conducted in the laboratory to understand the susceptibility of the oil immersed IGBTs when exposed to a higher background electric field. This study is explained in the upcoming section.

3.4 Influence of external electric field on the behaviour of oil immersed IGBTs

3.4.1 Background

As described in section 2.1, the physical size of all components in MMC will remain the same despite the insulating medium. The primary reduction in the size of converter is due to the reduction in clearances in oil. The clearance distance is inversely proportional to the electric field strength of insulating medium. For the given voltage, when submodules are tightly packed in oil compared to air, the IGBTs in submodules are exposed to a higher electric field in the surrounding environment. Hence, the susceptibility of IGBTs towards external electric field needs to be studied. However, it is to be noted that the electric field inside IGBT chip is very high when compared to the external field. So, the effect of the external electric field on the operation of the chip is relatively small. Hence a preliminary test was conducted to confirm the above-mentioned hypothesis. Since this test was not conducted for validation purposes, multiple samples of IGBTs were not tested and so the results were not statistically validated.

3.4.2 Experimental test setup

A basic schematic of the test setup is shown in figure 3.11. An IGBT was operated continuously at a low switching frequency (5 Hz). It was driven by a gate driver which in turn was controlled by a microcontroller. The IGBT was immersed in oil and was exposed to a high electric field by means of parallel field plates as indicated in figure 3.11. Upon application of voltage, across the plates, an electrical field was created between them. The IGBT also experiences this external electric field while in operation. The switching waveforms of the IGBT were observed to check for any discrepancy in the operation of the IGBT after application of the external field. The components used in the test setup is explained in detail below.

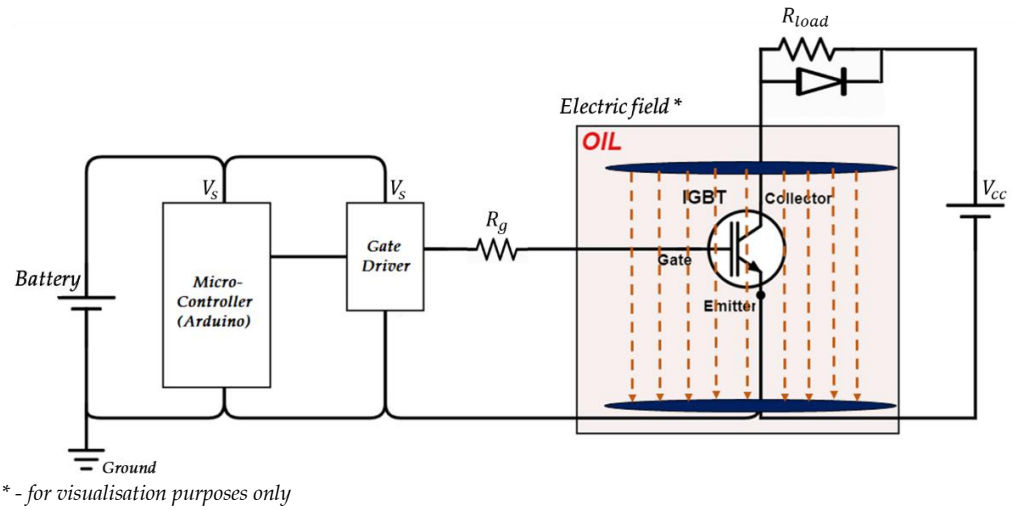

Figure 3.11: Basic schematic of the test setup

IGBT - This test was conducted using a 1200 V discrete IGBT with TO-247 package (IHW20N120R3) [56]. The construction and the package of the discrete IGBTs were described in section 3.2. Though the primary focus is on IGBT modules, this study was conducted with discrete IGBTs. The reason is that these packages are smaller than the IGBT modules. Hence, these packages are more vulnerable to the background field when compared to modules. If the operation of discrete IGBTs is not influenced by the external field, then its influence on the IGBT modules is an unlikely event.

Collector-Emitter Voltage supply - Since this test is to study the operation of the IGBTs at high electric field, there is a possibility of a breakdown across the collector-emitter terminals of the IGBT during the test. This can damage the collector-emitter voltage supply (V_{cc}). Hence a cheaper and isolated power supply was designed for the testing purpose. A block diagram of the supply is as shown in figure 3.12.

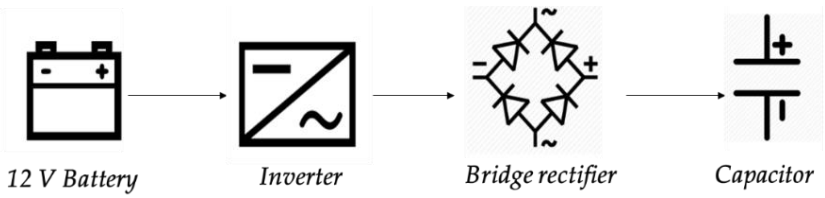

Figure 3.12: Block diagram of the collector emitter voltage supply (V_{cc})

A 12 V battery was used as an isolated source. An inverter was used to convert 12 V DC to 230 V AC followed by a diode bridge rectifier for rectification of the AC to pulsating DC voltage. Finally, a smoothing capacitor was added to obtain a DC voltage.

Load - A resistive load of 0.6 kΩ was used to limit the collector current. Since the resistive load was wire wound, there was relatively large parasitic inductance which created inductive spiking. Henceforth, to overcome it, an antiparallel diode was added to the load resistance. An image of the Collector-Emitter Voltage Supply along with the resistive load is shown in figure 3.13. The components of the supply are marked in the image.

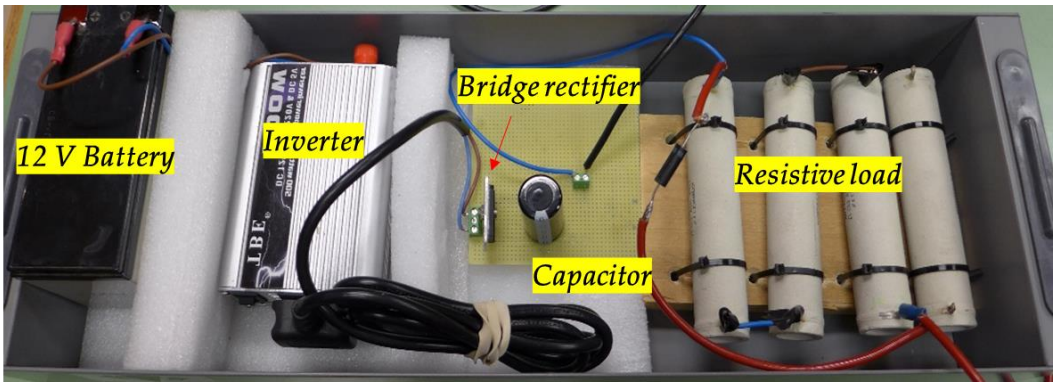

Figure 3.13: Collector Emitter Voltage Supply and load

Gate Emitter Voltage supply – An image of the gate driver circuit is shown in figure 3.14. L298N motor driver module was used as a gate driver to provide a voltage across the gate-emitter terminals of IGBT. This module was controlled using a microcontroller (Arduino UNO). The supply voltage to Arduino and the motor driver module was provided by 9V batteries as shown in the image.

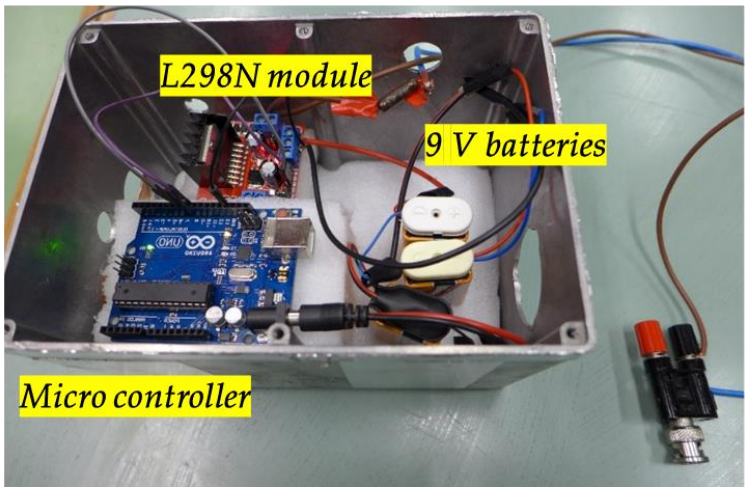

Figure 3.14: An image of the gate driver circuit

Shell Diala S4 ZX-I was the mineral oil used for all the experimental work in this thesis [57]. This oil is typically used in power transformers as an insulating medium, thereby possess good insulation capabilities.

As described in section 3.2, the base of the TO-247 package is copper and is therefore connected to collector potential. Though there is a background electric field *(E)* existing between top and bottom field plates, the base plate of the IGBT also acts as a field plate. During switching operation, the potential of IGBT base plate varies according to collector potential from 0 to V_{CC}. Therefore, the effective electric field strength *(E')* was limited with respect to IGBT base plate instead of field plate at the bottom. This concept is illustrated in figure 3.15. The distance between the upper and lower field plates and distance between the upper field plate and IGBT base plate are given by d and d' respectively. Since d is greater than d', the effective electric field strength *(E')* is greater than background field strength *(E)*. Please note that the actual field lines between parallel field plates are not shown in the image.

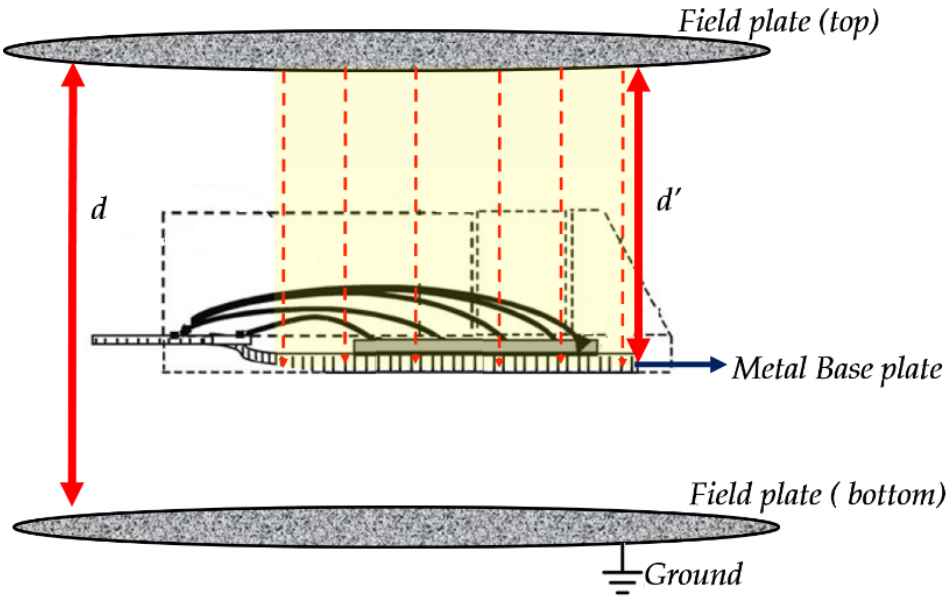

Figure 3.15: Representation of the effective field strength
(with horizontal orientation of the IGBT)

The test was repeated for two orientations of the IGBT with respect to the field plates, both vertical and horizontal. Figure 3.16 and 3.17 show the mounting arrangement of the IGBT in both the orientations under oil. In horizontal orientation, the IGBT was mounted in such a way that the metal base plate is facing the bottom field plate as shown in figure 3.15. In both orientations, the effective field strength is considered with respect to the base plate of IGBT. The base plate is visible in figure 3.17 where the IGBT is vertically mounted.

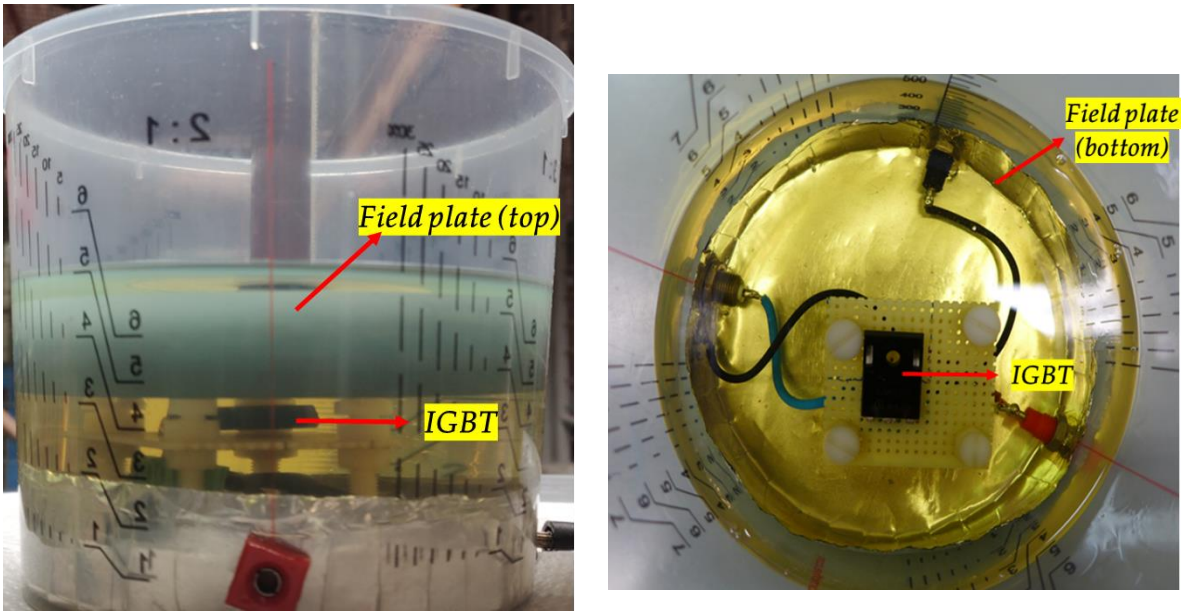

(a): Front view (b): Top view

Figure 3.16: Horizontal orientation of the IGBT

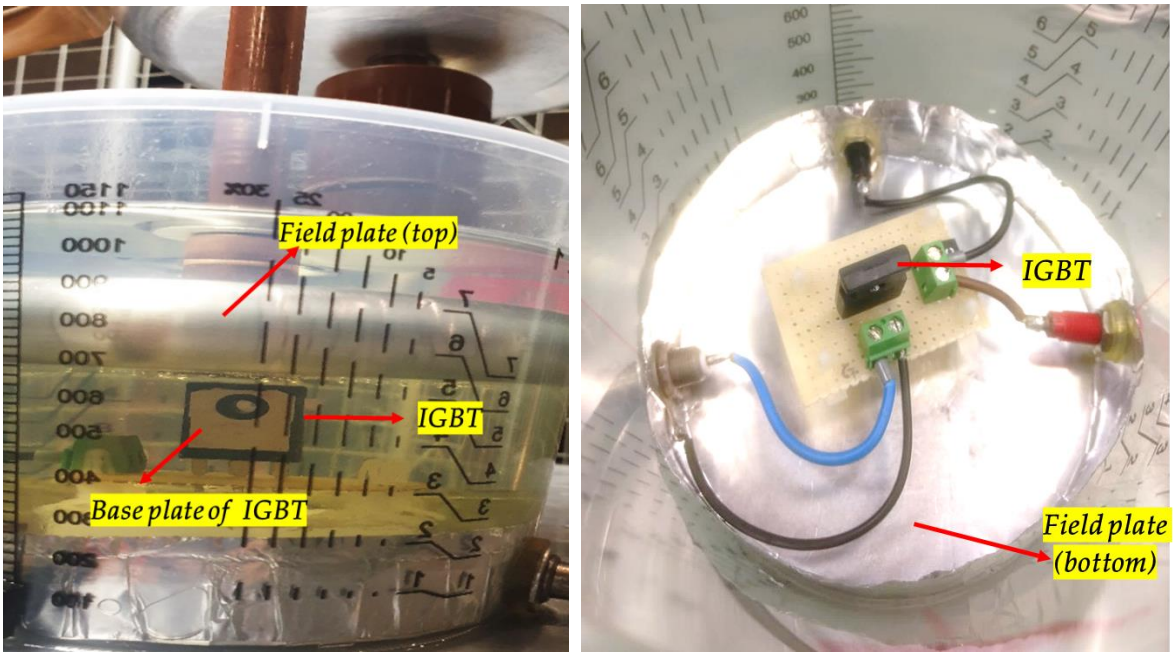

(a): Front view (b): Top view

Figure 3.17: Vertical orientation of the IGBT

It can also be noted that in figure 3.17 (b), the bottom field plate is made up of an aluminium foil and is bent in all the sides of the container. This was done to make the electric field lines more uniform in the region where the IGBT is placed. The entire test setup is shown in figure 3.18. The voltage across field plates was applied using a cascade transformer as shown in the image to create the background electric field.

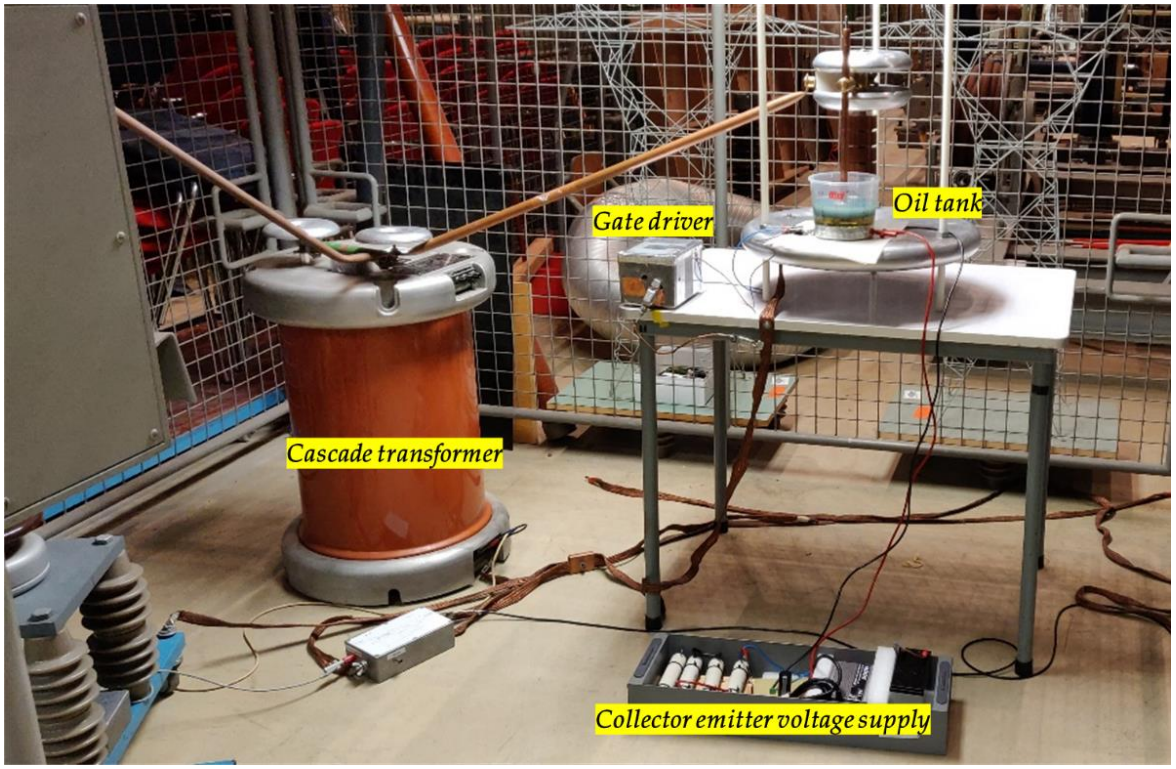

Figure 3.18: The complete test up

3.4.3 Results

An effective electric field strength of up to 6 $\frac{kV}{mm}$ was applied across the IGBT under test in oil. The term effective electric field strength is illustrated in figure 3.15. The distance between the upper field plate and the IGBT base plate (d) was set to be 2.5 mm during the test. Hence, a voltage of 15 kV was applied to the field plate to achieve the effective field strength *(E')* of 6 $\frac{kV}{mm}$ .The switching waveforms were compared before and after the application of the external electric field across the IGBT. There was no discrepancy observed in the switching waveforms of the IGBT in both the orientations. It can be observed that the IGBT package has sharp edges which lead to field enhancement in those regions. So, going to higher voltages can create a breakdown across the IGBT which in turn could damage the collector-emitter voltage supply. In addition, according to [37], the permissible field strength in oil under AC voltage is given as 6 $\frac{kV}{mm}$. So, the effective field strength was not further increased above 6 $\frac{kV}{mm}$. From this experimental study, it can be understood that the IGBT could withstand relatively higher background electric fields than in air. Hence, the IGBTs could be densely packed in oil, but with careful consideration of field enhancement due to the package. However, as mentioned earlier in this section, this study was not statistically validated by testing with multiple samples. Proper validation will be required in the future by repeating the same test procedure for multiple samples.

3.5 Long-term tests

Though there is ongoing research in the field of pressure tolerant power electronics as described in section 3.1, most of the available literature gives extensive information on short-term tests conducted to evaluate the performance of IGBT modules immersed in oil [58] or focusses on pressure tolerance of the semiconductors under oil [42]. Hence, the short-term performance of IGBTs is not investigated in this thesis. Instead, the long-term operation of IGBT modules is analysed by conducting preliminary experiments. From the results obtained in these experiments, the road map of tests required to validate the stable operation of IGBT modules over a long time is proposed in section 3.8. The tests conducted to investigate the long-term behaviour of the IGBT modules in oil is explained in the upcoming sections 3.6 and 3.7.

3.6 Voltage endurance test

3.6.1 Background

The primary aim of the experimental investigation is to check the extent of compatibility of off-the-shelf IGBT modules with the mineral oil. As shown in figure 3.9 (a), an IGBT module is built up of several heterogeneous materials, such as silicon chip, aluminium wires, DCB substrate, copper baseplate, solder, silicone gel and is enclosed in a plastic housing. As mentioned earlier, these modules are not hermetically sealed. So, when immersed in oil, it can penetrate into the IGBT module. If oil enters the plastic housing of the IGBT module, the first point of contact for the oil is the silicone gel. The silicone gel will shield the areas of high electric fields in the IGBT chip structure from impurities in the oil. But, according to the results obtained in [59], the silicone gel was found to be decomposing into the mineral oil over a period of operation (120 days). Therefore, there are possibilities of oil getting in contact with the chip surface of the IGBT. In reality, every IGBT chip has a finite size with a well-defined active area surrounded by an **edge termination** as indicated in figure 3.19.

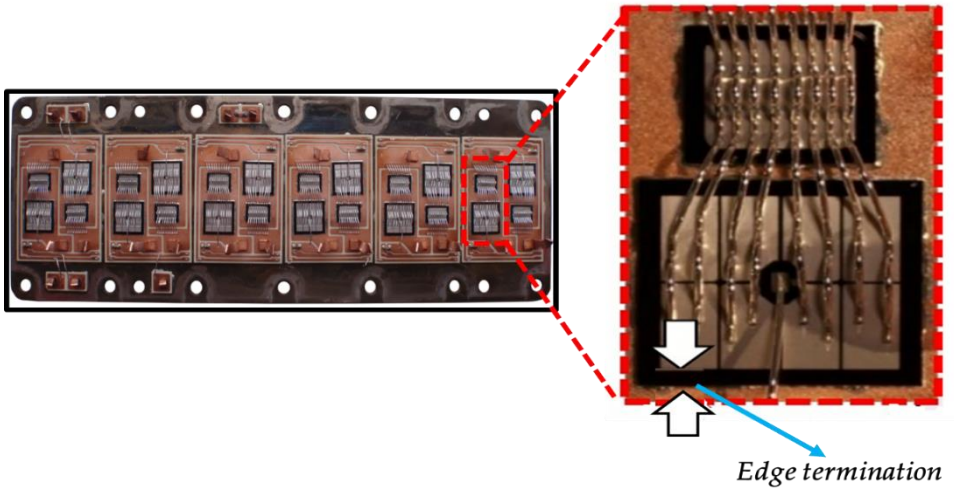

Figure 3.19: Representation of the edge termination in an IGBT chip [51]

Edge termination is applied to lower electric field strength at the edges of IGBT chip. Thus, the voltage blocking capability of IGBT structure is limited by the design and performance of edge termination. There are different types of edge termination structures which are explained in detail in [46]. In addition to edge terminations, it is also necessary to treat the chip surface to obtain a well-defined surface and to terminate the free bonds of the silicon atoms present at the surface of the chip. This treatment is called **surface passivation** and involves cleaning processes and subsequent deposition of an insulating material [46]. Hence, once the edge structure is processed during the manufacturing process, the area is sealed off with a passivation layer. Polyimide, silicon dioxide (SiO_2) are often used as a passivation layer. The compatibility of the oil with the passivation layer is also unknown. As described above, if the oil reaches IGBT chip surface, then the purity of oil becomes extremely important. The presence of any impurities in oil or mobile charge close to the semiconductor surface can lead to alterations in electric fields at the edges during device operation producing changes in breakdown voltage.

Therefore, in order to verify the stable operation of IGBT chips under oil, long term voltage endurance test was carried out on the IGBT modules when immersed in oil. The details and specifications regarding the test are explained in the next section.

After completion of endurance test, the following aspects are to be analysed inside IGBT module.

1) Analysis of the silicone gel to assess its condition and to check if there are any signs of degradation.
2) Microscopic analysis of the edge termination area to examine if there is any sign of foreign particles. An example of the presence of impurities in the edge termination region is shown below in figure 3.20

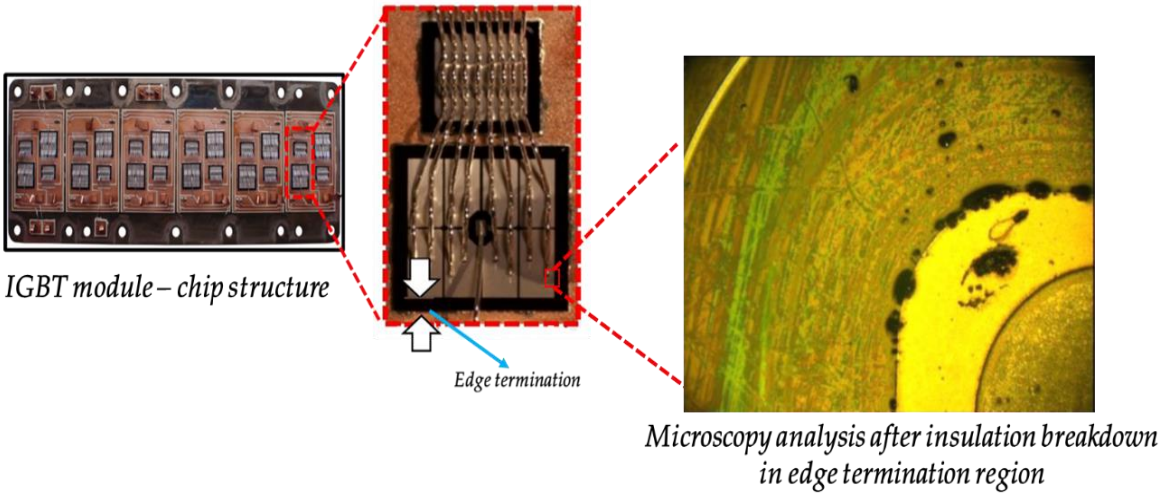

Figure 3.20: Microscopic analysis of edge termination region [60]

3.6.2 Test specifications

Discrete TO-247 IGBTs (IKW40N120H3FKSA1) [61] and IGBT power modules (FF50R12RT4) [62] which are commercially available were chosen for the test. Discrete IGBTs are relatively more tightly packed and the rate of penetration of oil should be lower than that of the IGBT module. Though the primary focus was on the IGBT modules, the discrete packages were also tested immersed in oil to check the extent of oil penetration inside the package. Both the discrete IGBTs and the modules were rated for 1200 V. The discrete package had a single IGBT as shown in figure 3.21 whereas the IGBT module had two IGBTs in series as shown in figure 3.22. However, for the test, only the upper IGBT in the module was used.

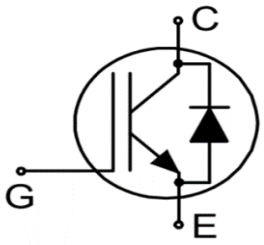

Figure 3.21: Symbolic representation of discrete IGBT [61]

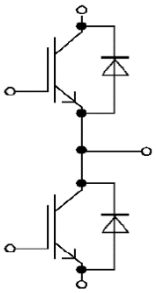

Figure 3.22: Symbolic representation of IGBT module [62]

During the test, IGBTs were operated in the forward blocking mode. It was turned off, i.e. 0 V was applied at the gate with respect to the emitter terminal. A blocking voltage of 960 V was applied across the collector-emitter terminals of the IGBT which is 80% of the device rated voltage similar to that of the High Temperature Reverse Bias (HTRB[3]) test. Though the IGBT is turned off, there is a leakage current I_{CES} between the collector and emitter. The ambient temperature during the test was maintained at 60° C. The primary reason for an elevated temperature was to increase the leakage current. The test was planned for a period of 1000 hours of operation. A table with a summary of the test conditions is shown in table 3.1.

Parameters	*Values*
Collector-Emitter Voltage (V_{CE})	*960 V (80% of rated* V_{CE})
Gate Emitter Voltage (V_{GE})	*0 V*
Duration of the test	*~ 1000 hours*
Failure criteria	*Collector emitter leakage current* (I_{CES}) > 2· (I_{CES_ref})
Ambient temperature	*60° C*

Table 3.1: Main test conditions for voltage endurance test

This test can determine weakness in the field depletion structures at the device edges and in the passivation layer. Due to the increased electric field strength, in certain areas of the chip movable ions can accumulate and create a surface charge.

[3] HTRB is a reliability test which focuses on the edge structure and the passivation layers of IGBT.

The source of the movable ions can be any impurities from the oil. The failure criteria for this test is the increase in leakage current by two times the initial reference value as indicated in table 3.1.

3.6.3 Electrical characterization of IGBTs

Electrical characterization of the IGBTs was conducted before starting the test for having a reference. It was repeated after completing the test to compare the measurements obtained in the pre-characterization and check if there was any change in the parameters. Generally, there is equipment available for characterization of the semiconductor devices such as a Power Device Analyzer / Curve Tracer [63]. Due to the unavailability of such equipment, separate test setups were built for every characterization during the thesis. The characterization curves of the upper IGBT in IGBT modules before and after the endurance test are compared in section 3.6.5. The procedure followed during characterization is given below.

Leakage current characterization - The definition of leakage current is given in the previous section. During characterization, the gate-emitter terminals of IGBT were short-circuited, thereby operating it in blocking mode. The IGBT was then tested up to 1000 V in steps of 200 V and the corresponding leakage current was measured. In case of modules, the upper and lower IGBT were tested separately. The schematic for the characterization of leakage current is shown in figure 3.23. The terminals 1, 2 and 3 of the IGBT represent gate, collector and emitter terminals respectively. The characterization was performed at ambient temperature.

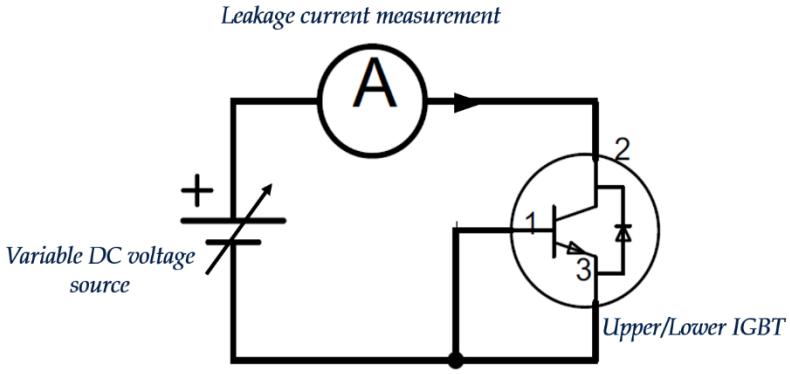

Figure 3.23: Schematic for characterization of leakage current [58]

Gate threshold voltage characterization – Gate threshold voltage (V_{GEth}) is the minimum voltage across gate and emitter terminals at which collector current (I_c) begins to flow. An adjustable low voltage DC-source is connected to provide the same voltage potential across gate-emitter and collector-emitter terminals of the IGBT. The voltage is increased in steps until a value of collector current (I_c) is reached as mentioned in the datasheet. I_c is given as 1 mA and 1.60 mA for discrete packages and modules respectively. The voltage on the DC-source is then measured using a voltmeter. The schematic of V_{GEth} characterization is shown in figure 3.24. Similar to the previous case, the upper and lower IGBTs were tested separately in IGBT module.

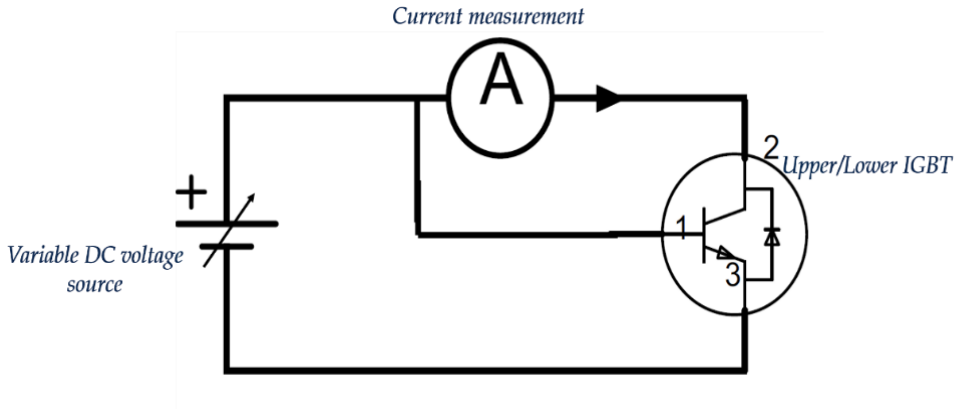

Figure 3.24: Schematic for V_{GEth} characetrization [58]

3.6.4 Experimental test setup

The schematic of the voltage endurance test is shown in figure 3.25. This test was conducted in a climate chamber wherein the ambient temperature was maintained at 60° C (within a tolerance of ±2°C). The IGBTs used for the test are labelled from Q1 to Qn. A programmable DC source (Spellman) was used to apply the blocking voltage to the IGBT. A dedicated LabVIEW software program in combination with a data acquisition system (DAQ) was designed to provide an automated control setup and reliable long-term data acquisition of the leakage current and temperature values. The 34972A LXI Data Acquisition / Data Logger Switch Unit was used for this purpose [64]. S1 to S6 are the switches in the DAQ switch unit. The Keithley 6485 Pico ammeter was used for the measurement of the leakage current [65].

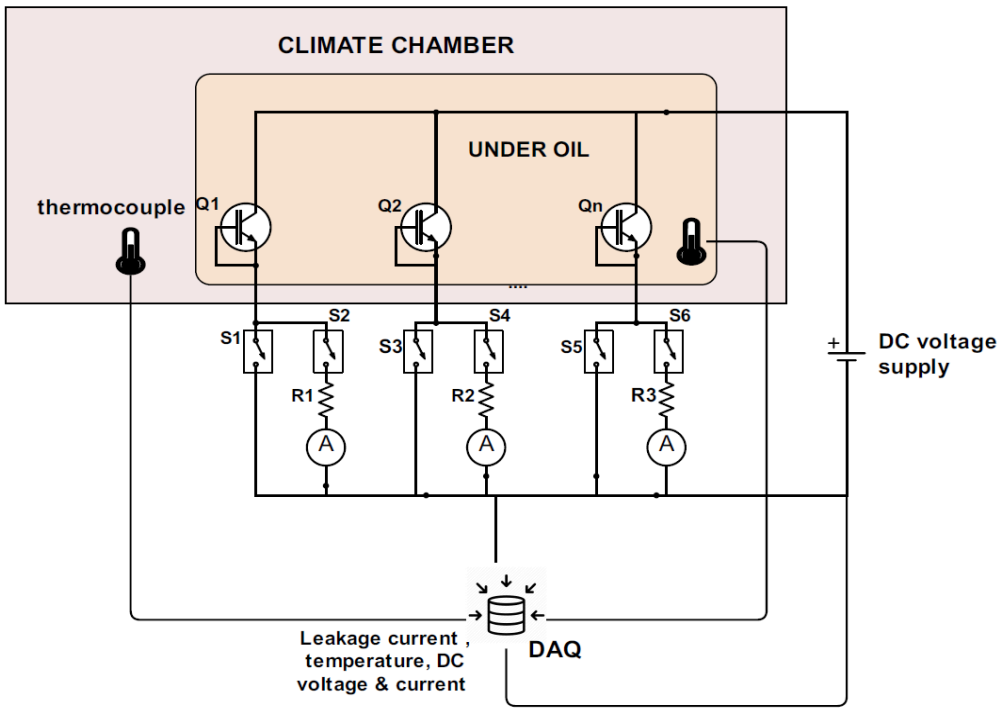

Figure 3.25: Schematic of the voltage endurance test

There are two modes of operation, normal mode and measurement mode. For example, in the case of Q1, when the IGBT is in a normal blocked state, the switch S1 is closed and S2 remains open. In case of leakage current measurement of Q1, switch S2 is closed followed by the opening of S1. The current measurement unit is connected to switch S2. A resistor R1 of large resistance (in MΩ) was connected in series with the Pico ammeter for limiting the current in case of any breakdown of the IGBT. After measurement of Q1 is completed, switch S1 was closed followed by the opening of S2. This procedure continues for all the other switches in a repeating sequence. This sequence was developed due to the availability of only one current measurement equipment. The temperature of oil tank and ambient temperature inside the chamber was monitored using thermocouples. The IGBT modules and discrete packed were placed into the oil tank as shown in figure 3.26 and kept inside the chamber.

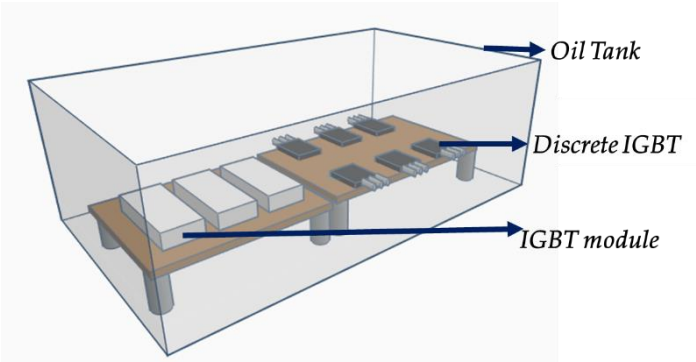

Figure 3.26: Mounting of the IGBTs inside the oil tank

The IGBTs were mounted on metal plates after application of thermal paste onto the base plate. The need for the application of the thermal interface material is explained as follows. When an IGBT module is mounted on a metal surface such as heat sink, the interface is non-uniform due to the presence of voids in microscopic level as shown in figure 3.27. These voids are usually filled with air which has relatively poor thermal conductivity ($\lambda_{air} \approx 0.03 \frac{W}{mK}$) [66]. Hence the main purpose of thermal interface material (TIM) is to displace this air with a material with higher thermal conductivity ($\lambda_{paste} \approx 0.5$ - $6 \frac{W}{mK}$). Different types of TIMs like thermal paste (or grease), soft-PGS (Pyrolytic Graphite Sheet) are used based on the application. In this thesis, a general-purpose thermal paste [67] was used to mount the modules on the metal plate during the experiments.

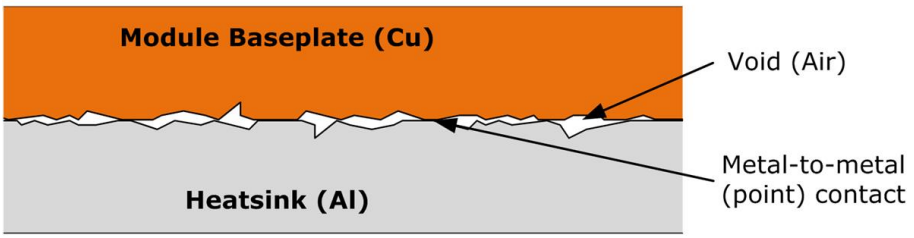

Figure 3.27: Microscopic cross-sectional view of baseplate-heatsink interface without TIM [66]

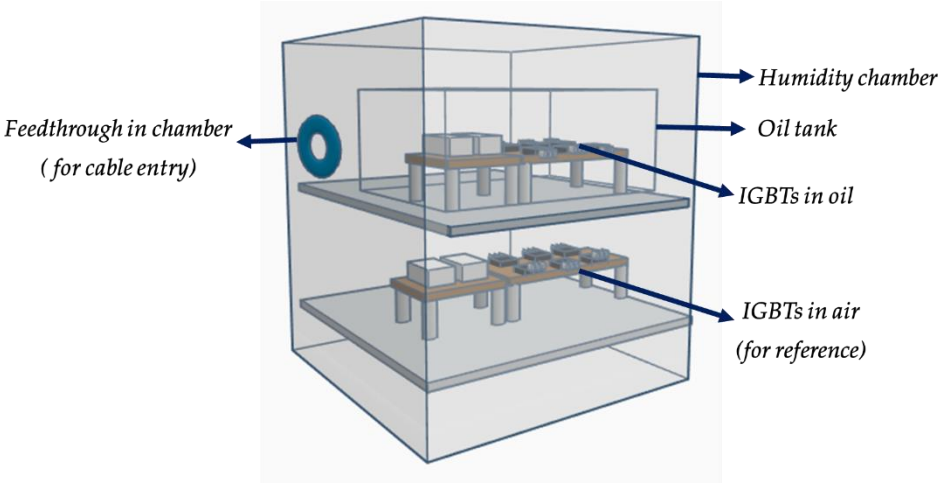

Figure 3.28: Complete arrangement of the test setup

A 3D representation of the complete test arrangement is shown in figure 3.28. The oil tank was placed in upper rack inside the climate chamber. There were three IGBT modules and five discrete IGBTs immersed in oil. As a reference, a similar IGBT fixture was made in air and mounted in the lower rack of the chamber wherein the same test conditions were implied. Two IGBT modules and six discrete IGBTs were tested in air. Images of the test setup and the devices under test (DUT) are shown in figure 3.29 and 3.30. To ensure the safety during the test operation, a safety interlock was integrated which stops the voltage supply to the IGBTs if the chamber's door was opened.

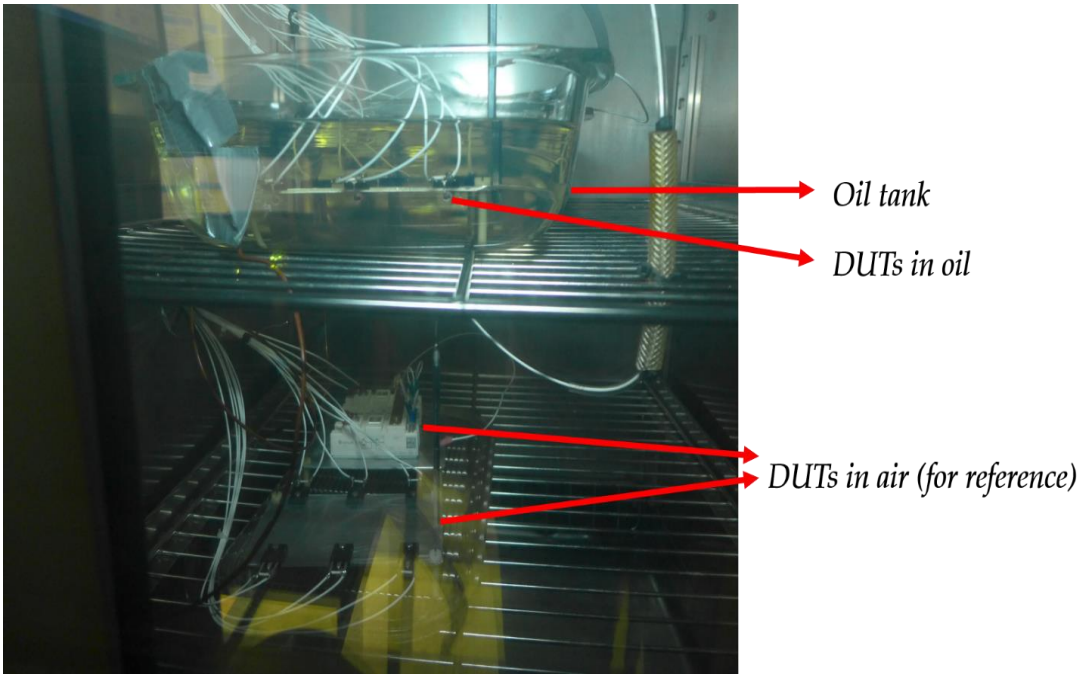

Figure 3.29: Arrangement of the IGBTS inside the humidity chamber

Figure 3.30: Entire test setup

3.6.5 Results

The voltage endurance test was successfully completed for nearly 960 hours with the above-mentioned test conditions. A 1000 hour of runtime was not possible due to practical reasons.

Leakage current measurements - A plot of the leakage current of an IGBT module immersed in oil and the corresponding temperature of the oil bath is shown in figure 3.31. The leakage current (I_{CES}) of the IGBT is dependent mainly on two parameters, blocking voltage and the ambient temperature of operation. Since both these parameters are usually maintained constant during the endurance test, it is expected to have a constant value of leakage current before any failure occurs. However, it can be seen that values of leakage current in figure 3.31 are not constant and have fluctuations. This is due to the variation in the test conditions which is explained as follows. For this purpose, the plot has been divided into three regions (indicated by a red dotted line) in figure 3.31. Initially, the temperature setpoint inside the humidity chamber was set to 60° C. However, it was noticed that the temperature display in the humidity chamber had an error offset to the actual temperature inside the chamber. Hence, the error offset was corrected by trial and error method. Therefore, region (1) has a lower leakage current compared to the final state in figure 3.31. Region (2) was the zone where manual correction was done for temperature. There is a dip in the region (2). This is due to the rework conducted in the test setup to prevent oil penetration into the measurement equipment. After a continuous operation of nearly 200 hours, it was noticed that oil was leaking via the thermocouple wires to measurement equipment by capillary action. Hence, the test was immediately stopped and rework was conducted by adding a connector and a terminal board inside the chamber. In this way, the thermocouple wires were isolated from the measurement equipment. In Region (3), the ambient temperature was nearly 60° C. There is a small dip in this region which indicates the instance when oil was refilled into the tank. The minor variations in the leakage current are due to the instantaneous variation in the ambient temperature.

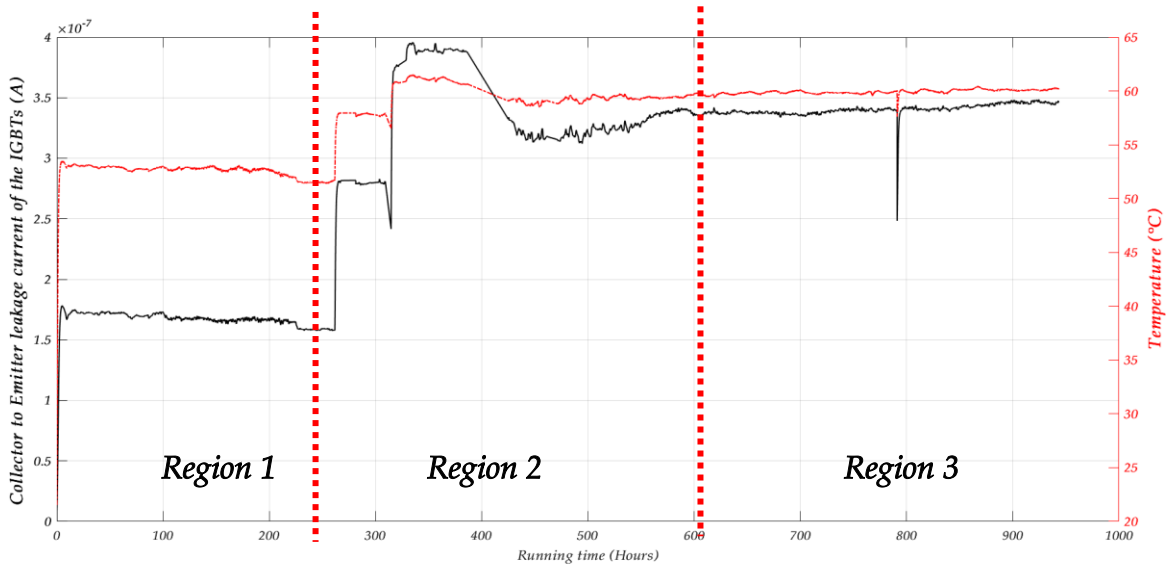

Figure 3.31: Plot of I_{CES} vs. time of an IGBT module and ambient temperature vs. time

In region 1, during the initial start-up phase, the temperature inside the climate chamber gradually increases, thereby increasing the temperature of oil bath. This results in rise of leakage current of IGBTs under test. The rate of increase of leakage current of IGBT module placed in air is compared with that of the IGBT module immersed in oil as shown in figure 3.32. The corresponding temperature values are also plotted. The dependence of leakage current with temperature can be clearly observed from the plot.

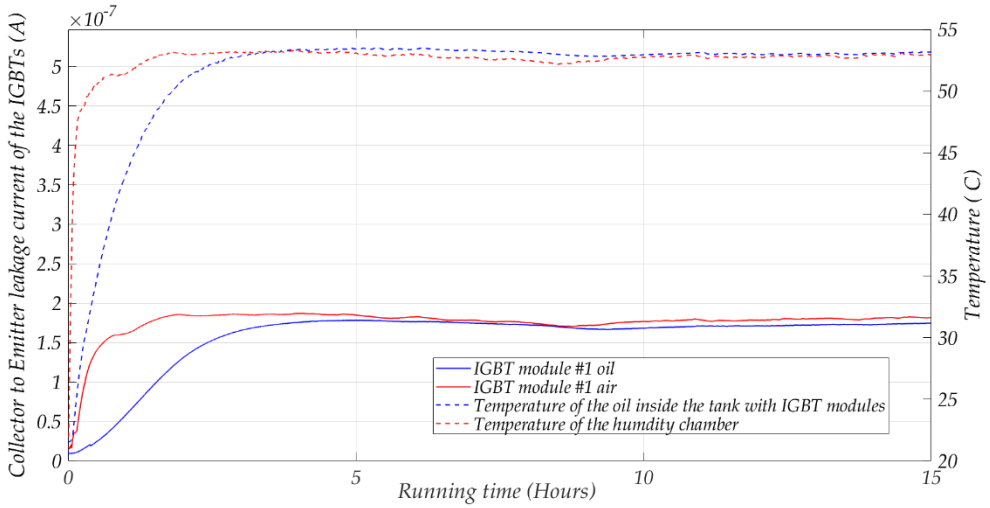

Figure 3.32: Comparison of I_{CES} vs. time of IGBT module in air and oil

A plot of leakage current measurements of all IGBTs under test vs. running time is shown in figure 3.33. Though the currents vary between each IGBT device, all the initial values (I_{CES_ref}) were within the nominal value as mentioned in datasheets [61,62]. After the completion of the test, there weren't any appreciable variation in the leakage current levels of all IGBT devices during the test as shown in the plot. So, none of the IGBTs had failed as per the chosen criteria $(I_{CES}) > 2 \cdot (I_{CES\_ref})$.

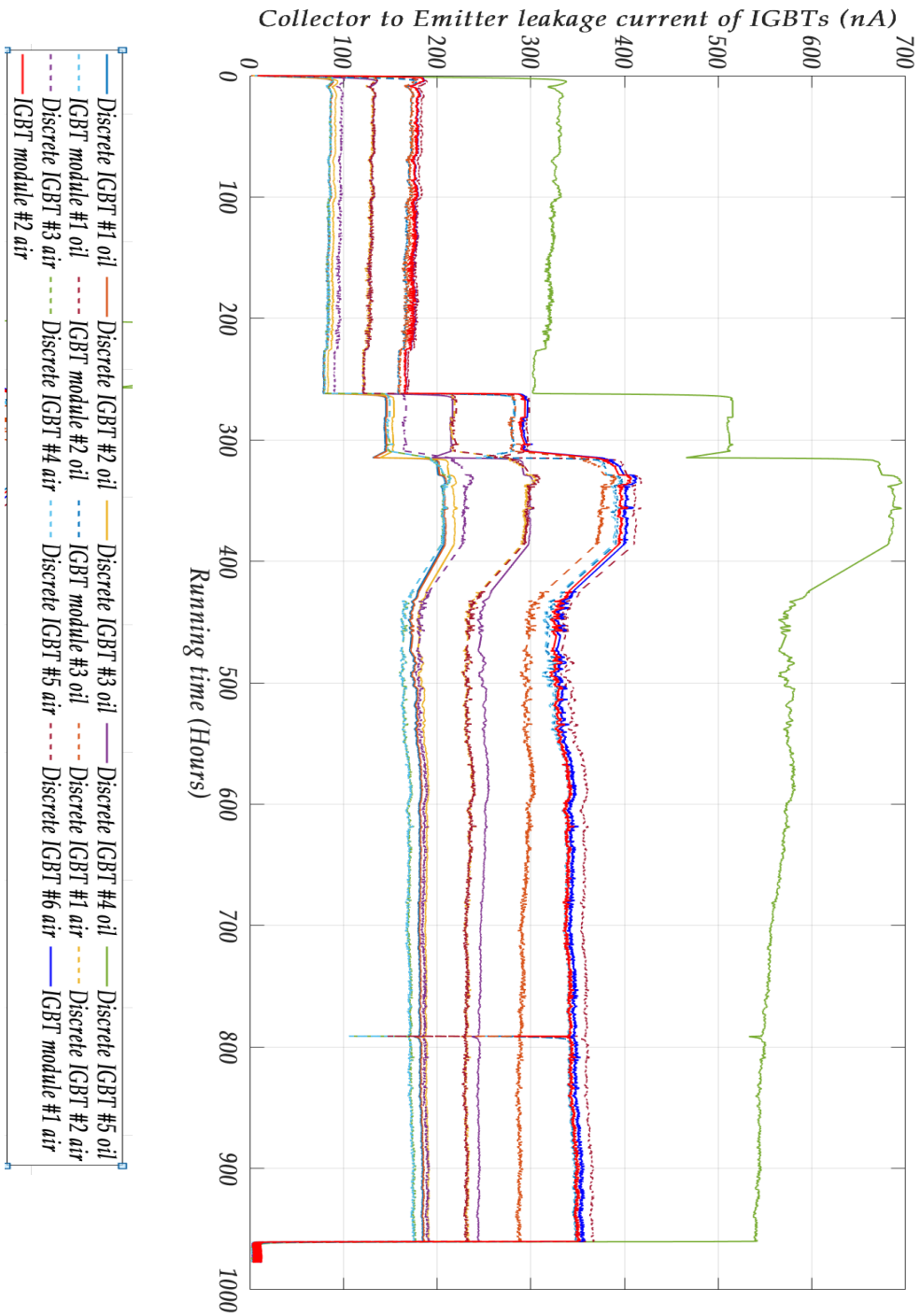

Figure 3.33: Plot of leakage current measurements of IGBTs vs. time

Comparison of pre and post characterization measurements - After completing the test, the IGBTs were characterized again to see if there is any deviation in the parameters. The electrical circuit used for the different characterization measurements was described in section 3.6.3. None of the parameters changed significantly, between the pre- and post-testing characterization. As an example, the pre and post characterization results of leakage current and gate emitter threshold voltage of one IGBT in an IGBT module are presented below in figure 3.34 and 3.35 respectively. The minor deviation observed in the results are within the tolerance and can be due to measurement inaccuracy.

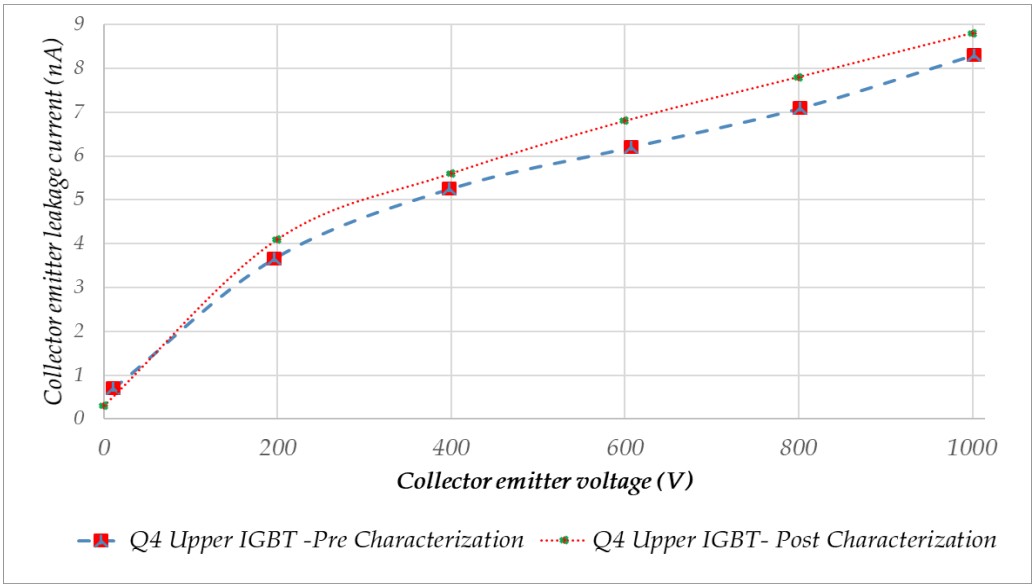

Figure 3.34: Collector Emitter leakge current characterization before and after the endurance test

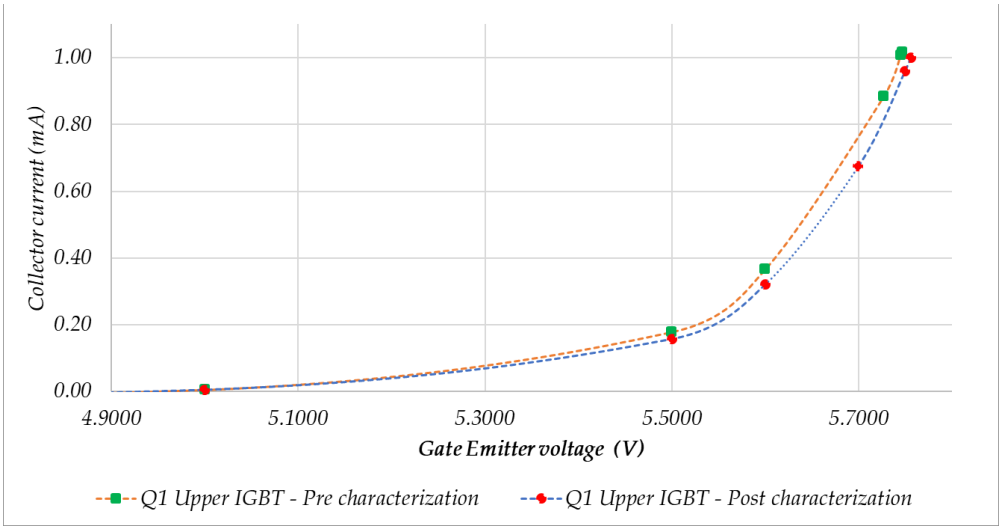

Figure 3.35: Gate Emitter Threshold voltage characterization before and after the endurance test

Visual inspection – After completing the test, a visual inspection of the oil tank was conducted wherein the IGBTs were immersed during the test. The following observations were made.

1) Mineral oil used for the experiment is usually transparent in nature. Oil in the tank with discrete IGBTs did not have any change in colour and was found to be transparent as shown in figure 3.36.

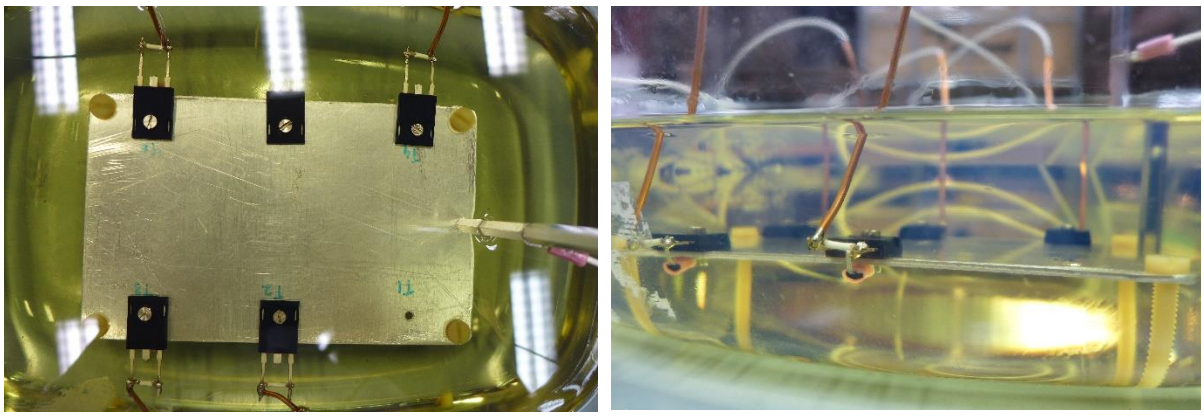

(a) (b)

Figure 3.36: Visual inspection of the oil tank with discrete IGBTs

2) Oil in the tank with IGBT modules was found to be cloudy as shown in figure 3.37. Figure 3.38 clearly indicates the comparison between the two oil tanks with discretes and modules.

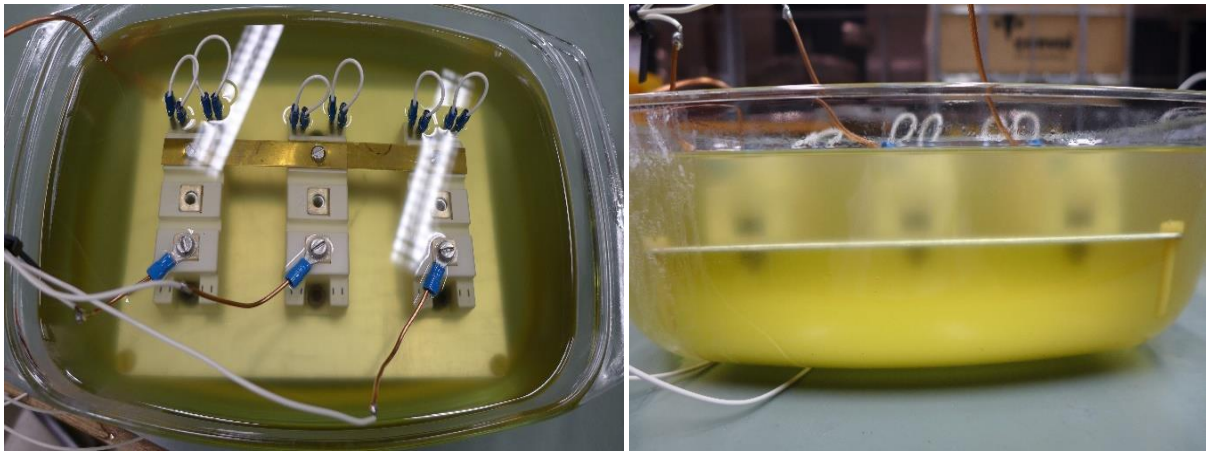

(a) (b)

Figure 3.37: Visual inspection of the oil tank with IGBT modules

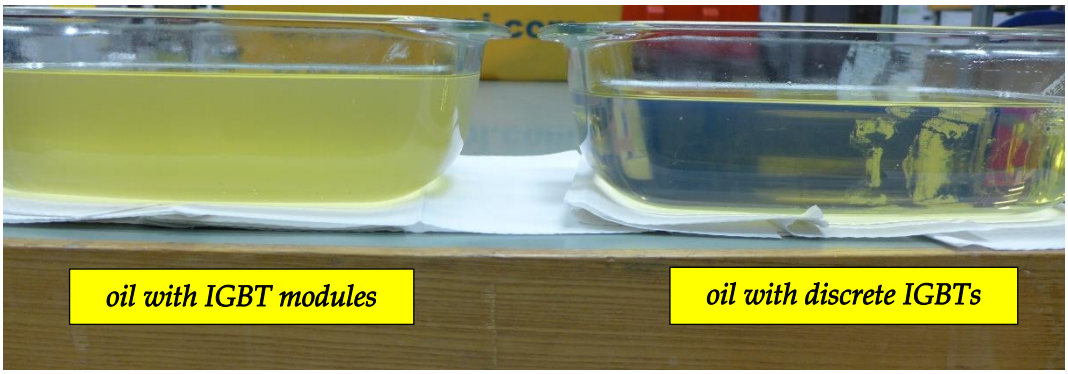

Figure 3.38: Comparison of oil tanks

Upon further investigation, it was found that the dissolution of the thermal paste was the reason behind the cloudiness of oil. As mentioned in section 3.6.4, this thermal paste is applied beneath the base plate of the IGBT modules before mounting them on a metal plate. Upon careful removal of the IGBT modules from the metal plate, the degradation of the thermal paste can be observed on the base plate of the IGBT module. An image of the thermal paste application before the test is shown in figure 3.39 and the degradation of the thermal paste after the test is shown in figure 3.40. This is an important observation which emphasizes the need for a detailed study on the choice of the thermal interface material for the IGBT when immersed in oil.

Figure 3.39: Thermal paste – before test

Figure 3.40: Thermal paste degradation – after test

Possible consequences of thermal paste degradation - As explained in section 3.4, thermal paste is applied to improve the thermal contact between the base plate of the IGBT module to the heatsink. For modules with a base plate, the thermal resistance of the interface between the case and heat sink is specified by a typical value in the datasheet R_{thCH}, which amounts to roughly 50% of the internal thermal resistance from chip to case [46]. Degradation of the thermal paste might lead to increased thermal resistance and ultimately IGBT module failure

when used in air environment. However, when IGBTs are immersed in oil, there are few other possibilities as follows,

1) Oil could fill in the voids between the two metallic surfaces and could act as a thermal interface material instead of the thermal paste itself.
2) A thermal interface material(TIM) compatible with the oil needs to be used in order to avoid their degradation in oil.

There are other factors like thermal conductivity of the oil and heat generated by the IGBT module during operation, which in turn depends on the power dissipation. Therefore, both these possibilities require further investigation.

Internal analysis of IGBT modules – After the endurance test, one test sample of the IGBT module was sent for internal analysis to Eurofins, a material science laboratory in the Netherlands. Figure 3.41 shows the internal view of a new IGBT module after the housing was partially opened. This IGBT module was used as a reference. Figure 3.42 shows the internal view of the IGBT module after the endurance test. The voltage endurance test performed with mineral oil has a significant influence on the silicone gel. Usually, the silicone gel is transparent as seen in figure 3.41. But, after the test, the gel completely became opaque.

Figure 3.41: Image of the silicone gel inside the new IGBT module

Figure 3.42: Image of the silicone gel inside tested IGBT module

Degradation of the silicone gel under the influence of the mineral oil was determined using Fourier Transform Infrared (FTIR) spectroscopy[4]. A sample of the gel was taken from the oil tested IGBT and compared with a reference sample of the silicone gel which was taken from a new non-tested IGBT module. Detailed explanation about the working principle of FTIR is given in [68].

[4] FTIR - When IR radiation is passed through a sample, some radiation is absorbed by the sample and some passes through (are transmitted). The resulting signal at the detector is a spectrum representing a molecular 'fingerprint' of the sample. The usefulness of infrared spectroscopy arises because different chemical structures (molecules) produce different spectral fingerprints.

Figure 3.43. shows the FTIR spectra of new silicone gel, silicone gel from the tested IGBT module and mineral oil. It can be observed that the spectrum of silicone gel of the IGBT module under test (red) is a combination of the IR spectrum of new silicone gel (blue) and mineral oil (green), thereby clearly indicating the migration of oil into the silicone gel.

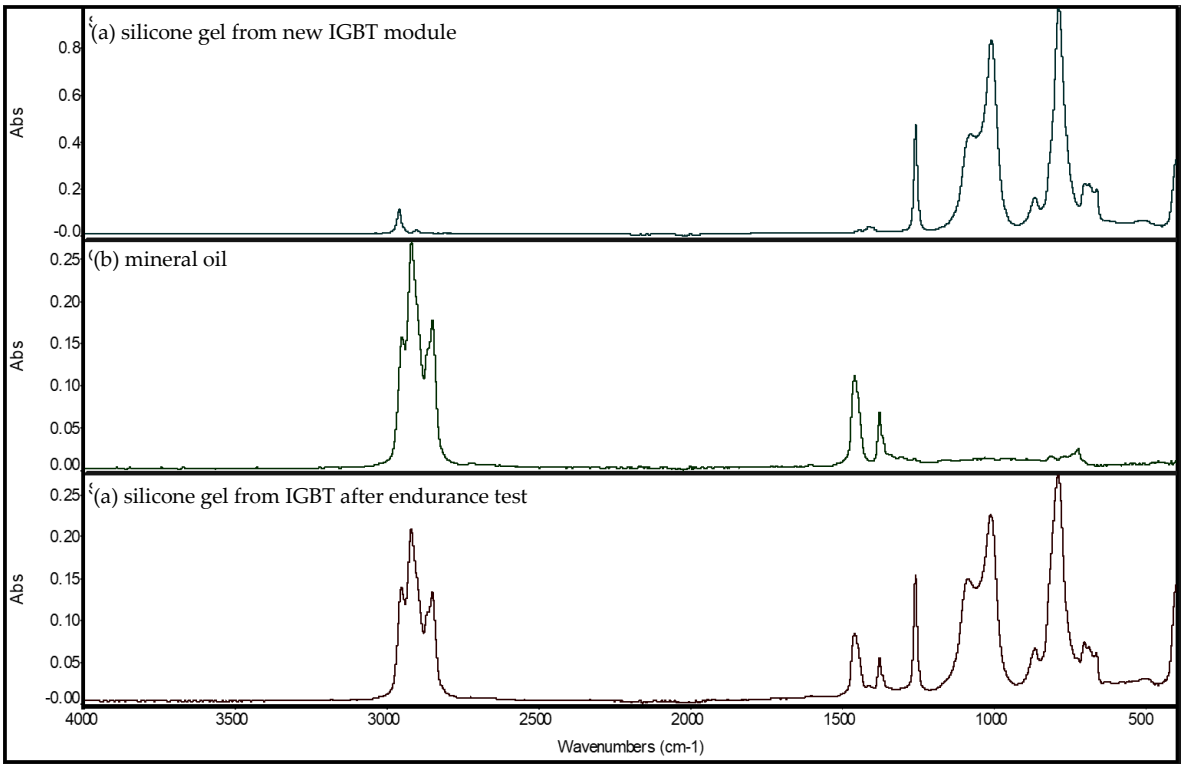

Figure 3.43: FTIR spectra of (a) silicone gel from new IGBT (b) mineral oil sample
(c) silicone el from IGBT module after endurance test

Internal analysis of discrete IGBTs – As described in section 3.6.2, few discrete IGBTs were also used for the voltage endurance test, to check the extent of oil penetration into the package. Pieces of packaging material were removed to check whether mineral oil had entered via the poles and/or through the plastic material.

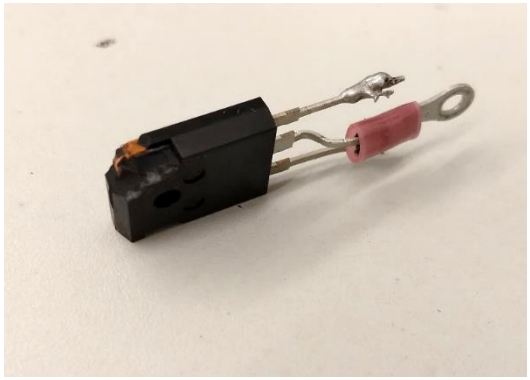

Figure 3.44: Half opened discrete IGBT

In figure 3.45, FTIR spectra of two discrete IGBTs are shown. For the IGBT under endurance test, some remains of oil at the outside can be detected (which is indicated at wavenumber 2900-3000 cm^{-1}), the IGBTs were this tight packed that no droplets of oil or other contamination

could be detected on the inside of the package. No oil has migrated into the package, neither via the terminals nor through the packaging material.

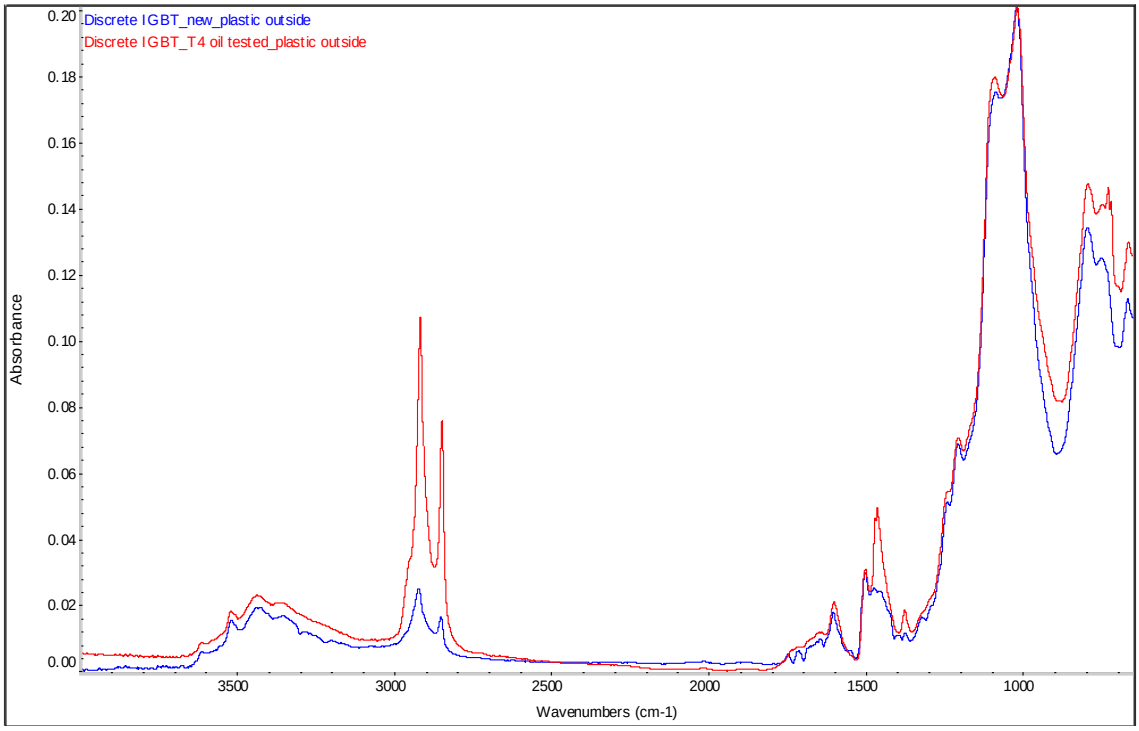

Figure 3.45: FTIR spectra of discrete IGBTs (new vs oil-tested)

3.7 Thermal cycling test

3.7.1 Background

Different layers of materials used in the construction of a wire-bonded IGBT module were described in detail in section 3.3. The layer sequence is shown in figure 3.46.

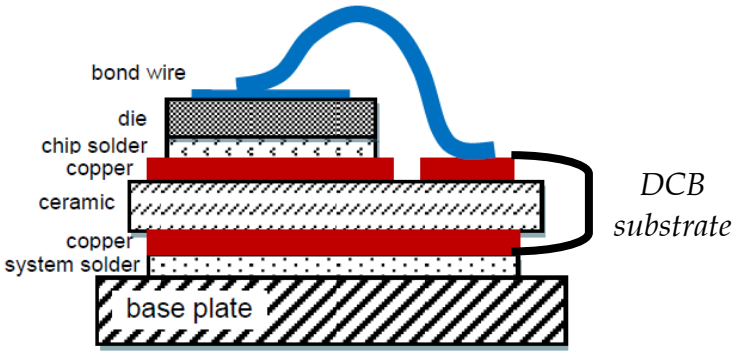

Figure 3.46: Layer sequence of IGBT module [54]

Amongst various construction elements, copper is mainly present in the IGBT module in the form of a base plate (in IGBT modules with copper baseplate) and in the DCB substrate as shown in figure 3.10. From [69-71], it can be concluded that there is a tendency of dissolution/corrosion of copper in mineral oil. This phenomenon is predominantly observed in transformers immersed in mineral oil. In [69], R. Maina et al. claims that mineral oils may react with the copper conductors in oil-impregnated transformers, leading both to the

formation of dissolved and suspended copper in the oil. This also results in the deposition of copper onto the paper surface of the solid insulation in the transformer. As already mentioned in the previous section, there are possibilities of oil reaching the internal chip surface of the IGBT module. If any copper dissolution or corrosion occurs on the substrate layer beneath the IGBT chip, it would result in an increase in the thermal resistance of the IGBT leading to premature ageing of the module. Therefore, it is vital to ensure the module reliability especially with respect to the substrate, base plate, system solder area between substrate and baseplate.

This is done by conducting thermal cycling on IGBT modules when immersed in oil. In a thermal cycling test, the IGBT module is heated and cooled for a certain number of cycles. There are different ways of performing thermal cycling tests. It is broadly classified into active and passive cycling as shown in figure 3.47. It is to be noted that there are other types of thermal cycling tests which are not included in this classification since they are not relevant to this study.

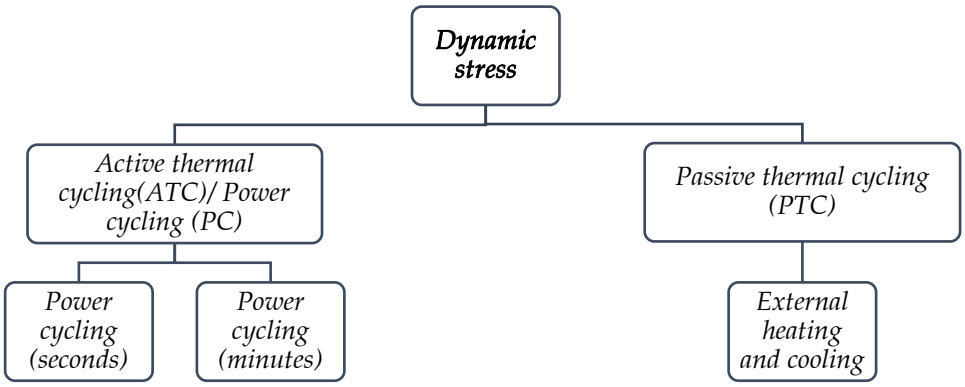

Figure 3.47: Classification of thermal cycling tests

In an active thermal cycling test, heating is done by applying a load current, which leads to heating of the junction of the semiconductor. Hence, the IGBT chips are actively heated by the losses generated by the IGBT themselves Once the required maximum junction temperature of the chip has been attained, the power is turned off and the module is cooled down quickly (e.g. by water cooling). Hence, this test is also called as power cycling (PC). Furthermore, power cycling test is classified into two types based on the test conditions. The first entry listed is called power cycling (seconds) test, wherein the cycle times are typically smaller than 15s [47]. These short cycles mainly stress the die connections, i.e. the bond wires or the interconnection between die and substrate. The second entry listed is the power cycling (minutes) test with longer cycle times (2-10 min) and smaller currents compared to PC(sec). The latter primarily affects the layers beneath the die including the system solder.

In contrast to the PC test, passive thermal cycling test involves external heating and cooling of the IGBT module. The test conditions of the passive thermal cycling are equivalent to the PC(min) test with longer cycle time in the range of a few minutes (2-10 minutes). Hence, this test also stresses the layers beneath the die surface.

As mentioned earlier, since the primary focus is on the reliability of the module with respect to the substrate and the system solder area, only PC(min) or passive thermal cycling test will be of relevance. A comparison between both these tests is presented in [54] which claims that passive thermal cycles induce stronger solder delamination underneath the substrate edges of IGBT modules compared to thermal cycles due to internal active heating. Hence, amongst the two, the choice of the test was decided to be passive thermal cycling.

The passive thermal cycling raises and lowers the case temperature at relatively long intervals in a time frame of minutes. The case temperature is measured on the base plate. For a thermal measurement, as close to the chip as possible, it is necessary to place the temperature sensor below the chip to be measured. In those cases, knowledge of the exact chip positions in the IGBT module is therefore essential [72]. Figure 3.48 shows thermal cycling(TC) curve for different types of IGBT modules, which provides information on achievable stress (in terms of number of temperature cycles) vs. case temperature swing (ΔT_{case}) during the lifetime of the system solder [73]. The typical cycle time of 5 minutes is considered for this TC curve. The IGBT modules used for the experiment in this thesis has a TC curve similar to the EconoPACK™ 4 package (as highlighted in figure 3.48). Hence, with a repetitive case temperature swing (ΔT_{case}) of 80 K, the IGBT module can withstand 5000 thermal cycles. This curve can be used as a reference to estimate the extent of thermal stress applied to the IGBT module.

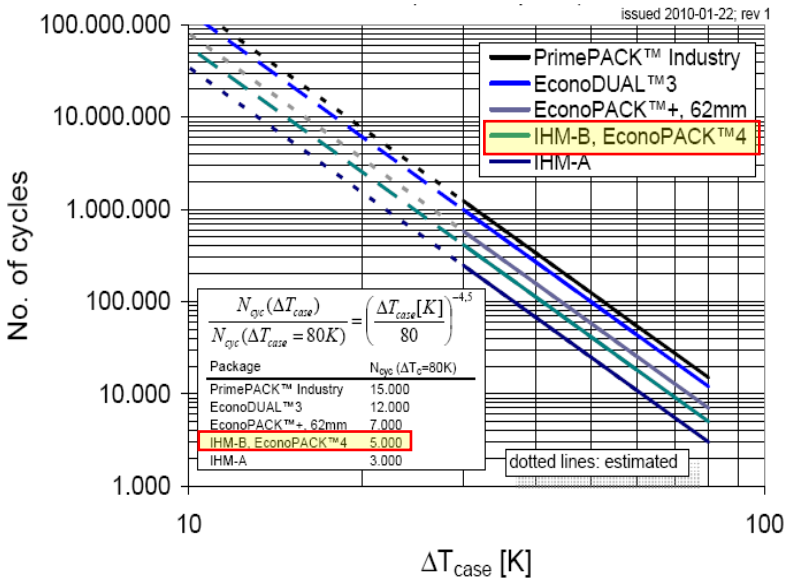

Figure 3.48: Thermal cycling capability curve of IGBT modules [73]

The details and specifications of the test setup are explained in the next section. After the completion of thermal cycling test, the following aspects of the IGBT's internal structure is to be analysed.

1) Analysis of the copper substrate and base plate layer to assess its condition and to check if there are any signs of degradation.
2) The status of the system solder layer to check for any delamination. This can be investigated with the help of a scanning acoustic microscopy (SAM). Example of

delamination of the solder between the baseplate and the DCB (system solder) is shown in figure 3.49 [74]. The thermal resistance in the region of the delaminated zones will be much higher than the original value.

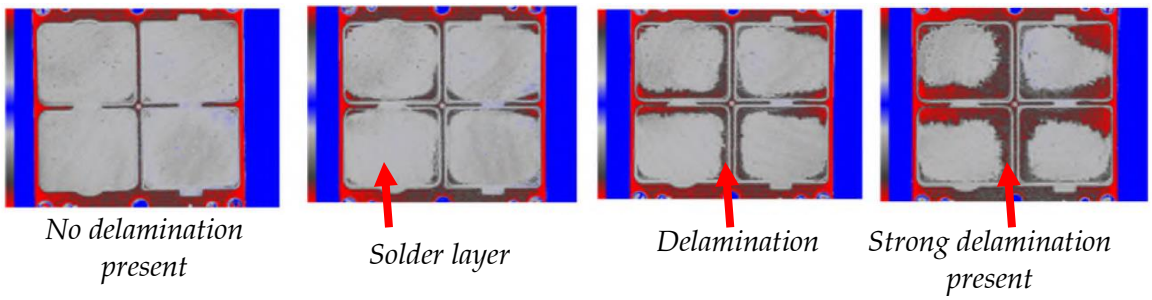

Figure 3.49: Example of delamination of the solder between the baseplate and the DCB (system solder) [74]

3.7.2 Test specifications

The IGBT power modules (FF50R12RT4) which were used during the voltage endurance test were reused for this test except for one IGBT module which was stored for internal analysis. The case temperature was cycled from 20° C to 100° C to achieve a ΔT_{case} of 80 K. Though the typical cycle time of 5 minutes was maintained while obtaining the TC curve as shown in figure 3.48, it was found that the minimum time required for the heating and cooling phase was approximately 2 minutes and 6 minutes respectively to achieve a ΔT_{case} of 80 K during the experiment. Especially, the large cooling phase is due to the insufficient capacity of the cooling system. Due to the increase in the cycle time, the thermal stress on the IGBT will be lower when compared to the TC curve for the same number of thermal cycles.

3.7.3 Test setup

The passive thermal cycling test is performed by mounting the module on a combination of an electrical heater, Peltier element and water cooling block as shown in figure 3.50. This entire setup was immersed in an oil bath which was placed in a climate chamber. The role of every component in the test setup is explained.

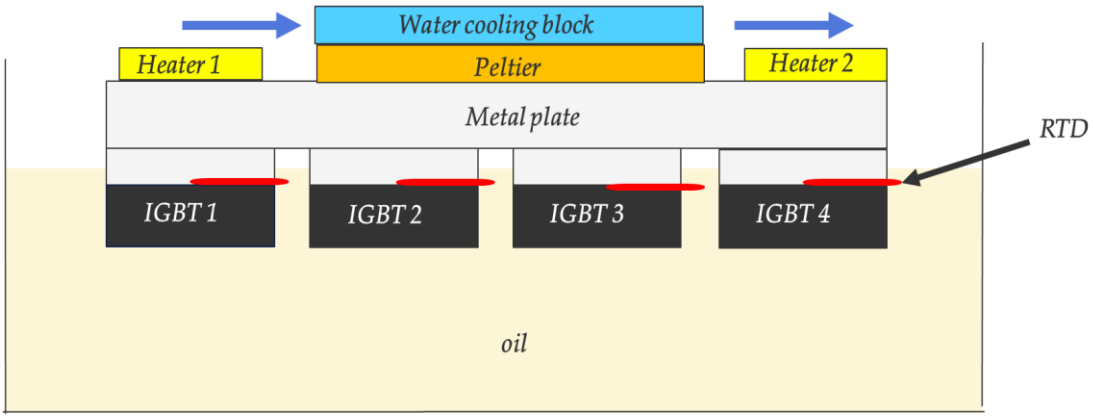

Figure 3.50: Diagrammatic representation of the experimental setup

Peltier element - It is a thermoelectric module which operates in accordance with the Peltier effect[5]. A Peltier element with dimensions of 62 mm x 62 mm x 4.57 mm was used for the test [75]. A typical image indicating the components of the Peltier element is shown in figure 3.51.

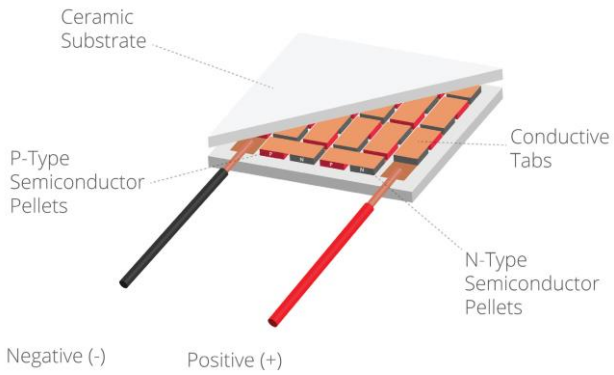

Figure 3.51: Typical construction of a Peltier element [76]

Temperature controller - The Peltier element was controlled by a temperature controller. A 5300 series TECSource from Arroyo instruments as shown in figure 3.52 was used for this purpose [77].

Figure 3.52: Temperature controller – Arroyo instrument [77]

5 Peltier effect -The effect creates a temperature difference by transferring heat between two electrical junctions. If an electric current is passed through a dissimilar material junction, then the heat may be generated or absorbed. Reversing the direction of the current flow will cause the heating and cooling effects to switch junctions.

Temperature sensor – The temperatures of the base plate of IGBT modules and the water cooling block was monitored by Platinum Resistance Thermometer (RTD) PT100. An image of a typical PT 100 is shown in figure 3.53. The RTD was connected in a 4-wire configuration to increase the accuracy of resistance measurement as the resistance error due to lead wire resistance is zero in this connection [78]. The temperature of the oil bath and the ambient temperature inside the climate chamber was measured by thermocouples.

Figure 3.53: Platinum Resistance Thermometer PT100

Figure 3.54: Electrical heater

Electrical heaters – In addition to the Peltier element, two electrical heaters, attached to the metal plate were turned on and off during the heating phase and cooling phase of the thermal cycle respectively. Each electrical heater was rated for 225 W. Figure 3.54 shows an image of the heater.

Water cooling block – A water cooling block was mounted on the Peltier element to cool the hot side of the element during the cooling phase. The water flow for the cooling block was controlled by an electronic valve. Figure 3.55 shows an image of the arrangement of the water cooling block on top of the Peltier element.

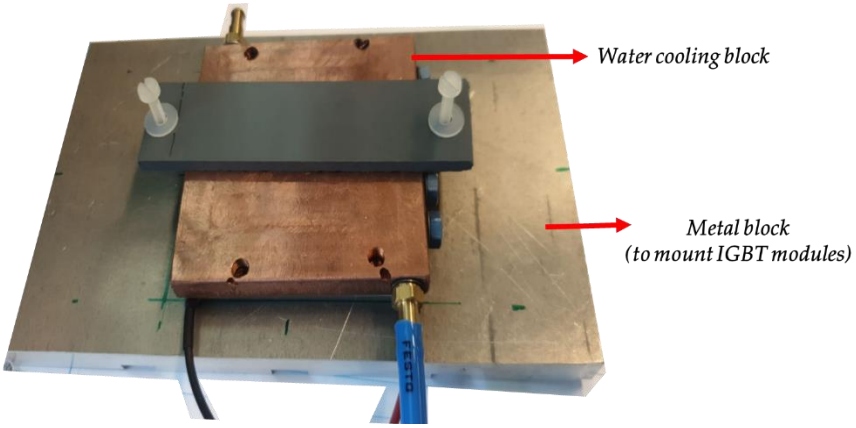

Figure 3.55: Arrangement of the water cooling block

The IGBT modules were mounted on a specially designed metal block as shown in figure 3.56. In order to keep the Peltier element outside the oil, the entire structure was kept inverted inside the oil bath. The RTDs, electrical heater and water cooling block were mounted after the application of thermal paste to improve the thermal conductivity. An image of the test setup kept inside the chamber is shown in figure 3.57.

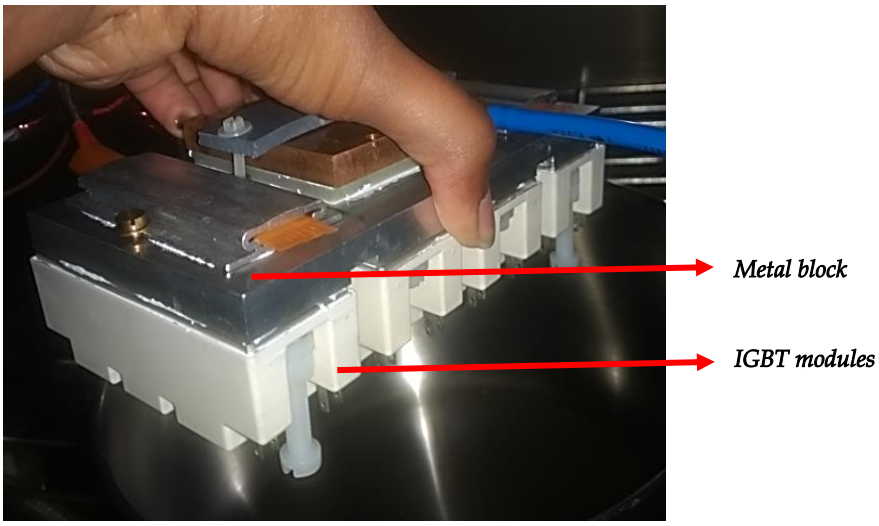

Figure 3.56: Mounting of the IGBT modules on the metal block

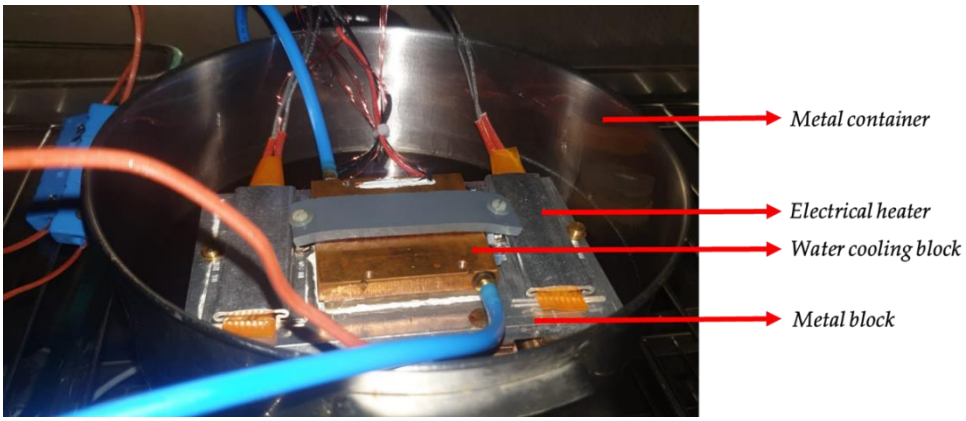

Figure 3.57: Arrangement of the setup inside the climate chamber

Grooves were created in the metal plate to mount the RTDs to measure the case temperature of the IGBT modules. As mentioned in section 3.7.1, to measure temperature closer to the chip, the case temperature beneath the IGBT chip area needs to be measured. But, the exact location of the chip inside the IGBT module was not known and was not disclosed by the IGBT manufacturer. Hence the RTD was placed in the centre of the IGBT module. However, unlike the active thermal cycling wherein the heat spreads from the IGBT chip, in passive thermal cycling, the entire surface area of the base plate is heated externally. So, the location of the RTD is trivial.

The case temperature of the IGBT modules was increased up to 100° C by means of the Peltier and the external heaters. Upon cooling, water is circulated through the cooling block until a temperature of 20° C is reached. Similar to the voltage endurance test, a dedicated LabVIEW software program in combination with the data acquisition system (DAQ) was designed to provide an automated control setup and long-term data acquisition of various temperatures. The 34972A LXI Data Acquisition / Data Logger Switch Unit was used for this purpose [64]. Figure 3.58 shows an image of the entire test setup.

Figure 3.58: Entire test setup for the thermal cycling test

3.7.4 Results

The temperature profile of the IGBT modules during the thermal cycling test is plotted in figure 3.59. It can be seen that the temperature of the oil gradually increases and reaches a steady-state temperature. The temperature of the water cooling block, mounted on top of the Peltier element varies in accordance with the thermal cycle. The ambient temperature inside the chamber was maintained to be constant at 8° C. This temperature was maintained in order to improve the rate of the cooling during the cooling phase of the thermal cycle as per Newton's law of cooling[6].

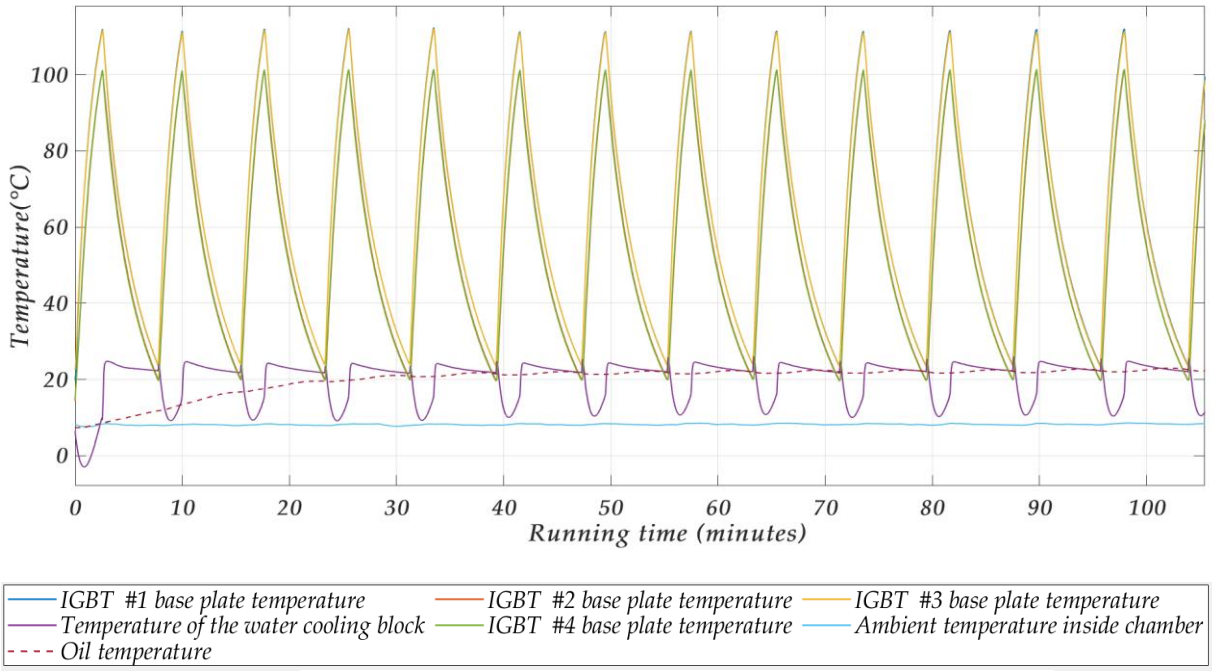

Figure 3.59: Temperature profile during the thermal cycling test

6 Newton's law of cooling states that the rate of heat loss of a body is directly proportional to the difference in the temperatures between the body and its surroundings.

One thermal cycle from the temperature profile is shown in figure 3.60. It can be observed from the plot that the heating and cooling phase spans for 2 and 6 minutes respectively.

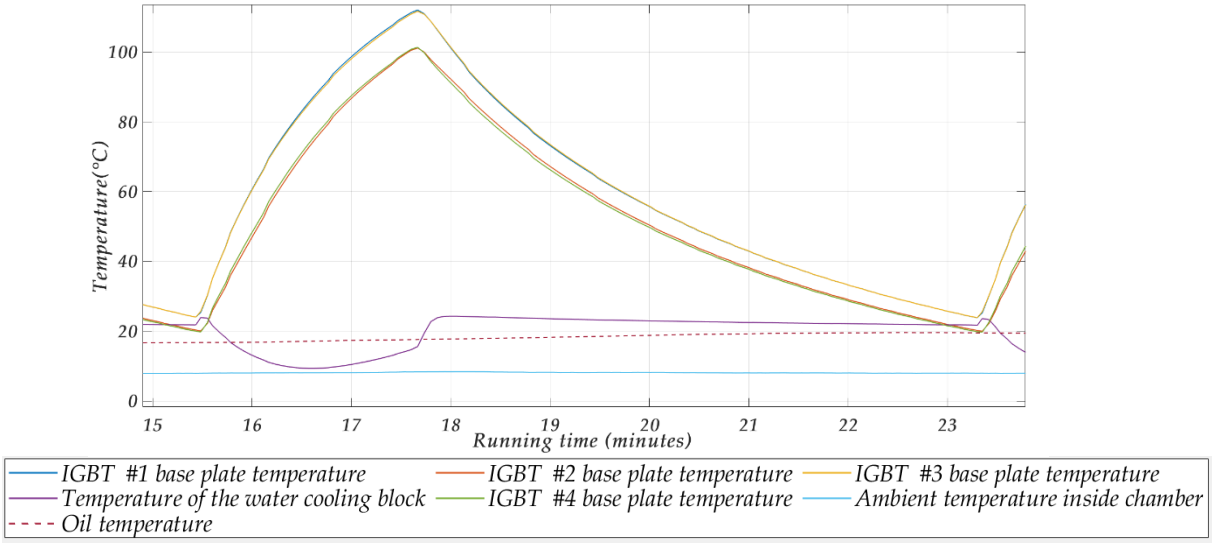

Figure 3.60: One thermal cycle from the case temperature profile

The time taken for the cooling phase of the thermal cycle highly depends on the temperature of the oil and the ambient temperature inside the climate chamber. Hence it is very important to maintain a constant ambient temperature inside the chamber.

Failure in the test system - After completion of nearly 800 thermal cycles, there was an unexpected failure in the control software of the test. This failure had happened during the heating phase of the IGBT modules wherein the heaters were kept on. Due to a software failure, the heaters failed to switch off and continuously heated the base plate of the IGBT module and thus the oil in the tank. Since the test setup was completely controlled by the software, the test did not stop when the temperature of the IGBTs and oil increased. This resulted in overheating of the IGBT modules resulting in its failure.

Solution to avoid failure - This failure was primarily due to the absence of an external safety device which can operate independently of the control software. Hence a possible solution to avoid such failure is to use additional 'thermal switches' on the base plate of the IGBT and inside the oil tank. These are electromechanical devices which cuts off the power supply to the test system when a temperature limit is exceeded, thereby preventing potential burn out or failure [79]. The usage of such thermal switches proved to be necessary in order to protect the IGBTs under test.

The IGBT modules were damaged due to the failure and so they couldn't be used for further testing. Hence the thermal cycling test was not continued further.

3.8 A Roadmap for future testing

This thesis is a part of a large study aimed at investigating possibilities for operating power electronic components under oil. Hence a road map of minimum tests required to verify the reliable operation of the IGBTs is proposed in this section.

Compatibility of passivation layer with mineral oil – As mentioned in section 3.6.5, FTIR analysis of the silicone gel inside the IGBT modules after the voltage endurance test has indicated the penetration of the mineral oil into the silicone gel, thereby turning the gel opaque. The initial prediction of direct contact of mineral oil to the chip surface is proved to be highly possible. After oil reaches the chip surface, it is important to know the compatibility of the passivation layer to mineral oil. A detailed description about the passivation layer is given in section 3.6.1. This is a protective layer of the chip from its external environment, e.g. against contaminations influencing on the flow of carriers inside the chip. For this analysis, the IGBT modules without the gel could be investigated by immersing them directly in oil. In this way, the passivation layer will already be in direct contact with oil, thereby creating the worst-case scenario.

Effect of contaminants on the chip surface – Since the oil is circulating inside the entire container, there are possibilities of the presence of contaminants in mineral oil which can reach the IGBT chip surface. Hence a study regarding the potential contaminants and their effect on the chip surface at high electric field areas is required.

Compatibility of the substrate in mineral oil - Since the passive thermal cycling test as described in section 3.7, could not be completed within the thesis timeline, the test needs to be completed in future. But, the passive cycling test aimed at applying cyclic thermal stress to the substrate in order to observe any degradation. In addition to this test, the copper used in the substrate of the IGBT module needs to be separately tested in mineral oil to investigate its chemical compatibility in mineral oil.

Active power cycling test of the IGBT module - In addition to the passive cycling test, the active power cycling test is also an essential test to simulate the real-time operation of the IGBT modules.

From the literature study and results from the experimentation, it can be found that the chemical compatibility of the components inside the IGBT module with the mineral oil plays a very important role for the reliable operation of the IGBT modules. Hence, the chemical compatibility of mineral oil with every component of the IGBT module must be investigated.

Choice of oil – If mineral oil is found to be a bad candidate through experimentation, other types of oil such as synthetic ester oils, natural ester oils, polyether fluorinated fluids [59] could be investigated as an alternative.

3.9 Summary

In this chapter, the need for experimental investigation of the power electronics components in oil was explained. The construction of the existing IGBT packages were described followed by the identification of critical regions in the IGBT module structure which required investigation under oil. Consequently, two test setups were built to test the operation of the IGBT modules focussing on critical areas. The chapter is concluded by providing a road map of future tests required to assure the feasibility of IGBT modules under oil.

4

Conclusions and Recommendations

This is the last chapter of the thesis report. It concludes the work of this master's thesis with recommendations for future work.

4.1 Conclusions

The main objective of this master's thesis is successfully achieved by proving the feasibility of oil immersed design of MMC based mobile high voltage test source for onsite testing. This feasibility study covers both system level aspects, as well as component-level aspects. The system-level part covers the estimation of achievable percentage of size reduction of the test source in oil when compared to one with air as external insulating medium. As the proposed test source is immersed in oil, its components must be compatible with oil. Hence, a preliminary component-level investigation was conducted to analyse the operation of Insulated gate bipolar transistor (IGBT) under oil. Based on the results obtained from the experimental work, future test procedures and validation methodologies are proposed to realize an oil immersed mobile test source.

The following conclusions can be drawn from this master's thesis work:

1) From the literature study, it is found that there are no existing power converters available with oil immersed design in high voltage applications such as HVDC and FACTS. Hence, experimental investigation on the design and reliability of components when immersed in oil is necessary.
2) A long-term voltage endurance test was conducted on discrete IGBTs and IGBT modules when immersed in oil. The results revealed no oil migration inside the discrete packages, whereas the migration of oil inside the IGBT module was confirmed. Despite oil migration, the operation of the IGBT module was not influenced by mineral oil for the entire test duration.
3) A dimensioning tool developed in this master's thesis can be used to choose the appropriate converter layout for the MMC based test source with air or oil, both for stationary and mobile testing purposes. A primary investigation on electric field distribution of the proposed converter layout in air was conducted. Results show that the converter design can meet the basic insulation requirements with optimal design of the corona rings and shields around the submodules.
4) Initial estimate obtained from the tool shows that the voltage capability of the test source is around 4 times higher in oil than that of air for the given standard trailer dimensions. A test source rated for 320 kV is possible with oil immersed design. This voltage capability is nearly 25% higher than the voltage rating of existing mobile AC resonant test system used for onsite cable testing (by KEMA Laboratories).

5) In this thesis, the dimensions of submodule for MMC were considered based on off-the-shelf DC capacitors. However, by customising the design of DC capacitor, specific to the test application, the size of the submodule could be reduced further. This could result in even higher voltage capability of the test source.

4.2 Recommendations for Future Research

This thesis is the first step of a bigger study aimed at investigating possibilities for oil immersed design for the power electronics based test source. Hence, this section indicates possible areas for future research and improvements of the work performed in this thesis.

1) A preliminary test to investigate the operation of IGBT module in oil was conducted during this thesis timeline. Hence, a road map with a series of tests is proposed in section 3.8, which are at least needed to investigate if the existing off-the-shelf IGBT modules can reliably operate in oil. These series of tests need to be performed.
2) There are primary differences between MMC design, proposed for test source and traditional MMC, employed in HVDC application. Hence, the design requirements of the test source submodule need to be customised based on the test application.
3) Apart from MMC, a feasibility study of the on-site test source based on other power converter topologies like the cascaded H bridge configuration, needs to be conducted in order to find an efficient solution.
4) After conducting the feasibility study on other topologies, a comparative study between potential candidates needs to be conducted based on economic aspects to realise a cost-effective solution.

Appendix

A.1 AC resonant cable test system

A block diagram of the AC resonant test system for on-site testing of extruded cables is shown in figure A.1 [80]. This test system is used for AC withstand testing after installation of cable in the field. Tests are performed according to IEC 60840 and 62067. These standards require testing with AC voltage in the frequency ranging from 20 Hz to 300 Hz. Detailed description about the components and operation of the test system is given in [80]. A detailed overview about various onsite testing techniques for other equipment is given in [81].

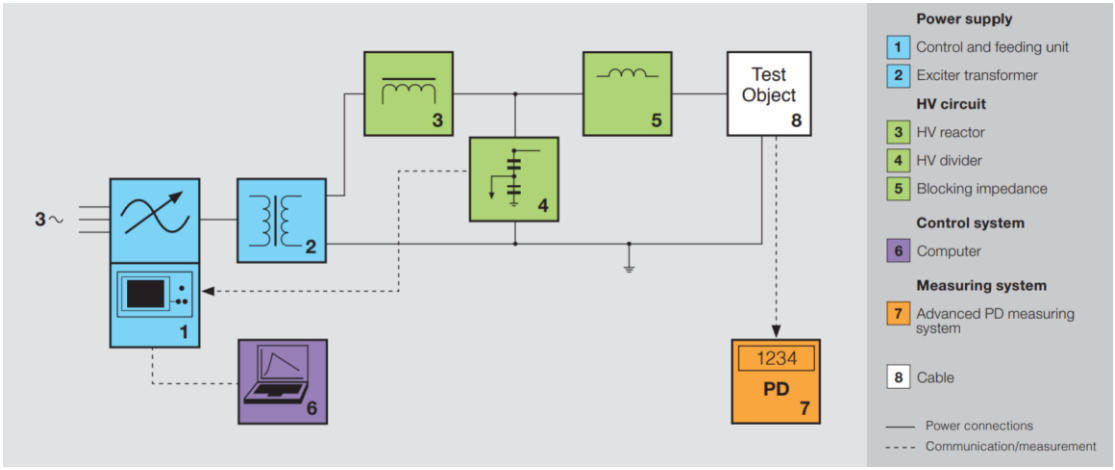

Figure A.1: Block diagram of AC resonant test system [80]

A.2 Volume estimation

The ratio of volume occupied by converter arrangement to the volume occupied by air insulation in a converter hall was calculated in an actual MMC based converter station.

To perform this estimation, typical dimensions of the converter tower and converter hall were taken from a case study [82]. The converter station used for this study was the Oberzier converter station (converter supplied from Siemens). The converter hall consists of 24 converter towers (six numbers of 2-layer towers and eighteen numbers of 4-layer towers). The geometry of the converter hall is given in figure A.2.

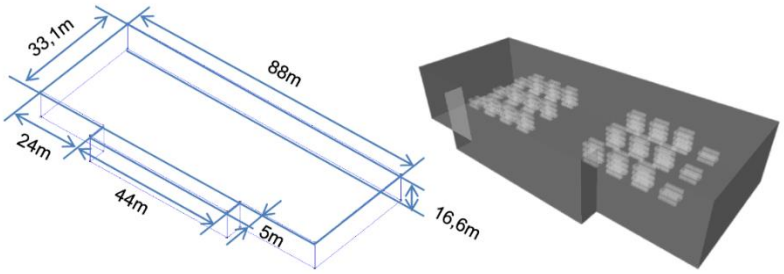

Figure A.2: Geometry of converter hall [82]

An image of a 2-layer converter tower by Siemens is shown in figure A.3 [83]. The geometry of the converter tower is given in figure A.4 [82].

Figure A.3. 2-layer converter tower (Siemens) [83]

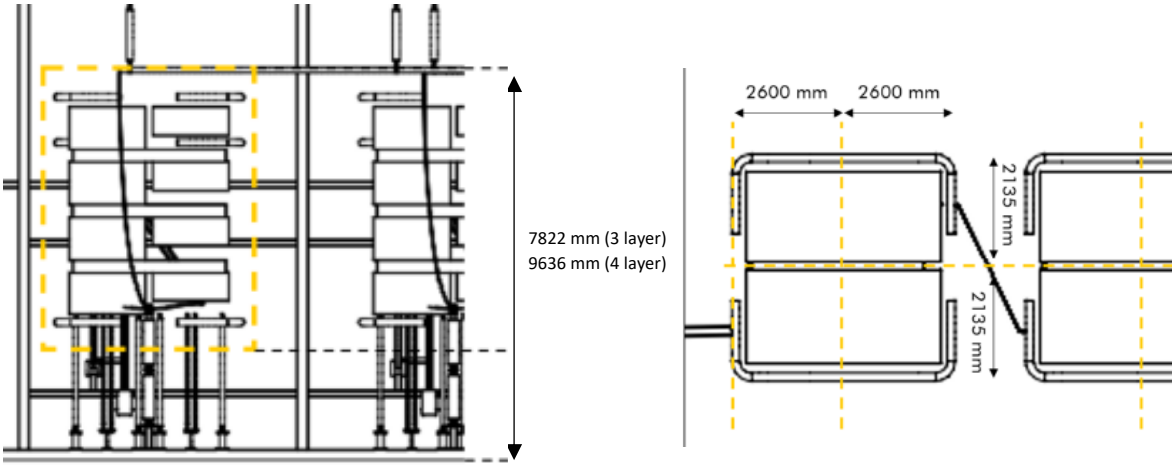

Figure A.4. Converter tower geometry [82]

The total volume of the converter hall is estimated to be 46464 m^3 according to the dimensions mentioned in figure A.2. The total volume occupied by the converter towers is approximately found to be 4872 m^3. Hence, only 10% of the total volume is occupied by the converter tower. This estimation could differ between converter stations.

A.3 Algorithm of the dimensioning tool in MATLAB

A dimensioning tool was used in this thesis work to estimate the total number of submodules that could be fitted into the trailer using a different converter layout. This tool was developed in MATLAB using optimisation. The constraints for the optimisation are the dimensions of the trailer. A flowchart elucidating the algorithm involved in developing the dimensioning tool is shown in figure A.5.

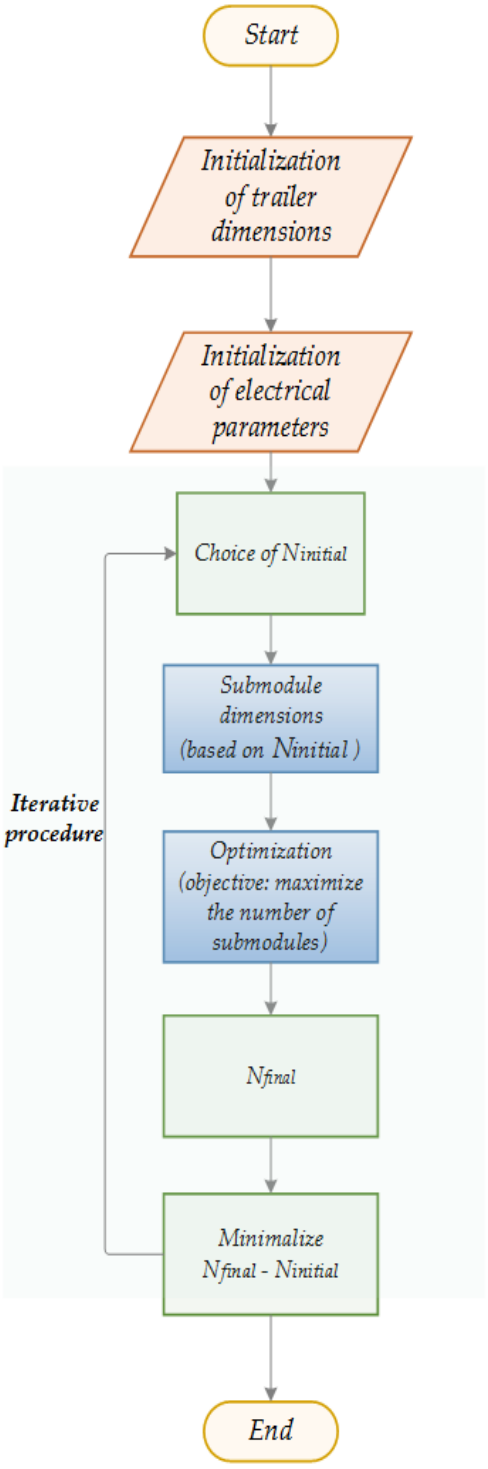

Figure A.5. Algorithm followed for dimensioning the test source

After initializing the trailer dimensions and other electrical parameters, the optimisation is repeated for different values of N. For every N, the dimensions of the module will change as explained in section 2.5.1 (with the dimensions of the submodule rated for 200 kV as reference). A snippet of the MATLAB script is given as an example to illustrate this procedure. In this example, the dimensioning of type I converter layout (of orientation I) in air is explained. A similar procedure is followed for other converter layouts in air. In oil, the

procedure remains the same except that the clearance criteria is different (as mentioned in section 2.6).

Initialisation of dimensions of trailer

```
prompt = 'What is the length of the truck (in m)? ';
L_truck = 100*(input(prompt)); % conversion into cm
prompt = 'What is the height of the truck (in m)? ';
H_truck = 100*(input(prompt));
prompt = 'What is the width of the truck (in m)? ';
W_truck = 100*(input(prompt));
```

Initialisation of electrical parameters

```
Submodule_voltage=4;%in kV
```

Clearances in air according to IEC 60071

```
Vm=[0,3.6,7.2,12,17.5,24,36,52,72.5,100,123,145,170,245,300,362,420,550
,800];%clearance in air per IEC 60071
Insul = 10^ 1*[0,60,60,90,120,160,270,480,630,780,900,1100,1300,
1500,1700,1900,  2100,2350,3350];%in cm
x1=1:1:10000000;
d_air = interp1(Vm,Insul,x1,'linear','extrap');
```

Distance between the levels of the converter according to insulator height

```
x=[0,20,28,38,50,70,95,140,185,230,275,325,360,395,460,500]; %
insulator length
y = 10^- 1*[0,190,215,255,305,445,560,770,1020,1220,1500,1700,1900,
2100,2300,2500];%in cm
y1=0:1:10000000;
d_level = interp1(x,y,y1,'linear','extrap');
clearance_submodule_air = 5;% in cm
```

Type I orientation I

```
fun = @(x)(1/(x(1)*x(2)));% optimisation function - maximise the layer
and tower for the given truck dimensions
A = [];
b = [];
Aeq = [];
beq = [];
lb = [2, 2]; % lower limit for the number of submodules per level and
level
ub = [30, 30]; % upper limit for the number of submodules per level and
level
```

```
IntCon = 1:2;
options = optimoptions('ga', 'Display', 'off');

k=0.2;
v=[];
mat=[];
for i=1:1:20
    L_module=60*(k^(1/3));
    H_module=30*(k^(1/3));
    W_module=25*(k^(1/3));
    for j=1:50
        [x,fval,exitflag,output,population,scores] = ga(@(x)fun(x),2,
A, b,Aeq, beq,...
            lb, ub,
@(x)function_type_1_orientation_1(x,L_truck,H_truck,
W_truck,L_module,H_module,W_module,Submodule_voltage,clearance_submodul
e_air,d_air,d_level),IntCon,options);
        v(j,:)= x;
    end
    n_mod = prod(v,2);
    mx= max(n_mod);
    loc = find(n_mod==mx);
    for l = 1: length(loc)
        SM_axis(l) = v(loc(l),1);
        lev(l) = v(loc(l),2);
    end
    l_a =find(lev == min(lev));
    level_air = lev(l_a(1));
    SM_X_axis_air = SM_axis(l_a(1));
    mod_air= SM_X_axis_air *level_air;
    mat(i,:) =horzcat((k*100),mod_air);
    k=k+0.1;
end
g=abs(mat(:,1)-mat(:,2));
mat = [mat,g];
[r l]=find(mat(:,3)==min(g));
```

Optimisation function

```
function [c,ceq] =
function_type_1_orientation_1(x,L_truck,H_truck,W_truck,L_module,H_modu
le,W_module,Submodule_voltage,clearance_submodule_air,d_air,d_level)
ceq = [];
% level and tower in the converter design TYPE I
SM_X_axis= x(1);
level = x(2);
```

```
v_level = (SM_X_axis*Submodule_voltage);
N_level_air= SM_X_axis*level; % number of submodules in one level
Volt_air= (N_level_air*Submodule_voltage)/2; % voltage rating of test
source

% calculation of the dimensions of the converter
Act_height_air= (level*H_module)+(d_level(v_level)*(level-1))+
(2*d_air(Volt_air)); Act_width_air = (2*L_module)+
d_air(2*Volt_air)+(2*d_air(Volt_air));
Act_length_air = (W_module*SM_X_axis)+((SM_X_axis-1)
*clearance_submodule_air)+ (2*d_air(Volt_air));
c= [Act_width_air-W_truck,Act_height_air-H_truck,Act_length_air-
L_truck]; % comparison with the trailer dimensions
end
```

Published with MATLAB® R2018b

A.4 Electric field simulation of the converter layout (type I- orientation I)

In section 2.7, electric field analysis was conducted on the converter layout which could contain the maximum number of submodules. This section shows an example of electric field simulation of another type of conveter layout – type I (orientation I). The 3D representation of the conveter layout is shown in figure A.6 (repeated from figure 2.30).

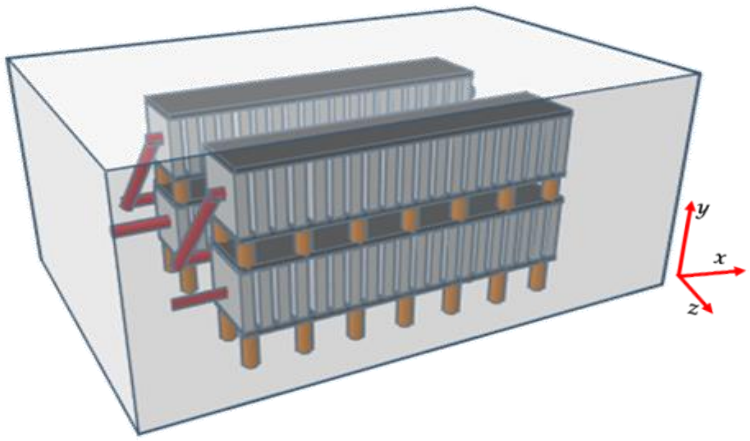

Figure A.6: Submodule arrangement of type I connection (orientation I) inside the trailer

With this layout, 18 submodules were found to fit in one converter arm (with 9 submodules in one layer). The corresponding 3D model of the layout is shown in figure A.7.

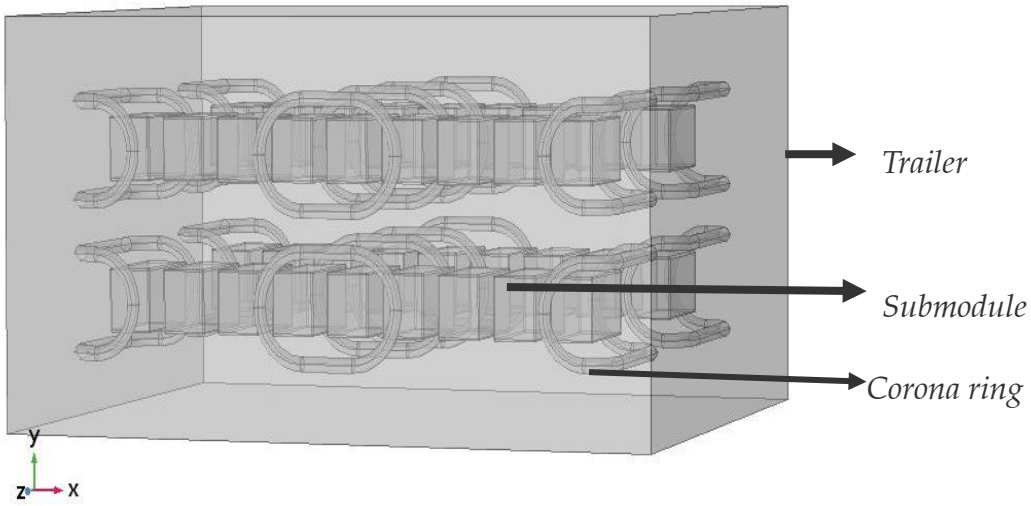

Figure A.7: Simplified 3D model of type I (orientation I) in COMSOL

A.8 shows the potential distribution of the submodules in the converter arrangement. In this case, all modules in upper arm are inserted ($N_u = 18$) and all the modules in lower arm are bypassed ($N_l = 0$). The output voltage for this state of the converter is -V_{dc} which is -36 kV in this case.

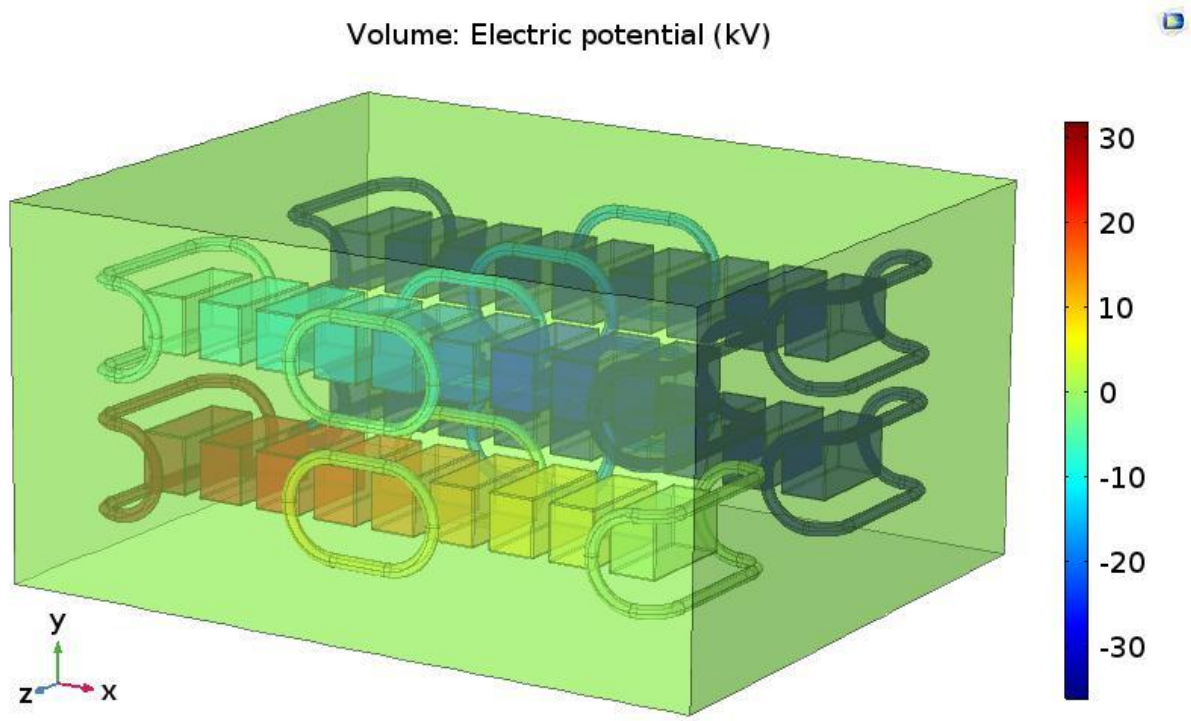

Figure A.8 Potential distribution of submodules

The field distribution on the surfaces of converter tower arrangement is shown in figure A.9. It can be seen that, with the addition of the corona rings, the maximum field is nearly 1.2 $\frac{kV}{mm}$. However, the corona rings in this design are not optimised according to the converter structure. With accurate design, the maximum field could be reduced further below 1 $\frac{kV}{mm}$.

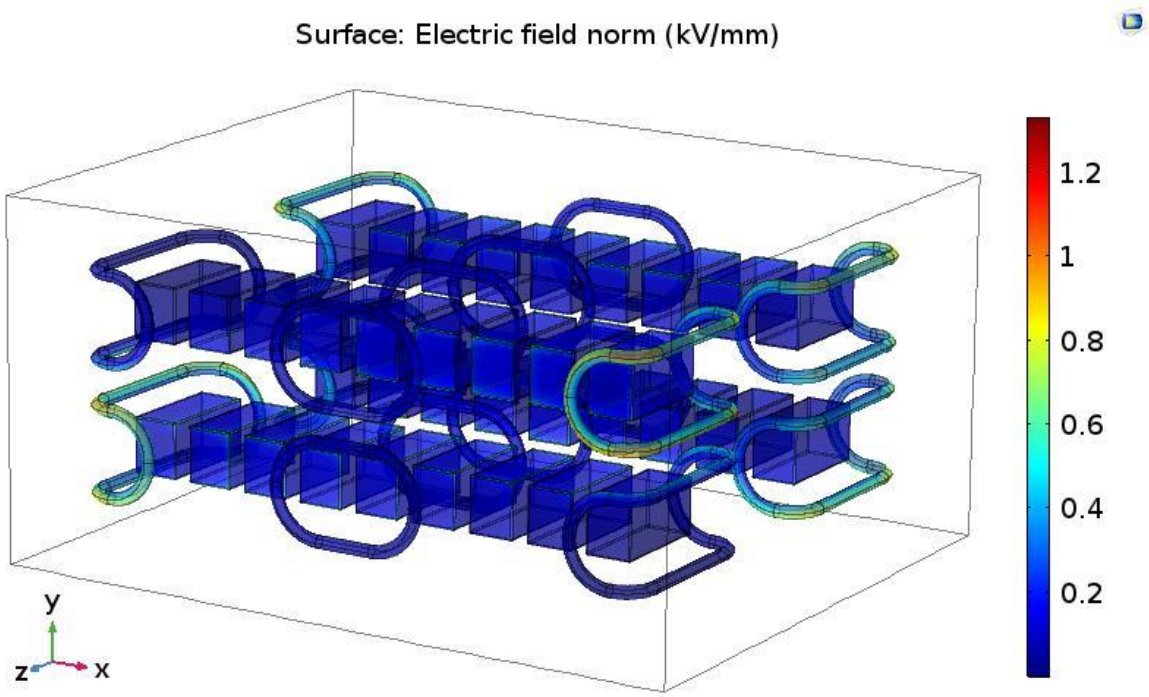

Figure A.9 Surface field distribution of the converter arrangement

Bibliography

[1] Eaton, "Blackout Tracker" [Online]. Available: http://blackouttracker.powerware.com/uk.html Accessed on: 15 June 2019.

[2] IEC 60071-1, Insulation co-ordination - Part 1: Definitions, principles and rules.

[3] IEC 60060-3 High Voltage test techniques –Part 3: Definitions and requirements for on-site testing.

[4] GE, "Mobile substations" [Online]. Available: https://www.gegridsolutions.com/products/brochures/AlstomEnergy/GIS/Grid-ACS-L2-Mobile_Substations-0311-2016_03-EN.pdf Accessed on: 10 June 2019.

[5] Power Diagnostix, "On-site Measurements" [Online]. Available: https://www.pdix.com/services/on-site-measurements.html Accessed on: 12 June 2019.

[6] DNVGL, "On-site testing" [Onsite]. Available: https://www.dnvgl.com/services/on-site-testing-20965 Accessed on: 11 June 2019.

[7] E. Gulski, P. Cichecki, F. Wester, J. Smit, R. Bodega, T. Hermans, P. Seitz, B. Quak, F. Vries, "On-site Testing and PD Diagnosis of High Voltage Power Cables", *IEEE Trans. Dielectr. Electr. Insul.*, vol. 15, pp. 1691-1700, 2008.

[8] Energy Solutions Co. "HVAC testing of underground cable up to 400 kV" [Online]. Available: http://www.energysolutionskwt.com/hvac-testing-of-underground-cable-up-to-400-kv.html Accessed on: 12 June 2019

[9] D.A. Ganeshpure, "Modular Multilevel Converter (MMC) based High Voltage Test Source", Master thesis in Electrical Engineering, Delft University of Technology, 2018

[10] S. Yang, A. Bryant, P. Mawby, D. Xiang, L. Ran, P. Tavner, " A High Voltage Multi Level Arbitrary Waveform Generator for Insulation Testing", IEEE Trans. Power Electron., vol. 26, no. 2 pp. 405 - 411, May 2019

[11] A. Dragonas et al, "High-Voltage High-Frequency Arbitrary Waveform Multilevel Generator for DBD Plasma Actuators," IEEE Trans. on Ind. Appl, vol. 51, no. 4, pp. 3334–3342, 2015.

[12] IEC 60664-2-1 Insulation coordination for equipment within low voltage systems - Part 2-1: Application guide - Explanation of the application of the IEC 60664 series, dimensioning examples and dielectric testing

[13] Samtec, "Creepage and Clearance and Why We Care About It" [Online]. Available: https://blog.samtec.com/post/creepage-and-clearance-and-why-we-care-about-it/ Accessed on: 29 June 2019

[14] PCIM, "Modular Multilevel Submodules for Converters, from the State of the Art to Future Trends" [Online]. Available: https://pcim.mesago.com/content/dam/messefrankfurtmesago/pcim/2019/documents/pdf/en/PCIM_2018%20Markus_Billmann.pdf Accessed on: 26 June 2019

[15] IEEE EPEC 2011," HVDC Plenary Session" [online]. Available: http://www.ieee.ca/epec11/admin/04-0800-hvdc_plenary_barker.pdf Accessed on: 29 June 2019

[16] Hans-Peter Nee and Lennart Ängquist, "Perspectives on Power Electronics and Grid Solutions for Offshore Wind farms," Elforsk AB, Stockholm, Technical Report, November 2010. [Online]. Available: http://www.elforsk.se/Rapporter/?download=report&rid=10_96_ Accessed on: 26 June 2019

[17] K. Sharifabadi, L. Harnefors, H. Nee, S. Norrga, R. Teodorescu Design, Control and Application of Modular Multilevel Converters for HVDC Transmission Systems, Wiley-IEEE Press 2016

[18] Alstom Grid, "HVDC-VSC: transmission technology of the future," France, THINK GRID #08: Magazine, 2011. [Online]. Available: http://www.alstom.com/Global/Gr-%20id/Resources/Documents/Smart%20Grid/Think-Grid-08-%20EN.pdf%20. Accessed on: 26 June 2019

[19] Electric Energy Online, "LSIS Introduces Full Lineup of the World's Top Smart Energy Solution". [Online]. Availablehttps://electricenergyonline.com/print_news.php?ID=5-92647 Accessed on: 26 June 2019

[20] Alstom Grid, "Tres Amigas and VSC Technology", http://www.ece.uidaho.edu-/hvdcfacts/Presentations/Kirby2011.pdf%20Accessed on: 29 June 2019

[21] Chen.H, et al.: "Hardware design and key submodule testing of the world's first single-level press-pack IGBT based modular multilevel converter for VSC HVDC", PEMD 2016, paper A10.2

[22] "Large-scale adoption of model-based design for production of HVDC technologies" [Online]. Available: https://www.mathworks.com/content/dam/mathworks/mathworks-dot-com/solutions/automotive/files/uk-expo-2013/large-scale-adoption-of-model-based-design-alstom.pdf Accessed on: 26 June 2019

[23] CEPRI "M2000 HVDC Flexible converter valve" [Online]. Available: http://www.cepri.com.cn/products/details_38_131.html Accessed on: 24 June 2019

[24] Trans bay cable, "Operations" [Online]. Available: http://www.transbaycable.c-om/operations.html Accessed on: 24 June 2019

[25] Siemens "HVDC PLUS. Voltage Source Converter Solution HVDC. Technology, Benefits, Applications"https://docplayer.net/50337438-Hvdc-plus-voltage-source-converter-solu-tion-hvdc-technology-benefits-applications.html Accessed on: 24 June 2019

[26] Xu, T., Jones, P.S., Davidson, C.C.: 'Electrical type tests for the voltage sourced converter valves based on modular multi-level converter'. Proc. 17th ECCE Power Electronics and Applications Conf., Geneva, Switzerland, September 2015, pp. 1–10.

[27] DNVGL, "GROW – two proposal ideas" – presentation

[28] Windpower, "Siemens wins order for HVDC link between Denmark and Holland" [Online], Available: https://www.windpowerengineering.com/electrical/siemens-wins-order-for-hvdc-link-between-denmark-and-holland/ Accessed on: 24 June 2019

[29] Siemens, "HVDC technology development for electricity networks" [Online] Available: https://www.suffolk.gov.uk/assets/planning-waste-and-environment/major-infrastructure-projects/National-Symposium-Siemens-HVDC-Steve-Aughton.pdf Accessed on: 24 June 2019

[30] A. Christe, E. Coulinge, D. Dujic, "Insulation coordination for a modular multilevel converter prototype", Proc. 18th Eur. Conf. Power Electron. Appl., pp. 1-9, 2016.

[31] Brugg Cables, "High Voltage XLPE Cable Systems" [Online] Available: http://www.nepa-ru.com/brugg_files/02_hv_cable_xlpe/03_web_xlpe_guide_en.pdf Accessed on: 24 June 2019

[32] KEMA Laboratories - General information of Series-Resonant test-set

[33] HVP, "general purpose pulse capacitors", https://www.hvproducts.de/files/wm_general_purpose_pulse.pdf Accessed on: 24 June 2019

[34] Infineon, "Datasheet" [Online] Available: https://www.infineon.com/dgdl/Infineon-FZ750R65KE3-DS-v03_02-EN.pdf?fileId=db3a304325afd6e00126461fd3936974 Accessed on: 24 June 2019

[35] Infineon, "Datasheet" [Online] Available: https://www.infineon.com/dgdl/Infineon-FZ250R65KE3-DS-v03_00-en_de.pdf?fileId=db3a3043382e8373013895a5f3f6169f Accessed on 24 June 2019

[36] PPC Insulators, PPC Porcelain Solid Core Post Insulators and operating Rods https://www.ppcinsulators.com/wp-content/uploads/2018/05/PPC_ANSI_Solid-Core_A-4_LQ.pdf Accessed on 2 August 2019

[37] F.H. Kreuger, Industrial High DC Voltage, Delft University Press, 1991.

[38] Liu, Chenyang, et al. "Electric-field Simulation of Insulation Type Test of±420kV HVDC Flexible Converter Valve." 2018 IEEE International Power Electronics and Application Conference and Exposition (PEAC). IEEE, 2018.

[39] "Upgrade of the Apollo HVDC converter station" [Online]. Available: https://library.e.abb.com/public/4b6d19b5e4afa385c12576640046ed66/Upgrade%20of%20the%20Apollo%20HVDC%20converter%20station.pdf Accessed on 2 April 2019

[40] "CIGRE 2004 ", [Online]. Available: http://www.ptd.siemens.de/Question14_Summary.pdf Accessed on: 28 June 2019

[41] A. Petterteig, R. Pittini, M. Hernes, Ø. Holt, "Pressure tolerant power IGBTs for subsea applications" in EPE, Barcelona, 2009.

[42] R. Pittini, M. Hernes, "Pressure Tolerant Power Electronics for Deep and Ultradeep Water", Oil and Gas Facilities, vol. 1, no. 1, pp. 47-52, 2012.

[43] U. M. Choi, Studies on IGBT module to improve the reliability of power electronic systems, Aalborg, Denmark, Feb. 2016.

[44] "Oil-filled capacitors", [Online]. Available: http://www.highenergycorp.com/HEC-Oil%20filled%20Capacitors.pdf Accessed on 27 April 2019

[45] Mohsen A Hajji ."A Transient model for Insulated Gate Bipolar Transistors (IGBTs)". Thesis, University of Pittsburg. 2002

[46] J. Lutz, U. Scheuermann, H. Schlangenotto, and R. D. Doncker, Semiconductor Power Devices: Physics, Characteristics, Reliability. New York, NY, USA: Springer, 2011.

[47] Infineon Technologies IGBT Modules -Technologies, Driver and Applications; A. Volke, M. Hornkamp, ISBN 978-3-00-032076-7

[48] "Press-pack IGBT, towards the next generation of a super switch", [Online]. Available: https://fhi.nl/app/uploads/sites/38/2014/01/KWx-IXYS-UK-IGBT-june14.pdf Accessed on 2 August 2019

[49] R. Simpson, A. Plumpton, M. Varley, C. Tonner, P. Taylor, X. Dai, "Press-pack IGBTs for HVDC and FACTS", CSEE Journal of Power and Energy System, vol. 3, no. 3, pp. 302-310, Sep. 2017.

[50] "GD Rectifiers", [Online]. Available: http://www.gdrectifiers.co.uk/news/june_2013_-_new_ixys_press-pack_igbts_high_power_sonic-frd/.

[51] Pedersen, Kristian Bonderup. "IGBT Module Reliability. Physics-of-Failure based Characterization and Modelling." (2014).

[52] R. Teixeira-pinto, "Multi-terminal DC network: System integration dynamics and control", 2014.

[53] Christian Zorn, "Alterung von Leistungshalbleitermodulen im Temperatur-Feuchte Spannungs-Test", Thesis, University of Bremen, 2019.

[54] Infineon Technologies, "Comparison between active and passive thermal cycling stress with respect to substrate solder reliability in IGBT modules with Cu baseplates", [Online]. Available:https://www.infineon.com/dgdl/InfineonPCIM_2014_Comparison_between_active_and_passive_thermal_cycling_stress-ED-v1_0en.pdf?fileId=5546d46146d18cb4014-7444462de296c Accessed on 3 August 2019

[55] Infineon, Material content datasheet-FF50R12RT4 [Online]. Available: https://www.infineon.com/dgd-l/Infineon-34mm-MaterialContentDataSheet-v04_00EN.pdf?fileId=db-3a30434358307d-0143666890af588b Accessed on 15 July 2019

[56] Infineon, Technical Datasheet - IHW20N120R3, [Online]. Available: https://www.infineon.com/dgdl/Infineon-IHW20N120R3-DS-v02_06EN.pdf?fileId=db3a304320d39d5901-21819187cb19a8 Accessed on 20 July 2019

[57] Shell Diala S4 ZX-I, "Technical Datasheet", [Online]. Available: http://tdc.ge/wp-content/uploads/2014/03/1_Diala_S4_ZX-I.pdf Accessed on 20 July 2019

[58] "Operation of IGBT-Modules in Insulation Liquids", [Online]. Available: https://ntnuopen.ntnu.no/ntnuxmlui/bitstream/handle/11250/2368059/13489_FULLTEXT.pdf?sequence=1 Accessed on 20 July 2019

[59] Liland KB, Lesaint C, Lundgaard L, Hernes M, Glomm WR, Liquid insulation of IGBT modules: Long term chemical compatibility and high voltage endurance testing. In: Proceedings of the IEEE International Conference on Dielectrics; 3-7 July 2016; France. p. 384-389

[60] SINTEF, "Enabling Pressure Tolerant Power Electronics – PTPE for Deep Water Applications", [Online]. Available: https://www.sintef.no/globalassets/project/press-pack/enabling-ptpe-for-deep-water-applications_pres_update.pdf Accessed on 20 July 2019

[61] Infineon, Technical Datasheet - IKW40N120H3, [Online]. Available: https://www.infineon.com/dgdl/Infineon-IKW40N120H3-DS-v02_01EN.pdf?fileId=db3a304325305e6d01-2591d4832f7032 Accessed on 20 July 2019

[62] Infineon, Technical Datasheet - FF50R12RT4, [Online]. Available: https://www.infineon.com/dgdl/Infineon-FF50R12RT4-DS-v02_00en_de.pdf?fileId=db3-a304327b89750012805fb1a356147 Accessed on 20 July 2019

[63] Keysight Technologies, "B1505A Power Device Analyzer / Curve Tracer" [Online]. Available:https://www.keysight.com/en/pd-1480796-pn-B1505A/power-device-analyzer-curve-tracer?cc=NL&lc=dut# Accessed on 20 July 2019

[64] Keysight Technologies, "34972A LXI Data Acquisition / Data Logger Switch Unit" [Online]. Available: https://www.keysight.com/en/pd-1756491-pn-34972A/lxi-data-acquisition-data-logger-switch-unit?cc=US&lc=eng Accessed on 20 July 2019

[65] Picoammeter, "Technical datasheet", [Online]. Available: https://www.tek.com/datasheet/series-6400-picoammeters/model-6485-picoammeter Accessed on 20 July 2019

[66] Semikron, "Thermal Paste Application", [Online]. Available: https://www.semikron.com/dl/service-support/downloads/download/semikron-application-note-thermal-paste-application-en-2018-01-19-rev-00/ Accessed on 20 July 2019

[67] RS Pro, "Technical Data Sheet- Silicone Heat Transfer Paste", https://docs-emea.rs-online.com/webdocs/1583/0900766b8158346a.pdf Accessed on 20 July 2019

[68] Thermo Fisher Scientific, "Introduction to FTIR spectroscopy" [Online]. Available:https://www.thermofisher.com/nl/en/home/industrial/spectroscopy-elemental-isotope-analysis/spectroscopy-elemental-isotope-analysis-learning-center/molecular-spectroscopy-information/ftir-information/ftir-basics.html Accessed on 20 July 2019

[69] R Maina, V Tumiatti, M. C. Bruzzoniti et al., "Copper dissolution and deposition tendency of insulating mineral oils related to dielectric properties of liquid and solid insulation", J. IEEE International Conference on Dielectric Liquids, pp. 1-6, 2011.

[70] A. Kalantar, M. Levin, "Factors affecting the dissolution of copper in transformer oils", *Lubrication Sci.*, vol. 20, pp. 223-240, 2008.

[71] P. Wiklund, M. Levin, B. Pahlavanpour, "Copper dissolution and metal passivators in insulating oil", IEEE Electr. Insul. Mag., vol. 23, no. 4, pp. 6-14, 2007.

[72] Infineon, "34mm and 50mm Solder Bond Modules Use and Installation Manual" [Online].Available:https://www.infineon.com/dgdl/Infineon-AN2017-07-Use%20and%20Installation%20Manual-34mm-and-50mm-Solder-Bond-Modules-AN-v01_02-EN.pdf?fileId=5546d462576f3475015775517f2622cd Accessed on 20 July 2019

[73] Infineon, "IGBT reliability in converter design", [Online]. Available: http://www.infineon.com/export/sites/default/cn/product/promopages/CSR/6.ppt Accessed on 20 July 2019

[74] Infineon Technology: AN2019-05 Use of power cycling curves for IGBT4; 2019

[75] Laird, "Ceramic Plate Series - Thermoelectric Modules", [Online]. Available: https://assets.lairdtech.com/home/brandworld/files/Laird-ETS-CP-Series-CP2-127-06-Data-Sheet.pdf Accessed on 20 July 2019

[76] arcTEC™ STRUCTURE, "Improved Performance and Life Span in Peltier Modules" [Online]. Available: https://www.cui.com/catalog/resource/arctec-structure-improved-performance-and-life-span-in-peltier-modules.pdf Accessed on 2 August 2019

[77] Arroyo Instruments, 5300 Series TECSource – user manual. [Online]. Available: http://www.arroyoinstruments.com/manuals/Arroyo5300TECSourceUsersManual.pdf Accessed on 20 July 2019

[78] Labfacility, "Platinum Wound Detector Elements", [Online]. Available: http://www.farnell.com/datasheets/1918881.pdf?_ga=2.227160093.1473037429.1564336028-726660352.1564336028 Accessed on 20 July 2019

[79] Control Products, Inc. "What is a Thermal Cutoff Switch?" [Online]. Available: https://www.cpi-nj.com/thermal-cutoff-switches/ Accessed on 20 July 2019

[80] HighVolt, "AC Resonant test system for on-site testing of extruded HV cables [Online]. Available:https://www.highvolt.de/portaldata/1/Resources/HV/Downloads/8-02-4.pdf Accessed on 20 July 2019

[81] W. Hauschild, E. Lemke, High-Voltage Test and Measuring Techniques, Springer-Verlag, 2014.

[82] Marc Torras Garcia." Design and viability analysis of a new HVAC system". Master Thesis, Escola Tècnica Superior d'Enginyeria Industrial de Barcelona

[83] Siemens, "Converter technology for successful grid expansion", [Online]. Available:https://press.assets.siemens.com/content/siemens/press/ui/en/search.html#/asset/sid:b3b3043a-f151-416e-96b8-fd1556a18ccf Accessed on 20 July 2019

List of abbreviations

HV	High Voltage
MV	Medium Voltage
LV	Low Voltage
MMC	Modular Multilevel converter
IEC	International Electrotechnical Commission
HVDC	High Voltage Direct Current
IGBT	Insulated Gate Bipolar Transistor
DC	Direct Current
SM	Sub Module
HTRB	High Temperature Reverse Bias
STATCOM	Static Synchronous Compensator
FACTS	Flexible Alternating Current Transmission System
DUT	Device Under Test